Mineralogy, geochemistry and sulfur isotope characterization of Cerro de maimón (Dominican Republic), San Fernando and Antonio (Cuba) lower cretaceous VMS deposits: Formation during subduction initiation of the proto-Caribbean lithosphere within a fore-arc

L. Torró, J.A. Proenza, J.C. Melgarejo, P. Alfonso, J. Farré de Pablo, J.M. Colomer, A. García-Casco, A. Gubern, E. Gallardo, X. Cazañas, C. Chávez, R. Del Carpio, P. León, C.E. Nelson, J.F. Lewis

PII: S0169-1368(15)30071-8
DOI: doi: 10.1016/j.oregeorev.2015.09.017
Reference: OREGEO 1620

To appear in: *Ore Geology Reviews*

Received date: 22 May 2015
Revised date: 9 September 2015
Accepted date: 16 September 2015

Please cite this article as: Torró, L., Proenza, J.A., Melgarejo, J.C., Alfonso, P., Farré de Pablo, J., Colomer, J.M., García-Casco, A., Gubern, A., Gallardo, E., Cazañas, X., Chávez, C., Del Carpio, R., León, P., Nelson, C.E., Lewis, J.F., Mineralogy, geochemistry and sulfur isotope characterization of Cerro de maimón (Dominican Republic), San Fernando and Antonio (Cuba) lower cretaceous VMS deposits: Formation during subduction initiation of the proto-Caribbean lithosphere within a fore-arc, *Ore Geology Reviews* (2015), doi: 10.1016/j.oregeorev.2015.09.017

Mineralogy, geochemistry and sulfur isotope characterization of Cerro de Maimón (Dominican Republic), San Fernando and Antonio (Cuba) Lower Cretaceous VMS deposits: Formation during subduction initiation of the Proto-Caribbean lithosphere within a fore-arc

L. Torró[a,*], J.A. Proenza[a], J.C. Melgarejo[a], P. Alfonso[b], J. Farré de Pablo[a], J.M. Colomer[a], A. García-Casco[c], A. Gubern[a], E. Gallardo[d], X. Cazañas[e], C. Chávez[f], R. Del Carpio[f], P. León[f], C.E. Nelson[g], J.F. Lewis[h]

[a]Departament de Cristal·lografia, Mineralogia i Dipòsits Minerals, Facultat de Geologia, Universitat de Barcelona (UB), Martí i Franquès s/n, 08028 Barcelona, Spain

[b]Departament d'Enginyeria Minera i Recursos Naturals, Universitat Politècnica de Catalunya. Av. Bases de Manresa 61-73, 08240 Manresa, Catalonia, Spain

[c]Departamento de Mineralogía y Petrología, Universidad de Granada, Fuentenueva s/n, 18002 Granada, Spain & Instituto Andaluz de Ciencias de la Tierra, CSIC-UGR, Av. Las Palmeras, 4, 18100 Armilla, Granada, Spain

[d]Central Geological and Mining Enterprise, Santa Clara, Cuba

[e]Instituto de Geología y Paleontología, Vía Blanca y Carretera Central, Havana, Cuba

[f]Corporación Minera Dominicana, C/ José A. Brea Peña #3, Edificio District Tower, Level 3, Ensanche Evaristo Morales, Santo Domingo, Dominican Republic

[g]Recursos del Caribe, S.A., 2360 23rd Street, Boulder, Colorado 80304, USA

[h]Department of Earth and Environmental Sciences, George Washington University, Washington, DC 20052, USA

To be submitted to Ore Geology Reviews

* Corresponding author: Lisard Torró i Abat

Departament de Cristal·lografia, Mineralogia i Dipòsits Minerals, Universitat de Barcelona. C/ Martí i Franquès s/n 08028 Barcelona, Catalonia, Spain.

Phone number: (+34) 934021344

E-mail: lisardtorro@hotmail.com

Abstract

The volcanic-arc Lower Cretaceous Maimón (Dominican Republic) and Los Pasos (Cuba) Formations, representative of the oldest magmatism recorded in the Caribbean island arc, host most of the known volcanogenic massive sulfide (VMS) deposits in the Greater Antilles. On the basis of new lithogeochemical data, basalts of the Maimón Formation are classified as fore arc basalts (FAB), boninites and less abundant low-Ti (LOTI) and normal island-arc tholeiites (IAT), and those of the Los Pasos Formation as LOTI and IAT. Felsic volcanics from the two formations are geochemically analogous and present mantle-type (M-type), boninitic and tholeiitic signatures, classifying as FIV-type, typical of post-Archaean VMS-bearing juvenile volcanic suites. This lithogeochemical data is indicative of formation in a fore-arc environment just after subduction initiation in association with initial extensional regimes and associated boninitic and tholeiitic melts that originated in the shallow mantle. Within this tectonic framework, rocks of the Los Pasos Formation and associated VMS deposits likely formed at a slightly later stage than those of the Maimón Formation.

Primary syngenetic ore mineral assemblages from VMS deposits in the Cerro de Maimón (Maimón Formation), San Fernando and Antonio (Los Pasos Formation) are similar. They are composed mainly of pyrite in a matrix with variable proportions of chalcopyrite, sphalerite and tennantite. However, variable metamorphism and deformation have imprinted distinct deformation/recovery textures on the three deposits. Relict sedimentary-diagenetic sulfide growths are preserved only in Antonio ore in the form of local framboidal and colloform growths and microcrystallite textures. Spongy texture, dominant in the Antonio deposit and sparse in San Fernando ores, along with overgrowths of pyrite are interpreted as representative of syn-depositional hydrothermal replacement. Annealing texture among pyrite grains and rotated pyrite porphyroclasts with adjacent asymmetric pressure shadows, combined with cataclastic textures in Cerro de Maimón ore denote higher metamorphic grade and more intense deformation. Syn-metamorphic sulfide recovery/recrystallization led to the remobilization of trace elements and subsequent crystallization of discrete minerals (galena, tellurides, tetrahedrite, arsenopyrite/löllingite, Ag-sulfosalts and electrum).

The chemical composition of sphalerite from the three deposits suggests ore formation in a sediment-starved environment. Estimated minimum venting fluid temperature calculated from the composition of sphalerites from stratiform mineralization in the three deposits is in the range of 242 to 302 ºC. Tennantite crystals from the three deposits returned low Sb and Ag contents, typical of VMS mineralization formed in juvenile intraoceanic island-arc settings. A broad trend toward Sb

enrichment in stratiform ores in the San Fernando and Antonio deposits parallels lower concentration of Se and As and higher contents in the more incompatible Sb, Te and Bi in galena with respect to Cerro de Maimón. These nuances in ore geochemistry are in good agreement with the slightly more primitive setting of formation of VMS mineralization hosted in the Maimón Formation, as indicated by the lithogeochemistry of the volcanic host rocks.

The sulfides from Cerro de Maimón display $\delta^{34}S$ values of -1.3 to +3.0 ‰, whereas those from the San Fernando and Antonio deposits were in the range of -0.5 to +7.0 ‰ and of 0.0 to +5.8 ‰ respectively. The relatively narrow scatter of $\delta^{34}S$ suggests homogeneous fluid sulfur composition and similar physico-chemical conditions during the ore forming processes, and is consistent with sulfide derived from the inorganic reduction of seawater and/or from a magmatic source.

Although the three deposits are classified as non-auriferous, significant Au contents are described in Cerro de Maimón ore (to 7.6 g/t) and in intermediate (to 1.44 g/t) and upper (to 0.88 g/t) mineralized zones of the San Fernando deposit.. Gold, probably precipitated as invisible gold during exhalative mineralization, shows evidence for later metamorphism- and deformation-triggered remobilization and re-precipitation as subordinate electrum. Solid-state mechanical transfer was apparently the dominant upgrading mechanism in the Cerro de Maimón deposit whereas liquid-state chemical transfer would have governed the upgrading process in the San Fernando deposit.

Keywords: Fore-arc, FAB, boninite, LOTI, VMS, volcanic arc, Caribbean

1. Introduction

Volcanogenic massive sulfide (VMS) deposits form at or near the seafloor as a result of the exhalation of metalliferous hydrothermal fluids in submarine volcanic environments (Doyle and Allen, 2003; Tornos, 2006; Galley et al., 2007). They are largely syngenetic and are coeval with associated volcanism which often exhibits specific petrochemical signatures that are indicative of formation at anomalous high temperature (Herzig and Hannington, 1995; Piercey, 2011). Volcanogenic massive sulfide deposits have been described from a variety of volcanic and rift-related tectonic settings in ancient and modern ocean floor. These settings include active divergent (oceanic spreading ridges) and convergent margins, with convergent margins characterized by subduction-related (arc and associated back arc basins) environments along oceanic and continental plate boundaries.

Although a few Greater Antilles VMS deposits have been exploited on a small scale since at least the 16th century, it was from the mid-1970's that sustained exploration for base metals resulted in the discovery of a number of Cu and Cu-Zn rich VMS deposits (Childe, 2000). Volcanogenic

massive sulfide deposits in the Greater Antilles are described in the Dominican Republic and Cuba, genetically linked to two main episodes of island-arc tectonic and magmatic evolution: 1) bimodal-mafic type deposits that formed during the earliest stages of island-arc volcanism, and 2) mafic (Cyprus) type that formed in mature back-arc basins (Kesler et al., 1990; Proenza and Melgarejo, 1998; Russell et al., 2002; Nelson et al., 2011). The bimodal-mafic VMS deposits are hosted primarily by Early Cretaceous tholeiitic volcanic rocks of the Maimón and Amina Formations in the Cordillera Central of the Dominican Republic and in the Los Pasos Formation and Purial Complex in central and eastern Cuba respectively (Fig. 1A). They are typically associated with basalt-rhyolite contacts. For a detailed description of the metallogenic evolution of the Greater Antilles within the framework of the tectonic evolution of the northern Caribbean, the reader is referred to Proenza and Melgarejo (1998) and Nelson et al. (2011). Mafic- (Cyprus) type VMS deposits of the Greater Antilles are not discussed in this article.

The Maimón Formation hosts the Cerro de Maimón and Loma Pesada deposits, and the Loma Barbuito, Río Sin, Loma la Mina and San Antonio occurrences (Lewis et al., 2000) (Fig. 1B); deposits hosted in the Amina Formation include Anomaly "B" and Cerro Verde. The Cerro de Maimón Cu-Zn-Au-Ag deposit is located 70 km northwest of the Santo Domingo and 7 km east of the town of Maimón, in the Monseñor Nouel Province; it is the only VMS deposit currently in production in the Caribbean realm. Discovered in the 1970's as a result of geochemical studies of the gossan outcrops by Falconbridge Dominicana, the deposit was sold to Globestar who put it into production in November of 2008. The mine is currently owned and operated by Perilya Limited through its subsidiary Corporación Minera Dominicana (CORMIDOM) (http://www.perilya.com.au/our-business/operations/cerro-de-maimon). Measured, indicated and inferred resources as of December 31st 2013 total 10,642,000 t of sulfide ore averaging 1.47 % Cu, 0.78 g/t Au, 26.01 g/t Ag and 1.49 % Zn, and 545,000 t of oxide ore averaging 1.04 g/t Au and 11.80 g/t Ag (NI 43-101-compliant). Production from 2008 through 2012 totals 2,367,778 t of sulfide ore mined plus 1,355,665 t of oxide ore mined for total production of 48,574 t Cu, 61,914 oz Au and 2,509,538 oz Ag (Trout and Chavez, 2013). Cerro de Maimón mine plant processes 1,300 tpd sulfide ore and 700 tpd oxide ore for a yearly production of approximately 12,000 t of copper concentrate, 12,000 ozs of gold and 325,000 ozs of silver. The first studies of the deposit and the sulfide mineralization carried out by Watkins (1990) and Astacio et al. (2000) were followed by a summary of the structure, petrography, whole rock and oxygen isotope geochemistry by Lewis et al. (2000). Andreu et al. (2015) published an extensive study on its weathering profile.

Volcanogenic massive sulfide mineralization in the Los Pasos Formation includes the San Fernando, Antonio and Los Cerros deposits and the Los Mangos, Independencia, La Ceiba and

Minas Ricas occurrences (Fig. 1C) (Tolkunov et al., 1974; Cabrera, 1986; Gallardo-Eupierre, 2001; Nelson et al., 2011). Updated Cuban databases mention a total of nineteen VMS deposits and occurrences within this formation (Torres-Zafra, 2013). The San Fernando and Antonio deposits are located in the Villa Clara province, about 20 km south of Santa Clara and 290 km east of Havana. The San Fernando deposit, located 13 km northeast of Manicaragua town, was mined intermittently from its discovery in 1827 to its closure in 1961, with an estimated production of 38,580 ozs Au, 2,636.444 ozs Ag, 11,000 t Cu and 28,000 t Zn; estimated current resources are of 2 Mt at 2.3 % Cu and 3.5 % Zn. Recent drilling conducted by the Holmer Gold Mines Ltd - GeoMinera S.A. joint venture proved that the mineralization is still open along strike. The Antonio deposit is located 15 km southeast of the town of Fomento and was mined through open pit and small adits. The past production of the Antonio deposit is estimated at 50,000 t at 2.5 % Cu in the period 1956-1957; current resources are estimated to be 2.7 Mt at 0.3 g/t Au, 18 g/t Ag, 0.64 % Cu and 3.89 % Zn (production and resource data for Cuban deposits are from Nelson et al., 2011).

Lithochemistry of the volcanic sequences of the Maimón and Los Pasos Formations, here revised and refined on the basis of new whole rock geochemical analyses, represents an exceptional record of the very first magmatic expressions connected to the onset of intraoceanic subduction. Hence, the study of VMS mineralization hosted by these two formations offers an extraordinary opportunity to examine VMS mineralizing systems related to the earliest stages of island arc volcanism. This article presents detailed mineralogy, ore mineral geochemistry and sulfur isotope data for the Cerro de Maimón, San Fernando and Antonio primary ores. In the light of the results, and attending particular features of each deposit, the conditions of ore deposition and the metamorphic recrystallization/recovery and upgrading mechanisms are contrasted and discussed. Furthermore, the tectonic environment in which the Maimón and Los Pasos Formation-hosted VMS deposits formed within the Early Cretaceous Caribbean island arc evolution framework is constrained.

2. Regional geology

2.1 PIA (Primitive Island Arc) series of the Caribbean Island Arc

The geology of the islands of Hispaniola and Cuba resulted largely from Cretaceous to Tertiary oblique convergence and underthrusting of the North American (Proto-Caribbean) Plate beneath the Greater Antilles island-arc since ca. 135 Ma (Rojas-Agramonte et al., 2011; Pindell et al., 2012, and references therein). Subduction and related arc magmatism ceased in Hispaniola and Cuba in the latest Cretaceous-earliest Tertiary as a result of volcanic arc-Caribeana terrane collision (García-Casco et al., 2008), though subduction and volcanism renewed in Hispaniola and eastern Cuba until the Eocene when the final collision of the arc and the Bahamas Platform took place (Lewis and

Draper, 1990; Mann et al., 1991; Rojas-Agramonte et al., 2006, 2008; Boschman et al., 2014). The Greater Antilles island arc hosts a wide record of subduction-related volcanism, which extended for more than 70 Ma. Geochemically, it comprises boninitic and island-arc tholeiitic (IAT) series of dominantly Lower Cretaceous age, commonly referred to as Primitive Island Arc (PIA/IAT) that evolved to calc-alkaline (CA) and high-K calc-alkaline (K-CA) series during Upper Cretaceous-Eocene time (Donnelly and Rogers, 1980; Kerr et al., 1999; Jolly et al., 2001). However, although in general PIA/IAT series predate CA series in the Greater Antilles, this transition apparently extended at least 40 million years, from the Barremian to the Turonian (ca. 130 to 90 Ma, Pindell et al., 2012 and references therein).

From east to west, PIA-volcanic rocks in the Greater Antilles include: The Water Island Formation in the Virgin Islands, pre-Robles Formation in eastern Puerto Rico, the Los Ranchos, Los Caños, Tortue-Amina and Maimón Formations and the El Cacheal Complex in Hispaniola, and Los Pasos and Téneme Formations in central and eastern Cuba (Fig. 1A; Proenza et al., 2006 and references therein).

Primitive Island Arc volcanic series include bimodal suites formed by basalts, basaltic andesites and lesser amounts of dacites and rhyolites generally affected by sea-floor metamorphism resulting in spilites and keratophyres, respectively. Similar to conventional IAT series, PIA-type lavas from the Greater Antilles have low LILE, LREE, HFSE and Th contents and near-horizontal to slightly enriched or depleted normalized LREE spectra (e.g. Jolly et al., 2001). However, geochemical studies of PIA-basalts from Eastern Cuba (Téneme Formation, Proenza et al., 2006) and central Dominican Republic (Maimón Formation, Horan, 1995; Lewis et al., 2002; Amina Formation, Escuder-Viruete et al., 2007a; and the basal unit of Los Ranchos Formation, Escuder-Viruete et al., 2006) revealed the presence of boninites. From reconstruction of magmatic relationships in the Puerto Plata ophiolitic complex in northern Dominican Republic, Escuder-Viruete et al. (2014) suggested the following steps during the birth of the Caribbean island-arc: 1) an extremely fast W/SW dipping roll-back of the Proto-Caribbean plate, with formation of boninitic magmas and associated LREE-depleted low-Ti IAT (>126 Ma) and later boninitic (126 Ma) volcanic rocks as the consequence of fertilization of supra-subduction mantle by fluids expelled from the subduction slab; and 2) normal IAT bimodal volcanism (122-110 Ma) formed from the melting of rising fertile mantle fluxed with fluids expelled from the downgoing oceanic crust in the mantle wedge.

2.2 Maimón Formation, Dominican Republic

The pre-Albian Maimón Formation, together with the Los Ranchos and Amina Formations, is part of the oldest and chemically most primitive island-arc volcanism in the Caribbean region (Lewis

and Draper, 1990; Lewis et al., 2002; Escuder-Viruete et al., 2007a, 2009). The Maimón Formation is a 9 km wide by 73 km long NW-SE trending belt (Fig. 1B) which can be divided into two structural provinces aligned parallel to the trend of the belt: (i) the Ozama shear zone to the SW, whose extreme deformation has obliterated most of the original igneous textures, and (ii) the much less deformed Altar Zone to the NE (Draper et al., 1996; Lewis et al., 2000). Both zones have been metamorphosed to greenschist facies. The Maimón Formation is in fault contact with the Loma Caribe peridotite and the Peralvillo Sur Formation (Lewis et al., 2002; Escuder-Viruete et al., 2007b) to the southwest and with the Los Ranchos Formation to the northeast (Fig. 1B). Draper et al. (1996) suggested that the Loma Caribe peridotite, a serpentinized harzburgite with minor dunites, lherzolites and pyroxenites forming part of a dismembered ophiolite complex (Lewis et al., 2006; Proenza et al., 2007), was tectonically emplaced over the Maimón Formation during the late Albian along a northward thrust; obduction resulted in deformation and metamorphism of the Maimón Formation, particularly in the Ozama shear zone. The Loma Caribe peridotite belt is separated from the Maimón Formation at their southern contact by the Peralvillo Sur Formation, a thin sequence of arc-related volcanic and volcanosedimentary rocks of Late Cretaceous (?) age (Martín and Draper, 1999; Lewis et al., 2000), documenting further tectonic movements of late Cretaceous-Tertiary age. The Maimón, Amina and Los Ranchos Formations are overlain by the Hatillo limestone, a massive micritic sequence deposited under shallow-water reefal conditions during Albian to Cenomanian time (Kesler et al., 2005). However, the Maimón Formation overthrusts the Hatillo limestone along the Hatillo Thrust. Both the Maimón and Hatillo Formations are intruded by diorites dykes and plugs of Paleocene (?) age (Bowin, 1966; Martín and Draper, 1999).

The Maimón Formation is composed of low-grade metamorphosed and variably deformed bimodal volcanic and volcaniclastic rocks containing scarce horizons of breccias and conglomerates. A belt of well-laminated rocks of sedimentary origin, mainly fine-grained meta-tuffs, cherts, dark shales and limestones, crops out in the north central part of the Maimón Formation and is conformable with the volcanic sequence (Kesler et al., 1991; Lewis et al., 2000). Geochemically, the mafic (basaltic) rocks range from low-Ti tholeiites with boninitic affinities to typical oceanic island-arc tholeiites. Felsic rocks are quartz-feldspar tuffs and porphyries that exhibit a similar depleted trace element signature indicating a common source (Lewis et al., 2000, 2002; Escuder-Viruete et al., 2007a).

The protoliths of the Maimón, Amina and Los Ranchos Formations have very similar elemental and isotopic (Sr and Nd) signatures, suggesting common magma sources and petrogenetic processes; however, the origin and relative position of these units within the primitive island-arc is still a

matter of debate (Torró et al., 2015). Horan (1995) concluded that the Maimón Formation formed in a back-arc basin. In contrast, Lewis et al. (2000) distinguished a fore-arc setting origin for the Maimón and Amina Formations and an axial island-arc context for the Los Ranchos Formation. On the other hand, Escuder-Viruete et al. (2007a) suggested a cogenetic origin for the three formations though lead isotope ratios ($^{206}Pb/^{204}Pb$, $^{207}Pb/^{204}Pb$ and $^{208}Pb/^{204}Pb$) of the Maimón and Amina Formations are lower than those of the Los Ranchos Formation (Horan, 1995). The fact that the Maimón and Amina Formations mainly host exhalative deposits in contrast to the epithermal character of those hosted by the Los Ranchos Formation is a further indication that they formed in different environments within a subduction setting (Nelson et al., 2011, 2015; Torró et al., 2014).

2.3 Los Pasos Formation, Cuba

The Early Cretaceous (Hauterivian?-Barremian: García-Delgado et al. 1998) bimodal Los Pasos Formation is the oldest unit of the Greater Antilles arc in Cuba (Díaz de Villalvilla et al., 1994, 2003; Kerr et al., 1999; Blein et al., 2002; Rojas-Agramonte et al., 2011). The Los Pasos Formation is only locally deformed by folding, and is not metamorphosed (Díaz de Villalvilla et al., 1994). It crops out to the southernmost part of the Cretaceous island arc unit of central Cuba, in a 3 to 5 km wide and 40 km long E-W trending arcuate belt (Fig. 1C). The Los Pasos Formation forms the southern limb of a synformal structure together with the other arc sequences (Iturralde-Vinent, 1998). It is intruded to the south by the mid-Cretaceous Manicaragua Batholith (Rojas-Agramonte et al., 2011), which also intrudes the volcanic-arc-derived metamorphic tectonic units of the Porvenir Formation and the Mabujina Amphibolite Complex (or lithodem). To the north, the Los Pasos Fm is covered by arc-related volcanic-volcaniclastic sequences of the Aptian-Albian Mataguà Formation. The Porvenir Formation consists of a bimodal volcanic sequence metamorphosed to the greenschist facies; it is interpreted as equivalent to the Los Pasos Formation (Rojas-Agramonte et al., 2011 and references therein). The 5 to 10 km-wide Hauterivian-Turonian Mabujina Amphibolite lithodem is tectonically below the Porvenir Formation and consists of intense to moderately deformed low-intermediate pressure amphibolites, meta-ultramafic rocks (serpentinites, metapyroxenites, hornblendites), intercalated metagranodioritic and granitic gneisses, discordant tonalitic-trondhjemitic-granitic bodies and veins and local metasilicites. This complex is interpreted as the metamorphosed roots of the island arc and its oceanic sole (Millán, 1996) or as an exotic volcanic arc terrane not related to the Greater Antilles arc (Blein et al., 2002; Rojas-Agramonte et al., 2011). The Manicaragua Batholith granitoids intruded the Porvenir Formation, the Mabujina Amphibolite Complex and the Cretaceous volcano-sedimentary arc at 81-89 Ma (Rojas-Agramonte et al., 2011).

The Los Pasos Formation rocks are mainly of volcanic origin, formed in a submarine environment where K-poor felsic lavas of dacitic-predominant composition with associated massive sulfide deposits are prominent. Basalts, basic tuffs and subordinate andesites are sandwiched between two rhyodacite units (Díaz de Villalvilla et al., 2003). The Los Pasos Formation also contains intercalations of pyroclastic, epiclastic, and sedimentary rocks. The volcanic rocks show a genetic relation with acid intrusive rocks and gabbroic bodies, suggesting a volcano-plutonic association. Geochemically, they are described as island-arc tholeiites (Kerr et al., 1999; Blein et al., 2002; Díaz de Villalvilla et al., 2003).

3. Geology and structure of the deposits

3.1 Cerro de Maimón

The Cerro de Maimón deposit is located in the Ozama shear zone, in the southern branch of the Maimón Formation, very close to the thrust-faulted contact with the Peralvillo Formation (Fig. 1B). Intense deformation, metamorphism and pervasive hydrothermal alteration (especially in the footwall rocks) have largely destroyed original features of the igneous rocks. Based on the least altered samples, the protoliths of the host rocks were described as mafic to intermediate submarine volcaniclastic and volcanic rocks by Lewis et al. (2000). Quartz-sericite-pyrite schists are the dominant foot wall rocks, grading to chlorite-quartz-feldspar schists at depth. Thin graphitic and hematitic chert horizons are more developed in the western hanging wall (Watkins, 1990). A high concentration of quartz veins associated with strong hydrothermal alteration in the westernmost area led Lewis et al. (2000) to the conclusion that the western foot wall zone could correspond to a sulfide stockwork whereas the eastern foot wall rocks would be distal to the feeding zone; nevertheless, such a stockwork has not been drilled.

The ore-body is 1000 m long, about 300 m wide and 15 m thick on average although the thickness reaches up to 40 m. The orebody dips 40° to the southwest with a general steepening of the dip to the northwest, and it flattens to 20° down plunge (Watkins, 1990) (Fig. 2A).

3.2 San Fernando

The ore zone at San Fernando occurs within the lowest unit of the Los Pasos Formation, which is largely composed of rhyodacite lapilli tuffs and local breccias (Fig. 2B). This unit is capped beneath an overlying basaltic flow with a strike of approximately 110º and northerly dips of 45º to 75º. Semi-porphyritic rhyodacite dominant flows cover these basalts and laterally and upwardly grade to rhyodacite tuffs and breccias (Gallardo-Eupierre, 2001). There are extensive zones of wall rock alteration, including proximal facies of chlorite+pyrite around stringer mineralization zones, and

local sericite-quartz+pyrite zones enveloped by more widespread sericite±pyrite zones. Bedded barite - chert horizons are located throughout the volcanic sequence. The lithostratigraphic sequence and ores are cut by NW-SE and NE-SE trending strike-slip faults and conspicuous diorite dykes and sills (Gallardo-Eupierre, 2001); further faulting is evidenced by sharp contacts between mineralized stockwork and relatively fresh rhyodacite rocks as well as by dismemberment of the stratiform sulfide body (Fig. 2B).

The mineralization is partly stratiform, although the majority of the historic mine workings concentrated on the stringer or feeder zone which is marked by a series of cross-cutting breccias. The ore body crops out close to the Los Mangos Shaft, and plunges along strike (to the east) at 120º up to a depth of 100 m, where it flattens (Gallardo-Eupierre, 2001). Bottom to top, the following sulfide mineralization styles are recognized: 1) an extensive stockwork zone of unknown thickness, 2) several semi-massive (replacement) stratabound units of a few meters to 20 m in thickness and 3) a mineralogically vertically zoned (see section 6.2.3) massive stratiform lens reaching to 30m in thickness (Fig. 2B).

3.3 Antonio

The Antonio deposit lies above rhyodacite lapilli tuffs and flows of the lowest unit of the Los Pasos Formation which are pervasively quartz-sericite-pyrite altered, and is overlain by basaltic flows and breccias (Gallardo-Eupierre, 2001). The presence of pyritic siliceous exhalite horizons closely related to the sulfide body is remarkable. The orientation of conformable contacts between volcanic units and sulfide lenses is 130º with dips of 10º to 45º to the northeast. The volcanic sequence is cut by dykes of variable composition including diorites and tonalites, whose thicknesses range from a few centimeters to several meters (Fig. 2C).

Stratiform mineralization extends for 300 m along strike, 250 m down dip and averages 11 m in thickness. Close to the surface, the mineralization thins and flattens (Fig. 2C). However, two superimposed massive sulfide bodies a few tens of meters apart are described along the main portion of the deposit at depth (Gallardo-Eupierre, 2001); both massive sulfide lenses are separated and underlain by stockwork zones.

4. Sampling and analytical techniques

This study is based on 350 drill core and *in situ* field samples collected from the Cerro de Maimón, San Fernando and Antonio deposits and their hosting volcanic series over the past 20 years.

Whole rock geochemistry was determined for a total of 41 samples of volcanic rocks from the Maimón and Los Pasos Formations. Powdered samples were carefully prepared by removing secondary veins and weathering products before crushing and powdering in a tungsten carbide mill. Major element and Zr concentrations were determined on glass beads made up of ~0.6 g powdered sample diluted in 6 g of $Li_2B_4O_7$, by means of a Philips Magix Pro (PW-2440) X Ray fluorescence (XRF) equipment at the University of Granada (Centro de Instrumentación Científica, CIC). Precision was better than ±1.5% for an analyte concentration of 10 wt %. Precision for Zr was better than ±4% at 100 ppm concentration. Trace elements, except Zr, were determined at the University of Granada (CIC) by ICP Mass Spectrometry (ICP-MS) after HNO_3 + HF digestion of ~100 mg of sample powder in a Teflon lined vessel at ~180°C and ~200 psi for 30 min, evaporation to dryness, and subsequent dissolution in 100 ml of 4 vol.% HNO_3. Procedural blanks and international standards PMS, WSE, UBN, BEN, BR, and AGV (Govindaraju, 1994) were run as unknowns during analytical sessions. Precision was better than ±2% and ±5% for analyte concentrations of 50 and 5 ppm, respectively.

Ore mineralogy and petrology were studied on 123 polished sections (73 from Cerro de Maimón and 50 from San Fernando and Antonio) by means of reflected light microscopy. Morphological, textural and preliminary compositional features of selected samples were examined by SEM-EDS using an Environmental SEM Quanta 200 FEI, XTE 325/D8395 equipped with an INCA Energy 250 EDS microanalysis system. Operating conditions were an acceleration voltage of 20 kV and a beam current of 1 nA. Ore mineral chemical analyses were performed with a five-channel JEOL JXA-8230 electron microprobe (EMP) at 20 kV accelerating voltage, 20 nA beam current and 5 μm beam diameter. SEM-EDS and EMP analyses were carried out at the Centres Científics i Tecnològics (CCiT) of the University of Barcelona.

Sulfur isotope analyses were carried out on 85 single sulfide grains from the three studied deposits: 28 from Cerro de Maimón, 37 from San Fernando and 20 from Antonio. Sulfide grains were separated by hand-picking techniques. Purity of the samples was tested by examination with a binocular microscope. Isotopic ratios were obtained using a Delta C Finnigan MAT Delta-S mass spectrometer with an elemental analyzer at the Centres Científics i Tecnològics (CCiT) of the University of Barcelona. Standards used for calibration were IAEA S3, IAEA S1, NBS-123 and IAEA S2. Precision of the analyses is better than ±0.2 ‰. Sulfur isotope composition is expressed as the delta per mil (‰) values relative to the Canyon Diablo Troilite (CDT) standard.

5. Geochemistry of volcanic rocks

Rocks from the Maimón and Los Pasos Formations have undergone extensive sea-floor metamorphism as well as hydrothermal alteration linked to the formation of the VMS deposits (Lewis et al., 2000; Díaz de Villalvilla, 2003; Torró et al., 2015). As a result, a number of elements (Si, K, Na, Ca, Mg, Fe, Rb, Ba, Sr) are likely to have mobilized and hence their current values may not be indicative of their original concentrations. The extensive hydrothermal alteration of rocks from the Maimón and Los Pasos Formations is evident in the Alteration Box Plot of Large et al. (2001) (Fig. 3A). In the studied rocks of the Maimón Formation, increasing AI and CPPI values from the "least altered rhyolites, dacites and basalts" (least altered box in Fig. 3A) are indicative of chloritization, sericitization and sulfide mineralization (pyrite), that along with silicification were recognized in the petrographic study by Torró et al. (2015). Most of the rocks studied from the Los Pasos Formation for lithogeochemistry were sampled far from the mineralized centers; however, mafic rocks from this formation show trends towards sericitization and carbonatization and felsic rocks record albitization, both trends probably related to spilitization and keratophiritization processes. Due to the likely mobility of major elements, those considered immobile in such post-magmatic conditions (HFSE, REE, transition elements and Th; Pearce, 2014) will be used here for igneous rock classification and tectonic discrimination.

According to the Zr/Ti vs. Nb/Y classification diagram of Pearce (1996), rocks from the Maimón and Los Pasos Formations range from subalkaline basalts to rhyodacites (Fig. 3B). Studied samples from the Maimón Formation are predominantly basalts with less abundant andesites and basaltic andesites and rhyodacites. In contrast, studied rocks from the Los Pasos Formation show a marked bimodal trend and consist of basalts and rhyodacites. Rhyodacites and basalts from both formations show Zr/Ti and Nb/Y ratios equivalents to those of rocks from the bimodal Los Ranchos Formation (Escuder-Viruete et al., 2006).

5.1 Mafic assemblages

Geochemical analyses of volcanic rocks from the Maimón and Los Pasos Formations whose protoliths were identified as basalts returned remarkably low Nb contents (<2 ppm), that in the chondrite-normalized extended REE diagrams translate as marked negative Nb anomalies when compared to values of NMORB (Fig. 4C-F). Niobium depletion of studied basalts becomes evident in the Nb-Zr-Y discrimination diagram of Meschede (1986) as well, with the whole of the analyses plotting in the volcanic-arc and NMOR basalt field (Fig. 4A). High V/Ti ratios of studied basalts are indicative of formation in island-arc settings in opposition to low ratios that characterize those basalts formed in MOR or mature back-arcs according to the tectonic classification diagram of Shervais (1982; Fig. 4B). The bulk of the analyzed basalts have Ti/V ratios in the range of 10 to 20,

corresponding to IAT compositions (including slab-proximal fore-arc and back-arc basalts; Pearce, 2014); nevertheless Ti/V ratios close to or lower than 10 point to boninitic affinities. According to Finlow-Bates and Stumpfl (1981), V can be mobilized and removed under hydrothermal activity in volcanogenic submarine-exhalative environments and hence given V values would represent, anyhow, minimum values.

Following Pearce's (2014) guidelines, studied basaltic rocks from the Maimón and Los Pasos Formations have been classified according to their TiO_2 and Cr (used as immobile proxy for MgO) contents into three types: type I or boninites, type II or low-Ti IAT (LOTI) and type II or normal IAT.

Type-I basalts or boninites (TiO_2<0.5 wt. % and Cr>275 ppm) occur in the Maimón Formation; these rocks show general depletions in REE compared to NMORB (Fig. 4C), with chondrite-normalized REE patterns varying from slightly convex (depletion in MREE relative to LREE and HREE) to mildly LREE-depleted (positive slopes). Thorium and V contents are either enriched or depleted relative to NMORB. Studied boninites from the Maimón Formation show similar normalized patterns to those described by Escuder-Viruete et al. (2006) in the Los Ranchos Formation, although LREE values are occasionally higher, similar to boninites from the Izu-Bonin-Mariana (IBM) fore-arc (Pearce et al., 1992; Reagan et al., 2010). However, chondrite-normalized patterns of LREE-depleted boninites show indisputable similarity to basalts described as transitional (from fore arc basalts, FAB, to boninites) in the IBM fore-arc basin by Reagan et al. (2010).

Type-II or LOTI basalts (0.4<TiO_2<0.8 wt. % and Cr<275 ppm) show conspicuous depletion in REE compared to NMORB (Fig. 4D,E). According to their chondrite-normalized REE patterns, LOTI basalts can be grouped into two sub-types: IIa or LREE-depleted LOTI and IIb or normal LOTI.

Type-IIa or LREE-depleted LOTI basalts are in the majority among the studied basalts from the Maimón Formation, whereas they are not detected among the analyzed basalts nor described in published geochemical data (e.g. Díaz de Villalvilla et al., 2003) from the Los Pasos Formation. These basalts are characterized by strong LREE depletion and flat MREE and HREE segments in chondrite-normalized diagrams, paralleling the NMORB pattern (Fig. 4D). Thorium and V values are systematically lower and higher, respectively, than NMORB. Chondrite-normalized values of type-II basalts from the Maimón Formation describe similar patterns to those of LREE-depleted LOTI basalts described in the Los Ranchos Formation by Escuder-Viruete et al. (2006) and FAB from the IBM fore-arc (Reagan et al., 2010; Ishizuka et al., 2011), even if the REE values in our study case are lower as a rule. Relatively high V contents (206 to 374 ppm) and low V/Ti ratios (10

to 15) of the LREE-depleted LOTI basalts from the Maimón Formation are also consistent with those of FAB of IBM (Reagan et al., 2010). These observations permit the classification of our LREE-depleted LOTI basalts as FAB, a term coined by Reagan et al. (2010) for describing "MORB-like" subduction-influenced tholeiitic lavas originating in the IBM fore-arc.

Type-IIb or normal LOTI basalts are detected in both the Maimón and Los Pasos Formations. They show flat chondrite-normalized REE patterns, with slightly higher MREE and HREE abundances than the boninites and LREE-depleted LOTI basalts described above (Fig. 4E). They are variably enriched in V and Th compared to NMORB. Normal LOTI basalts from the Maimón and Los Pasos Formations show great similarity with basalts from the Los Ranchos Formation described as LREE-depleted LOTI and generally have lower REE contents than those described as normal IAT by Escuder-Viruete et al. (2006).

Type-III or normal IAT basalts (TiO_2>0.8 wt. %) are exiguous among the studied basalts from the Maimón Formation and relatively abundant in those from the Los Pasos Formation (Díaz de Villalvilla et al., 2003). The analyzed normal IAT basalt from the Maimón Formation show a near-flat chondrite-normalized REE pattern, whereas normal IAT basalts from the Los Pasos Formation show contrasting faint negative slopes (LREE/HREE>0) and higher LREE contents (Fig. 4F). Thorium and V are systematically enriched to NMORB values, with normal IAT basalts from the Los Pasos Formation registering the highest Th values among the whole studied basalt spectrum. Normal IAT basalts from the Maimón and Los Pasos Formations show similar HREE values to LREE-depleted LOTI basalts from the Los Ranchos Formation (Escuder-Viruete et al., 2006) and MREE and HREE concentrations in the range of normal IAT basalts of this Formation.

5.2 Felsic assemblages

Rocks of rhyodacitic composition from the Maimón and Los Pasos Formations show marked negative Nb anomalies and mild positive Th anomalies (Fig. 5A). Their chondrite-normalized REE patterns vary from near-flat to slightly LREE-depleted or, in those samples with lower REE contents, convex. Tholeiitic- and boninitic-like chondrite-normalized REE patterns, lacking LREE enrichment, and low REE, Zr and TiO_2 contents are distinctive to typical calc-alkaline felsic volcanic rocks. Hence the studied rhyodacites are interpreted to have tholeiitic and boninitic affinities (e.g. Lesher et al., 1986; Piercey, 2011). Studied rhyodacites from the Maimón and Los Pasos Formations are depleted in LREE relative to felsic volcanics from Los Ranchos Formation (Escuder-Viruete et al., 2006), even if their HREE contents are similar.

Felsic volcanic rocks in terranes prospective for VMS deposits are commonly plotted in the Nb-Y discrimination tectonic diagram for granites of Pearce et al. (1984) (e.g. Piercey, 2011; Hollis et al., 2014). Rhyodacites from the Maimón and Los Pasos Formations plot in the volcanic arc granite field, with typical compositions of VMS bearing rhyolites formed in primitive (juvenile) arc settings of the M (i.e. mantle derived)-type (Fig. 5B). In addition, analyzed felsic volcanics, with extremely low Zr/Y and La/Yb_{CN} ratios, systematically lie in the FIV field (Fig. 5C, D) of post-Archaean tholeiitic and boninitic felsic volcanic rocks potentially associated with VMS deposits (Hart et al., 2004; Piercey, 2007). The low overall trace element contents of felsic volcanic rocks from the Maimón and Los Pasos Formations likely reflects the low trace element abundance of their mantle-derived mafic sources (boninite and arc tholeiite melts).

6. Ore mineralogy and petrography

6.1 Cerro de Maimón

Overall, the major ore mineralogy of the Cerro de Maimón deposit is relatively simple. Textures are principally controlled by the degree of metamorphism and deformation, to the point that primary textures are completely obliterated. In general ore samples are aggregates of pyrite grains in a matrix with variable amounts of other sulfide and gangue minerals, with fabrics ranging from matrix to grain-supported (Fig. 6). From textural features described below, a five-stage paragenetic sequence has been deduced (Fig. 6A).

Within the massive sulfide lens, gangue minerals are basically quartz and white mica (including both sericite and well developed muscovite) and rare chlorite. Quartz forms veins and aggregates of sutured crystals often with feather shapes adjacent to bigger pyrite grain edges (pressure shadows, stage III; Fig. 6B). For quartz veins, a late generation (stages IV and V) is deduced as they contain angular fragments of all the sulfides including those of supergene nature. Minute sericite needles forming aggregates concentrated along layers (Fig. 6B) occur interspersed with quartz-rich levels. Schistosity is defined by bundles of tabular crystals of muscovite (and minor chlorite; stage III) locally displaying crenulation fabrics. Muscovite bundles often wrap around pyrite grains. Barite appears along with other gangue minerals and sulfides among the pyrite grains or as infilling or inclusions within pyrite (stages II and III). Only local late hydrothermal sparry to blocky calcite is observed forming veins up to 0.5 mm in width cutting the bulk rock or partially flooding the groundmass among pyrite crystals.

Pyrite is by far the most abundant sulfide. It varies in shape from cubic idiomorphic to completely rounded or very irregularly outlined (Fig. 6). Pyrite size covers a wide spectrum even within

individual rock samples, typically ranging from 250 microns to 1.5 mm, although sizes up to 4.5 mm are present. During deformation, stage II pyrite underwent breaking (grain size reduction) and welding of individual crystals; as result of the former, cataclastic textures and microfracturing with blow-apart structures are abundant, especially where interstitial material is quartz (Fig. 6F). Metablastic welded pyrite crystal aggregates show frequent foam or annealing textures among fine to medium sized metacrystals with triple junctions at 120º (Fig. 6H). In the outer parts of the sulfide lens, where the mineralization is semi-massive, stronger deformation is evidenced by muscovite wrapped around large pyrite crystals with rotation fabrics (Fig. 6G) and durchbewegt textures (Vokes, 1969). These observations imply that pyrite grains behaved as porphyroclasts during syn-metamorphic deformation.

Variable proportions of chalcopyrite, sphalerite, tennantite and galena are generally present along the entire drilled section of the Cerro de Maimón massive sulfide body. Chalcopyrite and sphalerite are more abundant than tennantite, while galena is very scarce as a rule. Sphalerite only presents local subtle chalcopyrite disease (blebs of chalcopyrite in sphalerite). Variable proportions of these sulfides appear along with gangue minerals between pyrite grains (Fig. 6C-D) with a variety of textures indicative of plastic deformation and recovery/recrystallization at lower temperature than pyrite (Pesquera and Velasco, 1993; Barrie et al., 2010). Also, the four sulfides appear as both single (only one mineral) and composite (Fig. 6E) inclusions within pyrite. Annealing textures observed in the complex inclusion in Fig. 6E among bornite, chalcopyrite, sphalerite and galena necessarily implies that at least part of the bornite formed previously or during metamorphism; bornite is well documented in a wealth of modern and ancient VMS hydrothermal systems (e.g. Hannington et al., 1999a; de Ronde et al., 2011; Berkenbosch et al., 2012) and in metamorphic sequences and metamorphosed sulfide deposits (e.g. Sales and Meyer, 1951; Ramdohr, 1980; Misra, 2000).

Trace small tellurides of some tens of microns in size occur within voids in pyrite and are interpreted to have precipitated at late stages (stageVI; Fig. 6I-J). They are in their majority Ag-tellurides (hessite, Ag_2Te) and rare Bi- (hedleyite (Bi_7Te_3)/pilsenite (Bi_4Te_3)/tellurobismuthite (Bi_2Te_3)?) and Pb-tellurides (altaite, PbTe). Hessite is largely concentrated along tetrahedrite margins (Fig. 6J) suggesting that they are alteration products of the latter.

Discrete minute (~15 microns) electrum grains crystallized in voids within pyrite or in the contacts between pyrite and the other sulfides. Electrum grains were systematically detected in the outer parts of the sulfide lens, where deformation is more evident (e.g. rotational fabrics on pyrite grains). Supergene minerals include bornite, covellite-chalcocite and minor djurleite ($Cu_{31}S_{16}$), digenite

(Cu_9S_5) and yarrowite (Cu_9S_8). Assemblages of covellite-chalcocite forming flame-like textures systematically replace bornite (Fig. 6K) in those samples in which supergene processes developed further (stage V).

6.2 San Fernando

Detailed textural study of the ores from San Fernando revealed a complex mineralization and alteration story that can be discerned beyond contact metamorphism caused by the intrusion of the Manicaragua stock. From textural observations described below, a five-stage paragenetic sequence has been deduced for each mineralization style (stockwork, stratabound and stratiform; Fig. 7A).

6.2.1 Stockwork

Hosted in pervasively silicified and sericitized rhyolites, stockworks are composed of veins of quartz and pyrite with subordinate chalcopyrite and sphalerite; disseminated euhedral pyrite in hosting rhyolites is abundant. Minor very thin sphalerite±barite, tennantite and rare hessite±galena veinlets largely within chalcopyrite complete this fissure-infilling sequence.

6.2.2 Stratabound

Prior to sulfide mineralization, a first stage of hydrothermal alteration resulted in sericitization and chloritization of the host rocks. Euhedral tabular barian-muscovite and Mn-rich chlorite are surrounded and partially replaced by sulfides (mainly poikiloblastic pyrite). Enrichment in Ba of sericite/illite in VMS-hosting rocks is characteristic (Herzig, 1988). Chlorite laths along muscovite exfoliation planes are present, suggesting that chloritization followed sericitization as as is typical in footwall pipes close to the VMS mineralization (e.g. Lydon, 1988; Large et al., 2001). Local biotite intergrown with muscovite may represent remnants of rhyodacite rocks. The second stage corresponds to sulfide mineralization from variable replacement of original and alteration silicates. Although sphalerite, chalcopyrite, pyrite and tennantite generally show annealing textures (Fig. 7D), local chalcopyrite veinlets across sphalerite grains are preserved. Barite is locally replaced by sulfides.

A lower temperature mineral assemblage composed of Ag-rich tetrahedrite+hessite±electrum in veins crosscutting the sulfides defines the third stage. Hessite and electrum grains have sizes of a few microns to some tens of microns. Tennantite, hessite and electrum display polymineralic foam or annealing textures (Fig. 7E) that include the hosting sulfides, hence indicating deposition before the metamorphic peak. Local hessite and galena crystallized as infillings in pyrite voids lack annealing textures (Fig. 7D) and therefore precipitated after the metamorphic climax (stage IV).

The fifth stage is characterized by late replacement processes of zinalsite ($(Zn,Al)_3((Si,Al)_2O_5)(OH)_4$) + armenite ($BaCa_2Al_6Si_9O_{30}\cdot 2H_2O$) (Fig. 7K). Far from depicting annealing textures, these minerals corrode sulfur grain boundaries.

6.2.3 Stratiform

The stratiform massive sulfide lens can be roughly divided into a lower pyrite-dominated unit with subordinate chalcopyrite and sphalerite, an intermediate gold- and silver-enriched unit composed of pyrite+chalcopyrite+tennantite and an upper unit composed of sphalerite along with minor pyrite+galena±chalcopyrite. Rare relicts of sericitized plagioclase are the only record of the host rocks in their contact with the sulfide lens (stage I in Fig. 7A).

The stage II corresponds to the massive mineralization (i.e. sedimentation/replacement and syn-depositional hydrothermal alteration or refining; Eldridge et al., 1983) and hence the formation of the main part of the current mineralization volume. Pyrite, chalcopyrite, sphalerite and tennantite precipitated in this stage largely exhibit strong indentation and recrystallization (annealing) textures due to contact metamorphism. However, subtle local spongy textures in the core of pyrite grains are preserved (Fig. 7B) resulting from the recrystallization of polyframboidal pyrite aggregates (e.g. Velasco et al., 1998). In the lower unit, minor quantities of chalcopyrite and sphalerite occurring as inclusions within pyrite are attributed to poikiloblastic growth of the latter. In the intermediate unit, pyrite is, in contrast, partially replaced and cut by veins of chalcopyrite+sphalerite±tennantite (Fig. 7C). In the upper unit, pyrite is cut by an assemblage of low-iron sphalerite, galena, chalcopyrite and tennantite; sphalerite is in turn locally cut by a chalcopyrite+quartz±torneböhmite ($(REE)_2Al(SiO_4)_2(OH)$) assemblage (Fig. 7H). In this upper unit, sphalerite, chalcopyrite and tennantite appear as inclusions within pyrite as well.

In the intermediate unit, the lower temperature assemblage of stage III is defined by veins of sphalerite along with small sized (around 20) silver-rich tetrahedrite, arsenopyrite and electrum grains observed to cut chalcopyrite (Fig. 7I). Stage IV widely developed in the intermediate unit as veins of chalcopyrite, sphalerite, galena and tellurides cutting previous assemblages and as complex symplectic replacements of tennantite (Fig. 7F) consisting of an intimate intergrowth of löllingite+chalcopyrite±sphalerite+Ag-bearing phases such as tetrahedrite, hessite, matildite ($AgBiS_2$) and pyrargyrite (Ag_3SbS_3) and trace amounts of stromeyerite (AgCuS) and acanthite (Ag_2S) (Fig. 7G). In the upper unit, replacements by galena and chalcopyrite are attributed to the fourth stage that, as in the intermediate unit, lacks evidence for textural re-equilibration (foam or annealing textures).

Finally, stage V is represented by minor remobilization in narrow veins where silver (and Ag-Hg amalgams) occur as replacements of acanthite (Fig. 7J).

6.3 Antonio

Metamorphic recrystallization of ores in the Antonio deposit is less intense than that recorded at San Fernando on account of its greater distance from the Manicaragua batholith. Petrographically, this is illustrated by the preservation of spongy textures in the cores of pyrite (recrystallization of polyframboid pyrite aggregates; e.g. Velasco et al., 1998) and local framboidal-spheroidal growth remnants (Fig. 8B-E); both textural characteristics are definitely a distinguishing feature with respect to San Fernando and Cerro de Maimón deposits. Detailed textural study of the ores resulted in a four-stage paragenetic sequence presented in Fig. 8A separately for the stockwork and the stratiform mineralization types.

6.3.1 Stockwork

Stock mineralization is composed of quartz+sulfide veins that cut a pervasively altered rhyodacite host-rock in which local plagioclase remnants are recognized even though they were extensively replaced by sericite. Ti-oxide and apatite inclusions occur within plagioclase which, together with muscovite (corroded by sulfides), is gathered as stage I. Stage II corresponds to the first generation of sulfides and is defined by the predominance of fine-grained pyrite and minor sphalerite and chalcopyrite. Sphalerite, commonly presenting chalcopyrite disease, cuts pyrite whereas chalcopyrite forms veins crosscutting both pyrite and sphalerite. Stage III is represented by barite±chalcopyrite and quartz veins. Radial aggregates of prehnite are interpreted to be metamorphic.

6.3.2 Stratiform

Whereas the upper stratiform massive sulfide lens is composed to a great extent of pyrite, with only subordinate sphalerite and chalcopyrite (less than 1%), the lower stratiform lens presents compositional zoning, grading downward from chalcopyrite- to sphalerite-rich. Muscovite is the only remnant of the initial alteration stage (stage I) and, in detail, it contains sulfide replacements along exfoliation planes and corroded outlines. The bulk of the massive sulfide mineralization formed during stage II; it is defined by fine to medium (less than 300 microns) pyrite grains with a wide spectrum of textures descriptive of sedimentary-diagenetic-, hydrothermal- and later metamorphic-driven processes. Framboidal-spheroidal and microcrystallite textures (Fig. 8B) are representative of the diagenetic-sedimentary processes. Hydrothermal replacement textures are dominant in the studied ores, with extensive spongy texture (Fig. 8C,E) and common zoned

overgrowths of porosity- (Fig. 8E) and/or inclusion-free rims (Fig. 8D) over spongy cores. Later metamorphic textures are restricted to local annealing and rare cataclastic textures. Inclusions within pyrite grains are of chalcopyrite, sphalerite and subordinate tennantite (Fig. 8D). Chalcopyrite disease in sphalerite is common. Chalcopyrite, sphalerite and minor tennantite occur between and as infilling of fractures in pyrite grains, always displaying evidence for textural re-equilibration (Fig. 8E).

Faint annealing affected minerals defining stage III in veins with variable proportions of quartz, tetrahedrite, barite (Fig. 8F) and galena that cut previous assemblages. Finally, the fourth stage led to late precipitation of galena and tellurides such as altaite (PbTe), kochkarite ($PbBi_4Te_7$) and/or rucklidgeite ($(Bi,Pb)_3Te_4$) (Fig. 8G).

7. Ore mineral geochemistry

Representative EMP analyses of ore minerals from Cerro de Maimón, San Fernando and Antonio deposits are gathered in Table 1. In addition, a summary of chemical composition of sphalerite, tennantite and tetrahedrite from the three deposits is given in Table 2. Element compositions by EMP were assessed for variability among the three deposits and relative to the stratigraphy and mineralization type (i.e. stockwork, stratabound, stratiform) position of the samples. All analyses returned contents of Co, Ni, Ge, and In below their respective detection limits.

Sphalerite shows remarkably low atomic Fe/Zn ratios (<0.12) and low to intermediate S contents (Table 2); negative correlation between Zn and Fe (Fig. 9A) indicates a substitution of Fe for Zn (e.g. Herzig, 1988). The Cu content of sphalerite is as much as 1.16 wt. % and hence is below the 2 wt. % threshold suggested by many authors (Kojima and Sugaki, 1985; Tesfaye Firdu and Taskinen, 2010; Keith et al., 2014) as indicative of preservation of primary compositions and minor impact of remobilization or chalcopyrite disease. Nevertheless, as trends towards Cu enrichment do exist in the analyzed sphalerite grains (Fig. 9B) we did not use analyses with higher Cu contents for estimating P-T conditions from sphalerite compositions (see Discussion).

Tetrahedrite group minerals (fahlores) from the three deposits were found to be largely tennantite (Fig. 9 D) with the exception of late tetrahedrite in the San Fernando stratiform mineralization (Fig. 7A,I). Tennantite crystals from Cerro de Maimón have the lowest Sb contents whereas tennantite crystals from the stratiform units of San Fernando have the highest Sb values In the case of San Fernando, the distinct populations of tennantite shown in Fig. 9D correspond to the two stratiform units of this deposit. Thus, tennantite from the upper stratiform mineralization has lower Ag and Fe contents and higher Cu and Zn contents than in the intermediate stratiform unit. Tennantite from the

massive stratiform mineralizations in Antonio returned homogeneously low Ag contents whereas Sb contentsare lower in the lower stratiform than in the upper stratiform unit.

Tennantite from the stratabound mineralization in San Fernando and especially in the stockwork in Antonio shows contrasting and more diverse compositions than in the stratiform mineralizations of both deposits. In San Fernando it is enriched in Sb and impoverished in Ag and Fe relative to the stratiform units. The composition of tennantite from the stockwork of the Antonio deposit shows remarkable dispersion in its content in S, As, Sb, Ag, Fe, Cu and Zn contents. Silver and Sb enrichments correlate with S, Cu and As depletion.

Tetrahedrite from the upper stratiform mineralization in San Fernando has similar Zn and Fe concentrations whereas that from the intermediate stratiform level is richer in Fe than in Zn. Enrichment in Ag is observed in tetrahedrite crystals from the intermediate with regards to the upper stratiform levels of San Fernando.

Galena was analyzed in Cerro de Maimón and in the upper stratiform unit of San Fernando ores. It is the only sulfide with significant concentrations of Se and Te, the former being higher in Cerro de Maimón (0.38 to 3.83 wt. %) than in San Fernando (of 0.22 wt. %) while the reverse occurs for the latter, more concentrated in San Fernando (0.37 to 0.43 wt. %) than in Cerro de Maimón (to 0.25 wt. %). Silver is higher in San Fernando (0.40 wt. %) than in Cerro de Maimón (to 0.26 wt. %).

Pyrite composition is relatively constant and only random Pb, Zn, and Cd (up to 0.31, 0.22 and 0.15 wt. % respectively) were detected. Chalcopyrite in Cerro de Maimón has Zn and Pb concentrations ranging from values under their detection limits up to 1.18 and 0.22 wt. % respectively. Gold concentrations are very low with only sparse values of up to 0.27 wt. %. Arsenopyrite from the intermediate stratiform mineralization of San Fernando has As contents ranging from 36.79 to 43.39 wt. % and Co and Ni concentration as high as 0.08 and 0.11 wt. %, respectively.

Electrum grains from the intermediate stratiform unit of the San Fernando deposit have Ag/Au ratios from 0.67 to 0.93 and the general structural formula $Au_{0.50-0.59}Ag_{0.40-0.47}Cu_{0.01}Hg_{0-0.01}Fe_{0-0.01}$. Although the minute size of electrum grains in Cerro de Maimón samples prevented valid EMP analyses, EDS analyses suggest Ag/Au ratios close to 1.

8. Sulfur isotopes

In the Cerro de Maimón deposit, the $\delta^{34}S$ values of the analyzed sulfides tightly span from -1.3 ‰ to +3.0 ‰ (Fig. 10; Table 3), with a mode value of 0.0 ‰ and an average of +0.4 ‰ (n=28). The

$\delta^{34}S$ values range from -1.3 ‰ to +3.0 ‰ on pyrite, from -0.7 ‰ to -1.5 ‰ on chalcopyrite and is of +1.5 ‰ on the sphalerite analyzed sample.

$\delta^{34}S$ values of sulfide minerals from San Fernando range from -0.5 ‰ to +7.0 ‰ (Fig. 10; Table 3), with a modal value of +2.5 ‰ and an average of +2.7 ‰ (n=37). $\delta^{34}S$ values of pyrite cover the entire range, whereas $\delta^{34}S$ of chalcopyrite ranges from +0.3 ‰ to +3.1 ‰. The two analyzed sphalerite grains returned almost coincident values of +1.7 ‰ and +1.9 ‰. The scatter of $\delta^{34}S$ values reduces to -0.5 to +3.7 ‰ for sulfides from the upper and intermediate stratiform mineralization.

Sulfide minerals from the Antonio deposit have $\delta^{34}S$ values ranging from 0.0 ‰ to +5.8 ‰ (Fig. 10; Table 3) with an average of +2.3 ‰ (n=20). The sulfur isotope signature for pyrite covers the entire range. The chalcopyrite grain analyzed returned a value of +5.7 ‰.

9. Discussion

9.1 Geodynamic setting of host volcanic rocks

Boninites and tholeiites of the Maimón and Los Pasos Formations are displaced from the mantle array (depleted mantle-MORB-OIB) defined in the Th/Yb vs. Nb/Yb diagram of Pearce and Peate (1995; Fig. 11A) towards higher Th/Yb ratios and plot within the field of oceanic arc basalts (Pearce, 2014). This indicates a subduction component in the magmas and that the sources of basalts from both formations were depleted or NMORB-type mantle wedges without any evidence of contribution from an enriched mantle (e.g. mantle plume influence). As a rule, FAB would have formed from a depleted mantle source whereas a more enriched NMORB mantle is the likely source of the studied normal IAT basalts.

Low LREE/HREE ratios (e.g. La/Yb<5; Fig. 11B) exhibited by the basalts from the Maimón and Los Pasos Formations denote a shallow mantle origin outside of the garnet stability field (Pearce and Peate, 1995; Pearce, 2008) in an intraoceanic setting (i.e. far from continental crust contamination; Hawkesworth et al., 1993). Compared to modern arc suites showing flat NMORB-normalized HREE segments (consistent with partial melting of spinel peridotite), most basalts from the Maimón and Los Pasos Formations overlap the Tonga and South Sandwich fields; however, normal IAT basalts from the Los Pasos Formation show great similarity to basalts from the less depleted mantle-derived Marianas arc, formed at slightly lower degrees of melting (<25%; Jolly et al., 2001 and references therein).

Fore arc basalts and boninites predominate among the studied basalts from the Maimón Formation and are not detected (nor described, Díaz de Villalvilla et al., 2003) in the Los Pasos Formation. In contrast, basalts from the Los Pasos Formation are characterized as LOTI and normal IAT. On the other hand, felsic volcanics from both formations are largely equivalent, and have clear M-type tholeiitic and boninitic affinities.

The presence of boninites in stratigraphic correlation with FAB, as observed in the Maimón Formation, is a major indicator of a subduction-initiation fore-arc ridge in opposition to a back arc basin setting (Ishizuka et al., 2014a, Pearce, 2014 and references therein). Subduction-initiation ophiolites are formed in fore-arc settings during the extensional event that accompanies initial sinking and ensuing slab roll-back of a newly subducting plate, immediately after subduction commences (Stern and Bloomer, 1992; Stern, 2004). In this setting, mantle (typically depleted) flows into the nascent mantle wedge and interacts with variable, although rather small, amount of volatiles expelled from the sinking plate, resulting typically in higher degrees of melting than in mid-ocean ridges. This scenario precludes the formation of the first products of arc volcanism, that is, boninites, and favor the formation of FAB (Ishizuka et al., 2011, 2014a) (Fig. 12A). Escuder-Viruete et al. (2014) inferred the extrusion of LREE-depleted LOTI volcanic rocks (here identified as FAB) at >126 Ma, previous to the deposition of layered troctolites of boninitic affinity (126 Ma) from the Puerto Plata Ophiolitic Complex (northern Hispaniola); however, these authors noted that LREE-depleted LOTI basalts were not found in Puerto Plata, probably because of their tectonic removal during the extensive regime linked to continued slab roll-back of the subducting plate. FAB from the Maimón Formation, therefore, likely represents the first extrusive magmatic products of the nascent Caribbean island-arc, perhaps as old as 135 Ma (cf. Rojas-Agramonte et al., 2011; Pindell et al., 2012). Progressive stabilization of the magmatic front and steady-state subduction and convection in the mantle wedge along with progressive fertilization of the suprasubduction mantle and decompression-melting of rising fertile mantle would have led to the generation of LOTI and, later, of normal IAT lavas. The association of LOTI and IAT basalts with M- and FIV-type felsic volcanics described in the Los Pasos Formation is strong argument for formation in a juvenile arc setting, most probably linked to a slightly later stage in the subduction initiation setting relative to lavas from the Maimón Formation (Fig. 12B). Other PIA volcanic series, such as the upper basaltic unit of the Los Ranchos Formation (Escuder-Viruete et al., 2006), are composed of normal IAT with higher REE contents and LREE enrichments and, hence, would have formed subsequently (111.6±0.5 Ma; Kesler et al., 2005) (Fig. 12C). Progressively higher Th contents from primitive to more evolved basalts (FAB > boninites > normal LOTI > normal IAT from Maimón Formation >

normal IAT from Los Pasos Formation > normal IAT from Los Ranchos Formation; Fig. 4C-F) support increasing contribution of slab derived fluids/melts to the mantle wedge (e.g. Plank, 2005).

Altogether, these observations indicate that VMS mineralization hosted in the Maimón and Los Pasos Formations formed in a fore-arc setting linked to an extensive regime just after the onset of subduction (convergence) and associated primitive boninitic and tholeiitic melts. In consequence, an association of FAB, LOTI and boninite with FIV-type felsic volcanics must be taken into account as prospective for VMS deposits in the Caribbean region.

9.2 Sulfide formation, deformation, geochemistry and deriving constraints

Pyrite, chalcopyrite, sphalerite and less abundant tennantite are the major (>99 % in volume) ore minerals in the three studied deposits. A variety of trace minerals such as galena, sulfosalts, arsenides, tellurides, etc. complete the assemblages.

Chalcopyrite, sphalerite and tennantite occur in the main as the matrix of pyrite grains and show evidences of plastic deformation and recovery/recrystallization at a lower temperature than pyrite. Pyrite, in contrast, displays a conspicuous variety of textures outlining an increasing metamorphic/deformation grade from Antonio to Cerro de Maimón through the San Fernando deposits (in the knowledge that the nature and age of metamorphism was different in the Cuban and the Dominican cases, dynamothermal vs. contact-thermal). Increase in metamorphic grade resulted in a progressive pyrite average grain-size augmentation and obliteration of primary textures. Relicts of the former were only preserved in Antonio ores in the form of local framboidal and colloform growths and microcrystallite textures. Spongy texture is the dominant one in this deposit whereas it is sparse in San Fernando and nonexistent in Cerro de Maimón. Along with spongy textures, free or impingement overgrowths of euhedral and subhedral pyrite crystals with spongy cores and inclusions- and/or porosity-free rims are interpreted to be representative of syn-depositional hydrothermal replacements. At Cerro de Maimón, the effects of deformation and metamorphism on sulfides become more important; annealing or foam textures with triple junctions at 120º in blastic pyrite alternate with intense microfracturing and blow-apart and porphyroclastic textures, locally developing pressure shadows. Very similar textural relationships and gradations are described in other VMS-bearing districts worldwide that underwent low-grade metamorphism, such as the Iberian Pyrite Belt (Velasco et al., 1998), the Appalachians (Brueckner et al., 2015) or the Norwegian Caledonides (Cook et al., 1993; Barrie et al., 2010; Lockington et al., 2014).

The coexistence of cataclastic and annealing textures in pyrite over short distances and even in single rock samples may seem confusing for extracting orebody's geological history on the basis of

the refractory nature of pyrite. Actually, pyrite grain sizes, mineral abundances and local deformation regimes are assumed to often impose larger differences in the textural response of sulfide minerals than differential metamorphism and deformation (McClay and Ellis, 1983; Barrie et al., 2010). In this connection, the abundance and composition of matrix phases surrounding pyrite grains have a major influence on its textural/structural evolution. For example, a soft sulfide matrix (i.e. chalcopyrite and sphalerite) will enhance pyrite grain growth whereas where pyrite grains impinge upon one another (i.e. little or nonexistent matrix), significant fracturing occurs. This correspondence is almost systematic in Cerro de Maimón and overlaps with the complex deformation history that certainly involved brittle deformation during retrograde metamorphic conditions (e.g. Cook et al., 1993). By means of orientation contrast (OC) imaging and electron backscatter diffraction (EBSD), Barrie et al. (2010) concluded that the preservation of annealing textures in greenschist-facies metamorphosed massive sulfides of the Norwegian Caledonides potentially represented surface-driven processes (re-arrangement by a dissolution/syntaxial overgrowth) during metamorphism This conclusion contrasts with the classical assumption that foam textures result from recrystallization (e.g. Vokes, 1969; Cook et al., 1993; Velasco et al., 1998; Craig, 2001), which certainly occurs at higher than greenschist facies metamorphic grade (McClay and Ellis, 1983). This conclusion is in good agreement with the limited mobilization of gold during metamorphic upgrading observed in Cerro de Maimón ores (discussed in section 9.4).

Syn-metamorphic (including pre-, syn- and post-metamorphic peak) sulfide recovery/recrystallization led to metamorphic remobilization (s.s.; Marshall and Spry, 2000) and local redistribution of trace elements, including base and precious metals. Subsequently, discrete minerals such as galena, Bi-, Ag- and Pb-tellurides, tetrahedrite, arsenopyrite/löllingite, Ag-sulfosalts (the last two only in San Fernando), electrum and (Ag,Hg) amalgams formed. These phases commonly concentrate along sulfide contacts and voids and show textural evidence for both textural/mineral equilibrium and non-equilibrium in the three deposits, indicating that (re)crystallization extended throughout the whole metamorphic history.

Sphalerite, because of its high relative abundance in the studied deposits, is a good candidate for being the phase that released most of the Bi, Pb and Ag, initially hosted as solid solution and/or as discrete micro-inclusions (Huston et al., 1995; Cook et al., 2009), for the subsequent crystallization of minor and trace minerals during late mineralization. Recent studies by Lockington et al. (2014) reported that the concentrations of Pb, Bi and to some degree Cu and Ag in sphalerite decrease with increasing metamorphic grade and, once released, these elements potentially form discrete minerals elsewhere. In contrast, these workers did not detect systematic changes in the concentration of Fe and Cd, and hence asserted that their concentration in recrystallized sphalerites offer potential

insights into ore genesis. This potential was yet inferred by Scott (1976) for sphalerite and contemplated for other relatively refractory sulfides such as molybdenite, pyrite or arsenopyrite (e.g. Toulmin and Barton, 1964; Kretschmar and Scott, 1976). The incorporation of Fe into sphalerite structure in exchange of Zn has long been recognized as a function of the pressure, temperature and sulfidation state of the hydrothermal fluid sphalerite precipitated from (e.g. Scott and Barnes, 1971; Scott, 1973, 1976, 1983; Herzig, 1988; Keith et al., 2014). Hannington and Scott (1989) even viewed in the composition of the sphalerite a powerful prospecting tool for Au in VMS deposits as those conditions influencing gold grades (roughly, T<300ºC and high S_2 activities) translate into low Fe contents (<10 mole % FeS) in coeval sphalerite. From the benchmark work by Scott and Barnes (1971), based on thermodynamic principles in the Zn-Fe-S system, the chemical composition of sphalerite has been widely used as geobarometer (e.g. Canet et al., 2009) and less usually as geothermometer (e.g. Browne and Lovering, 1973). Nevertheless, a number of limitations of this "classical" method for geothermobaromentric calculations exist (Mishra and Mookherjee, 1988; Keith et al., 2014); the most bothersome one is, probably, that the thermodynamic equations were calibrated for sulfide assemblages precipitated in equilibrium with pyrrhotite. Since pyrrhotite is not present in the VMS deposits studied here, the use of the Scott and Barnes (1971) method is inappropriate; the excessive pressures (>>10 Kb) equivalent to the remarkably low X_{FeS} (~0.5 to 10 atom. %) registered are proof.

Keith et al. (2014), in a study of the composition of sphalerite from a wide spectrum of active and inactive submarine hydrothermal vent settings, presented criteria for discriminating among sediment-covered or sediment-starved environments. In addition, for sediment-starved cases not affected by metamorphism of higher grade than upper greenschists facies, they propose an equation (obtained from simple regression among Fe/Zn ratios measured in sphalerite and temperature data of the active vents) for the estimation of minimum fluid temperatures of sphalerite precipitation. Sphalerites from our study have remarkably low Fe/Zn ratios and low to moderate S contents (Table 1) that match the typical compositions expected in a sediment-starved setting (Fig. 9C). The Maimón and Los Pasos Formations contain flow lithofacies (flow-dominated association; Franklin et al., 2005), including coherent mafic and felsic lava flows and abundant autoclastic deposits, but only minor amounts of sediment (Lewis et al., 2000, 2002; Díaz de Villalvilla et al., 2003). These lithologic associations are consistent with the recorded low Fe/Zn ratios of sphalerite from the studied VMS deposits.

Estimated minimum fluid temperatures using the regression equation by Keith et al. (2014) are in the range of 242 to 302 ºC on average in the three deposits.. These temperatures are in a reasonable range and agree with homogenization temperatures of fluid inclusions in sphalerite-bearing

assemblages in ancient VMS deposits (e.g. Iberian Pyrite Belt, Spain, Almodóvar et al., 1998; Hokuroku District, Japan, Pisutha-Arnold and Ohmoto, 1983) and directly in active vents (in TAG, of 265-366ºC, Hannington et al., 1998; in MARK, of 335 to 350ºC, Edmond et al., 1995; in black smokers from the Brothers Volcano, Kermadec Arc, of up to 302 ºC, Berkenbosch et al., 2012).

Fahlore, due to its capacity for solid solution, is a potential tracer for categorizing environments of ore deposition, compositional and temporal variability of fluids and/or retrograde reactions (Sack et al., 2003 and references therein). Fahlores analyzed in the three deposits are largely tennantite (As>Sb), with only traces of tetrahedrite, crystallized as low temperature replacements during pre- and post-metamorphic peak (Fig. 7A), are present in San Fernando. Concentration of Ag-tellurides in the borders of recovered/recrystallized tennantite suggests that this mineral would have been an important contributor of this metal for the subsequent crystallization of late (metamorphic) Ag phases. Antimony concentration in tennantite from the three deposits is remarkably low. Nonetheless, a fair trend towards mild Sb enrichment in the stratiform mineralizations from Cerro de Maimón (av.: 0.27 at. %, Sb/(Sb+As) = 0.02) throughout Antonio (av.: 0.61 at. %, Sb/(Sb+As) = 0.04) to San Fernando (av.: 1.39 at. %, Sb/(Sb+As) = 0.10) deposits is evident.

Tetrahedrite and tennantite are important accessory minerals in bimodal-mafic and bimodal-felsic when compared with mafic-ultramafic, mafic-siliciclastic and felsic-siliciclastic (Seal II and Piatak, 2012) VMS types. Economou-Eliopoulos et al. (2008) described tennantite-tetrahedrite assemblages in ophiolite-hosted (mafic-ultramafic) VMS deposits (Cyprus-type, Singer, 1986) in supra-subduction bimodal volcanic sequences (bimodal-mafic, Shanks III and Koski, 2012; Piercey, 2011) linked to initial stages of subduction in a fore-arc setting. This feature contrasts with the general absence of fahlores in Cyprus-type deposits hosted in mid-ocean ridges and mature back-arc basins (mafic, Piercey, 2011; mafic-ultramafic, Shanks III and Koski, 2012; back-arc mafic, Franklin et al., 2005). Similarly, Herzig and Hannington (1995) confirmed in polymetallic massive sulfides on the modern seafloor that tetrahedrite and tennantite can be abundant in back-arc spreading environments (both, intraoceanic and intracontinental) in contrast with mid-ocean ridges. In fairness, local tetrahedrite (s.s.; along with arsenopyrite and a series of Sn and Pb sulphosalts) is part of the very complex sulfide assemblage typical of sediment-covered mid-ocean ridges close to continental margins (Herzig and Hannington, 1995). Nevertheless, important primary tetrahedrite mineralization in VMS deposits is apparently restricted to intracontinental settings (Petersen, 1992 and references therein).

This inventory is no more than the statement that the geochemistry and mineralogy of massive sulfides largely depends on the source-rock lithology, which is reflective of the tectonic setting (i.e. seawater-rock interaction; Fouquet et al., 1993; Herrington et al., 2005; Glasby et al., 2008; Gilgen et al., 2014). Fouquet et al. (1993) and Herzig et al. (1993), compared mineralization in the southern Lau Basin (back-arc) with of mid-ocean ridges and basalt-controlled back-arc basins and noticed a general enrichment in As, Pb, Zn, Ag, Au, Hg and Ba that was attributed largely to the existence of differentiated (intermediate or felsic) series of volcanic rocks with island-arc affinities (i.e. differences in the relative amount of leached mafic versus felsic rocks). Direct and unreserved attribution to felsic stocks as the sources of elements such as As, Sb, Bi or Au continues to the present (e.g. Zheng et al., 2015). Several authors (Herzig and Hannington, 1995; Glasby et al., 2008) correlated higher average concentrations of Pb, As, Sb and Ag in sulfides from back-arc spreading centers of the W and SW Pacific to the presence of sediments in the hosting rock series unlike mid-ocean ridges. Over the past few years, focus in this respect seems to have moved towards the mantle. In intraoceanic settings, Timm et al. (2012) summarized that arc-related mafic lavas are enriched in most of the siderophile and chalcophile elements when compared to MORB; these workers attributed this fact to metasomatism of the suprasubduction mantle by hydrous melts derived from the downgoing slab, the input of which can be further traced from back-arc to arc-front positions. Chalcophile elements such as As and Sb are highly mobile in hydrous fluids under oxidizing mantle conditions (Noll et al., 1996) and can be fluid-transported from the slab to the melting region in the suprasubduction zone. Among other parameters (e.g. subduction zone geometry, convergence rate, slab dip, mantle source composition, degree of partial melting, fractional crystallization, etc.), slab composition play an important role in the composition of the derived magmas (Haase et al., 2002). Sediments, altered oceanic crust and serpentinized uppermost lithosphere within the slab are possible sources of these elements (Kessel et al., 2005; Deschamps et al., 2010, 2011 and references therein).

In general, the geochemical behavior of Sb is similar to that of Pb (Noll et al., 1996) and, in subduction environments, is described to be even more mobile (Jochum and Hofmann, 1997); therefore, an efficient transfer to continental crust is expected. The very low Sb contents in the analyzed tennantite crystals from the three deposits indeed reflect that fahlores (and hence massive sulfide mineralization in general) precipitated during very primitive stages in the formation of the intraoceanic island-arc, in opposition to tetrahedrite (Sb dominates over As) prevalence documented in well-developed continental crust settings. Unfortunately, whole rock As and Sb contents of samples from the Maimón and Los Pasos Formations are not available. Systematic increase observed in the concentrations of Sb in tennantite from the three deposits (Cerro de Maimón <

Antonio < San Fernando) could be related to 1) small differences in the proportions of sediments and/or the grade of alteration and serpentinization (Jochum and Verma, 1996) of the oceanic crust and lithosphere within the downgoing slab and/or 2) formation of the deposits at slightly different stages in the evolution of the subduction-related magmatism and/or 3) differences in the lithology of the hosting rock units (e.g. presence of sediments in the overriding or upper plate). The lithogeochemistry of the hosting volcanics presented in this work perfectly cover the two last options.

Fahlore compositions and part of the late (stages III-IV; Fig. 7A) trace mineral assemblage in San Fernando differ from the Antonio and Cerro de Maimón deposits and deserve a more detailed explanation. Indeed, local symplectic (i.e. exsolution intergrowths; Augustithis, 1995) replacements of tennantite crystals by an assemblage of sphalerite, tetrahedrite, pyrargyrite, hessite, matildite, stromeyerite and acanthite are exclusive to this deposit. Geothermometric calculations based on the chemical composition of tetrahedrite in close intergrown with sphalerite, pyrargyrite, hessite, matildite, stromeyerite and acanthite (Sack et al., 2002) yield 170 ºC average temperature; because of the apparent absence of miargyrite, this estimation would actually represent a minimum temperature (Sack et al. 2003). This temperature is consistent with miscibility gaps or unmixing into high-Ag and low-Ag tetrahedrite varieties stated by Sack et al. (2003). Tetrahedrite from San Fernando shows bimodality in its Ag (and Cu, Zn and Fe) contents depicting two separated populations in Fig. 9D; however, these two populations find direct correspondence with the level (upper and intermediate) along the stratiform massive lens in which the respective tetrahedrite crystals precipitated. This observation and the parallel behavior observed in tennantite crystals from these same levels would indicate that tetrahedrite compositions are rather a reflection of the composition of the tennantite crystals that they are replacing than a product of immiscibility. A similar trend (gain in Sb and Ag) is observed in tennantite from the Antonio stockwork. These features support the circulation of an epithermal or mesothermal fluid during prograde and especially during retrograde metamorphism; syn-metamorphic magmatic fluids exsolved from the cooling Manicaragua batholith granodioritic magmas are good candidates. In any case, the scope of the epithermal/mesothermal assemblage is limited and did not involve an important remobilization of metals.

Systematic trace element measurements in galena have revealed fair potential of this mineral as a marker for the source of elements and ore formation processes in deposits that have undergone superimposed metamorphism and deformation (George et al., 2015). Nevertheless, the availability of databases on trace elements in galena from different mineralization styles and geodynamic settings is still limited. Galena is the only mineral that yielded Se and Te concentrations consistently

above their detection limits; Se fractionation toward galena (rather than chalcopyrite and sphalerite) in hydrothermal systems is well-constrained (Bethke and Barton, 1971). Relatively high concentrations of Se in galena, particularly from Cerro de Maimón, are conspicuous. The chalcophile elements Se and the more incompatible Te are expected to be more enriched in subduction related (bimodal mafic and bimodal felsic) than in mid-ocean ridge (mafic-ultramafic) magmas and associated VMS deposits (König et al., 2012). When compared to Cerro de Maimón, galena from San Fernando yielded systematically lower concentrations of Se and As and higher contents of the more incompatible Sb, Te and Bi; this observation parallels the Sb enrichment observed in tennantite crystals from the Antonio and San Fernando deposits compared to those in Cerro de Maimón.

On the whole, the ore mineralogy and geochemistry are in good agreement with the ore assemblages and compositions expected for VMS deposits formed in intraoceanic island-arc juvenile settings. Moreover, subtle although decided nuances in ore mineral (fahlores and galena) geochemistry find clear correspondence with the above discussed (section 9.1) differences in the timing of deposition of the host rocks suggested by lithogeochemistry. Both whole rock and ore mineral geochemistry point to a more primitive setting of formation of VMS mineralizations of the Maimón Formation than those hosted in the Los Pasos Formation (Fig. 12).

9.3 Source of sulfur

In seafloor hydrothermal systems, sulfur isotope fractionation between aqueous species, mineral phases and microorganisms is characteristic (Shanks III et al., 1995). Three main sources of sulfur to precipitate sulfides in VMS deposits are inferred: 1) inorganic reduction of seawater sulfate; 2) magmatic sulfur, either from a direct contribution from a vapor-rich magmatic fluid or after leaching of the volcanic host rocks; and 3) sulfur from microbial activity in reduced sediments by means of bacterial sulfate reduction (Sangster, 1976; Ohmoto, 1986; Solomon et al., 1988, 2004; Stanton, 1990; Çagatay and Eastoe, 1995; Shanks III et al., 1995; Ohmoto and Goldhaber, 1997; Herzig et al., 1998; Hoefs, 2009; Brueckner et al., 2015).

The relatively narrow scatter of $\delta^{34}S$ in the studied samples suggests homogeneity in fluid sulfur composition and similar physico-chemical conditions during the ore forming process. The narrow and predominantly positive values (Fig. 10) largely rule out bacteriogenic reduction of sulfate as the source of sulfide. This range is, in contrast, in good agreement with sulfide derived from the inorganic reduction of seawater and/or a magmatic source. Inorganic thermochemical reduction of seawater sulfate favored by high temperature formation of the deposits and the Fe-rich nature of the host basaltic rocks (Shanks III et al., 1981) was surely dominant, leaving a string of $\delta^{34}S$ values as

high as 7.0 ‰; all the $\delta^{34}S$ values are consistently lower than that of the starting seawater sulfate, of ~15 ‰ during the Cretaceous (Claypool et al., 1980).

Sulfides from Cerro de Maimón returned lower values and more reduced scatter of $\delta^{34}S$ than those analyzed from the San Fernando and Antonio deposits. It is generally accepted that metamorphism tends to homogenize and reduce the range of $\delta^{34}S$ in a deposit (e.g. Sangster, 1971), in agreement with the higher metamorphic grade and deformation in the Cerro de Maimón ores here reported. However, studies such as those developed in the greenschist metamorphosed Iberian Pyrite Belt VMS deposits by Velasco et al. (1998) challenged this hypothesis.

Tentatively, homogeneously lower values in Cerro de Maimón and in the upper and intermediate stratiform mineralizations in the San Fernando deposits could be correlated with increasing magmatic sulfur contribution at a constant seawater input (as established in Noranda district VMS deposits by Sharman et al., 2015). However, the many parameters that can influence sulfur isotopic value and fractionation (e.g. water/rock ratios, physico-chemical parameters such as T, pH, fO_2, fS_2, the sulfur isotopic composition of igneous wall rocks etc., Brueckner et al., 2015) prevent developing strong arguments for the source(s) of sulfur. Magmatic fluid influence is further discussed in section 9.4 below.

9.4 Gold: on its original distribution and later metamorphic remobilization

The distribution of Au grades along the Cerro de Maimón massive sulfide lens is fairly constant and averages 1 g/t in the sulfide body; however, local higher Au concentrations up to 7.6 g/t are detected according to data provided by Perylia-CORMIDOM. Gold values show positive correlations with Cu, Zn, Ag and Pb and all together classify Cerro de Maimón as a non-auriferous/base-metal VMS deposit (Poulsen and Hannington, 1995).

Broad technical reports (Gallardo-Eupierre, 2001) do not describe Au as an economic commodity in the Antonio ores and its concentration values are not given. According to the few technical data available, apparently neither is Au an economic commodity in San Fernando deposit. However, non-exhaustive analytical work performed in a few samples by the Central Mining and Geological Enterprise (unpublished) returned Au values as high as 1.44 g/t in the intermediate unit of the stratiform sulfide lens that correlate with maximum Ag concentrations (194 g/t); Au and Ag concentrations seem to decrease towards the upper unit (0.88 g/t Au and 75 g/t Ag) and to be remarkably lower in the lower stratiform sector (0.15 g/t Au and 6 g/t Ag). This distribution of both precious metals is in fact in good agreement with the conspicuous occurrence of electrum and the higher Ag contents in tennantite (and in its alteration product tetrahedrite) in the intermediate

stratiform unit reported here. The higher Au and Ag values correspond to intermediate temperature (~270 ºC) of the intermediate stratiform unit; the contents of both metals decrease towards the higher-temperature (~302 ºC) upper sector and are very low in the lower temperature (~256 ºC) lower portion.

As summarized by Hannington and Scott (1989), Huston and Large (1989) and Huston et al. (1992), in modern massive sulfide-forming systems, Au is commonly transported as $Au(HS)_2^-$ complexes, Au solubility and transport being favored at low temperatures (<300 ºC) and near neutral pH; gold subsequently precipitates upon mixing with seawater by oxidation (above the HSO_4^--H_2S equal activity curve), a drop in temperature (<150 ºC) and dilution of H_2S. The starting composition of the hydrothermal fluid can further complicate the system. Enrichment in Au (not related to high-sulfidation-VMS systems, Hannington et al., 1999b) may also reflect processes such as seafloor boiling or contribution from a magmatic source deeper in the system. Therefore, the different Au contents recorded in the studied deposits and in each of their respective units or mineralization styles cannot be correlated on a linear basis with a unique parameter and must be understood as a complex interaction among several of them.

Beyond minor late (pre- and post- metamorphic peak) electrum occurrences in the Cerro de Maimón and San Fernando deposits, the mineralogical distribution of the bulk of Au remains unclear. This led the authors to the suggestion that the precious metal occurs as micro-inclusions within sulfide mineral lattices (i.e. the so-called invisible gold; e.g. Larocque et al., 1995). The occurrence and relative concentration of minute electrum grains in strongly sheared zones of the Cerro de Maimón sulfide lens indicate a later metamorphism- and deformation-triggered remobilization and re-precipitation of Au (and Ag) (cf. Larocque et al., 1993). Prograde metamorphism of VMS bodies can produce the release of Au from pyrite and its partitioning between electrum and chalcopyrite (Larocque et al., 1995; Marshall et al., 2000). In the Iberian Pyrite Belt, Velasco (2014) explains the precipitation of electrum and Au-Ag-Hg amalgams from invisible gold (precipitated at exhalative stages) by means of mobilization and concentration by hydrothermal fluids after the metamorphic peak and fragile/ductile deformation. Remobilization and upgrading during deformation and metamorphism may imply solid-state mechanical transfer, liquid-state chemical transfer or both (mixed-state transfer) (Gilligan and Marshall, 1987; Marshall and Gilligan, 1987, 1993; Marshall et al., 2000). Although fluid facilitation surely acted for gold and silver metamorphic remobilization in the case of Cerro de Maimón deposit, regional and textural observations reviewed here suggest that solid-state mechanical transfer was the dominant mechanism; in contrast, mineral paragenesis and textures in San Fernando ores points to liquid-state chemical transfer as the governing mechanism during metamorphic remobilization and upgrading.

Electrum composition from the San Fernando and Cerro de Maimón deposits have remarkably high Ag contents that contrast with the extreme fineness (>99% Au) of gold grains analyzed from the Cerro de Maimón gossan (Andreu et al., 2015), indicating that chemical refining (Freyssinet et al., 2005; Yesares et al., 2014) certainly took place during the weathering profile formation.

9.5 VMS deposits in fore-arcs

According to the lithogeochemistry, and supported by ore mineral assemblages and geochemistry, VMS deposits hosted in the Maimón and Los Pasos Formations formed in a fore-arc setting during the earliest arc-related magmatic activity of the nascent Caribbean Island Arc. Both, mafic and felsic volcanics from the two Formations show robust evidences of generation from high-temperature magmas formed at shallow levels within the mantle conductive to forming VMS deposits (Piercey, 2011).

In subduction-zones with stabilized magmatic-fronts, fore-arcs characteristically have lower heat flow and geothermal gradients than back-arcs (Currie and Hyndman, 2006); however, the great extension rates associated with subduction initiation and associated high liquidus temperature FAB-boninite-LOTI suite magmas in fore-arc ophiolitic sequences make fore-arcs suitable for the formation of VMS deposits (Schulz, 2012 and references therein). In fact, relatively abundant hydrothermal activity and associated disseminated sulfide mineralization apparently prior to and contemporaneous with boninitic volcanism are described in the Izu-Bonin intraoceanic forearc (Ishizuka et al., 2014b). Nevertheless, only a few cases of VMS deposits formed within a fore-arc setting are reported and, as stated by Piercey (2011), a boninite-LOTI association with VMS is not described in modern geodynamic environments. Tectonic removal during slab roll-back induced extension of the FAB-boninite-LOTI substrate by low angle detachment faulting (Stern, 2004), and/or overprinting by younger magmatic arcs are among the reasons invoked.

10. Conclusions

The integration of the lithogeochemistry from the Maimón and Los Pasos Formations and the ore mineralogy and geochemistry, and sulfur isotope data from the Cerro de Maimón (Dominican Republic), San Fernando and Antonio (Cuba) VMS deposits has led to the following conclusions:

1- Geochemically, basalts of the Maimón Formation include FAB (fore arc basalts), boninites and minor LOTI (low-Ti island arc tholeiites) and IAT (normal island arc tholeiites), whereas those studied from the Los Pasos Formation are characterized as LOTI and IAT. These results point to formation shortly after the onset of subduction (convergence) linked to initial extensional regimes and associated primitive boninitic and tholeiitic melts of

shallow mantle origin in a fore-arc setting. In this environment, rocks of the Los Pasos Formation and associated VMS deposits likely formed at slightly later stages than those of the Maimón Formation.

2- The lithochemistry of felsic volcanics from the Maimón and Los Pasos Formations is equivalent; both exhibit M-type, boninitic and tholeiitic signatures. They classify as FIV-type, typical of post-Archaean felsic volcanic rocks prospective for VMS deposits.

3- Primary ore mineralogy from the Cerro de Maimón, San Fernando and Antonio deposits is largely analogous and composed in the main of pyrite, chalcopyrite, sphalerite and tennantite. In the three deposits, ore textures evidence deformation/recovery; higher deformation and metamorphic grade recorded in ores from the Cerro de Maimón deposit are reflected in generalized annealing and cataclastic textures. Antonio ores register the lowest deformation/metamorphic grade of the three studied deposits and preserve relicts of framboidal and microcrystallite growths and spongy textures. Syn-metamorphic sulfide recovery/recrystallization led to the remobilization and local redistribution of trace elements, and subsequent crystallization of discrete minerals (galena, tellurides, tetrahedrite, arsenopyrite/löllingite, Ag-sulfosalts and electrum).

4- The chemical composition of sphalerite from the three deposits suggests ore formation in sediment-starved environments; calculated minimum temperatures of precipitation for sphalerite from the stratiform mineralizations are in the range of 242 to 302 ºC for the three deposits.

5- Tennantite crystals from the three deposits have conspicuously low Sb and Ag contents that characterize most VMS deposits formed in juvenile intraoceanic island-arc settings. A broad trend toward Sb enrichment in stratiform ores in the San Fernando and Antonio deposits with respect to Cerro de Maimón parallels lower concentrations of Se and As and higher contents of the more incompatible Sb, Te and Bi in galena. These nuances in ore geochemistry support the slightly more primitive setting of formation of VMS mineralizations hosted in the Maimón Formation indicated by the lithogeochemistry of the hosting volcanic units.

6- Sulfur isotope data on sulfides from the three deposits indicate that sulfide derived from the inorganic reduction of seawater and/or from a magmatic source.

7- The three deposits are characterized as non-auriferous, although fair Au contents exist in the Cerro de Maimón ores and in the intermediate and upper stratiform portions of the San

Fernando deposit. Gold, that probably precipitated as invisible gold during the exhalative mineralization stage, shows evidence of later metamorphism- and deformation-triggered remobilization and re-precipitation as electrum; whereas solid-state mechanical transfer appears to be the dominant upgrading mechanism in the Cerro de Maimón deposit, liquid-state chemical transfer would have governed upgrading in the San Fernando deposit.

Acknowledgments

This research has been financially supported by the Spanish projects BTE2001-3308, CGL2012-36263, the Catalan project 2014-SGR-1661 and a FPU Ph.D. grant to L.T. by the Ministerio de Educación of the Spanish Government. The company *Central Geological Mining Enterprise* is thanked for providing samples and maps of the Cuban deposits. The help and hospitality extended by the staff at Cerro de Maimón mine are also gratefully acknowledged, as well as the technical support in EMP sessions by Dr. X. Llovet. The authors would like to thank Prof. David Huston for the valuable comments and suggestions to improve the quality of the manuscript.

References

Almodóvar, G.R., Sáez, R., Pons, J.M., Maestre, A., Toscano, M., Pascual, E., 1998. Geology and genesis of the Aznalcollar massive sulfide deposits, Iberian Pyrite Belt, Spain. Miner. Deposita 33, 111-136.

Andreu, E., Torró, L., Proenza, J.A., Domenech, C., García-Casco, A., Villanova de Benavent, C., Chavez, C., Espaillat, J., Lewis, J.F., 2015. Weathering profile of the Cerro de Maimón VMS deposit (Dominican Republic): textures, mineralogy, gossan evolution and mobility of gold and silver. Ore Geol. Rev. 65, 165-179.

Astacio, V.A., Lewis, J.F., Campbell, A., Espaillat, J., 2000. Oxygen isotope and alteration geochemistry of the Cerro de Maimón deposit, Dominican Republic, in: Jackson, T. (Ed.), Caribbean geology in the new millenium, transactions 15th Caribbean geological conference, Kingston, Jamaica.

Augustithis, S.S., 1995. Atlas of the Textural Patterns of Ore Minerals and Metallogenic Processes. W. de Gruyter, New York.

Barrie, C.D., Boyle, A.P., Cook, N.J., Prior, D.J., 2010. Pyrite deformation textures in the massive sulfide ore deposits of the Norwegian Caledonides. Tectonophysics 483, 269-286.

Berkenbosch, H.A., de Ronde, C.E.J., Gemmell, J.B., McNeill, A.W., Goemann, K., 2012. Mineralogy and formation of Black Smoker Chimneys from Brothers Submarine Volcano, Kermadec Arc. Econ. Geol. 107, 1613-1633.

Bethke, P.M. and Barton, P.B., 1971. Distribution of some Minor Elements between Coexisting Sulfide Minerals. Econ. Geol. 66, 140-163.

Blein, O., Guillot, S., Lapierre, H., Mercier de Lépinay, B., Lardeaux, J.M., Millán Trujillo, G., Campos, M., García, A., 2002. Geochemistry of the Mabujina Complex, central Cuba: implications on the Cuban Cretaceous Arc rocks. J. Geol. 111, 89-101.

Boschman, L.M., van Hinsbergen, D.J.J., Torsvik, T.H., Spakman, W., Pindell, J.L., 2014. Kinematic reconstruction of the Caribbean region since the Early Jurassic. Earth-Sci. Rev. 138, 102-136.

Bowin, C.O., 1966. Geology of the central Dominican Republic. Geol. Soc. Am. Mem. 98, 11-84.

Browne, P.R.L. and Lovering, J.F. (1973). Composition of sphalerites from the Broadlands Geothermal Field and their significance to sphalerite geothermometry and geobarometry. Econ. Geol. 68, 381-387.

Brueckner, S.M., Piercey, S.J., Layne, G.D., Piercey, G., Sylvester, J., 2015. Variations of sulphur isotope signatures in sulphides from the metamorphosed Ming Cu(−Au) volcanogenic massive sulphide deposit, Newfoundland Appalachians, Canada. Miner. Deposita 50, 619-640.

Cabrera, R., 1986. Geología y regularidades de la distribución de los yacimientos de cobre y oro de la región mineral de las Villas. Instituto de Geología y Paleontología, ACC, Havana.

Çagatay, M.N. and Eastoe, C.J., 1995. A sulfur isotope study of volcanogenic massive sulfide deposits of the Eastern Black Sea province, Turkey. Miner. Deposita 30, 55-66.

Canet, C., Camprubí, T., González-Partida, E., Linares, C., Alfonso, P., Piñeiro-Fernández, F., Prol-Ledesma, R.M., 2009. Mineral Assemblages of the Francisco I. Madero Zn-Cu-Pb-(Ag) deposit, Zacatecas, México: Implications for ore deposit genesis. Ore. Geol. Rev. 35, 423-435.

Childe, F., 2000. Volcanogenic massive sulphide mineralization in the Greater Antilles, in: Sherlock, R., Barsch, R., Logan, A. (Eds.), VMS deposits of Latin America. Geol. Soc. Can. Spec. Publ. 2, 183-196.

Claypool, G.E., Holser, W.T., Kaplan, I.R., Sakai, H., Zak, I., 1980. The age curves of sulfur and oxygen isotopes in marine sulfate and their mutual interpretation. Chem. Geol. 28, 199-260.

Cook, N.J., Halls, C., Boyle, A.P., 1993. Deformation and metamorphism of massive sulphides at Sulitjelma, Norway. Mineral. Mag. 57, 67-81.

Cook, N.J., Ciobanu, C.L., Pring, A., Skinner, W., Shimizu, M., Danyushevsky, L., Saini-Eidukat, B., Melcher, F., 2009. Trace and minor elements in sphalerite: a LA-ICPMS study. Geochim. Cosmochim. Ac. 73, 4761-4791.

Craig, J.R., 2001. Ore-mineral textures and the tales they tell, Can. Mineral. 39, 937-956.

Currie, C.A. and Hyndman, R.D., 2006. The thermal structure of subduction zone back arcs. J. Geophys. Res. 111, B08404.

de Ronde, C.E.J., Massoth, G.J., Butterfield, D.A., Christenson, B.W., Ishibashi, J., Ditchburn, R.G., Hannington, M.D., Braithwaite, R.L., Lupton, J.E., Dziak, R.P., Kamenetsky, V.S., Graham, I.J., Zellmer, G.F., 2011. Submarine hydrothermal activity and gold-rich mineralization at Brothers Volcano, Kermade Arc, New Zealand. Miner. Deposita 46, 541-584.

Deschamps, F., Guillot, S., Godard, M., Chauvel, C., Andreani, M., Hattori, K., 2010. In situ characterization of serpentinites from forearc mantle wedges: timing of serpentinization and behavior of fluid-mobile elements in subduction zones. Chem. Geol. 269, 262-277.

Deschamps, F., Guillot, S., Godard, M., Andreani, M., Hattori, K., 2011. Serpentinites act as sponges for fluid-mobile elements in abyssal and subduction zone environments. Terra Nova 23, 171-178.

Díaz de Villalvilla, L., Pérez, M., Sukar, K., Marí, T., Méndez, I., Rodríguez, R., Piñeiro, E., et al., 1994. Consideraciones geoquímicas acerca de los arcos volcánicos de Cuba. Resúmenes del Segundo Congreso Cubano de Geología y Minería 173-174.

Díaz de Villalvilla, L., Milia-González, I., Santa Cruz Pacheco, M., Aguirre, G., 2003. Formación Los Pasos: Geología, Geoquímica y su comparación con el Caribe, in: Estudios sobre los

Arcos Volcánicos de Cuba, Centro Nacional de Información Geológica, Instituto de Geología y Paleontología de Cuba, Havana.

Donnelly, T.W. and Rogers, J.W., 1980. Igneous series I island arcs: the northeastern Caribbean compared with worldwide island arc assemblages. B. Volcanol. 43, 347-382.

Doyle, M.G. and Allen, R.L., 2003. Subsea-floor replacement in volcanic-hosted massive sulfide deposits. Ore Geol. Rev. 23, 183-222.

Draper, G., Gutiérrez, G., Lewis, J.F., 1996. Thrust emplacement of the Hispaniola peridotite belt: orogenic expression of the mid Cretaceous Caribbean arc polarity reversal? Geology 24, 1143-1146.

Economou-Eliopoulos, M., Eliopoulos, D.G., Chryssoulis, S., 2008. A comparison of high-Au massive sulfide ores hosted in ophiolite complexes of the Balkan Peninsula with modern analogues: Genetic significance. Ore Geol. Rev. 33, 81-100.

Edmon, J.M., Campbell, A.C., Palmer, M.R., German, C.R., Klinkhammer, G.P., Edmonds, H.N., Elderfield, H., Thompson, G., Rona, P., 1995. Time-series studies of vent fluids from the TAG and MARK sites (1986, 1990) Mid-Atlantic Ridge: a new solution chemistry model and a mechanism for Cu/Zn zonation, in: massive sulfide ore bodies, in: Pearson, L.M., Walker, C.L., Dixon, D.R. (Eds.), Hydrothermal vents and processes. Geol. Soc. Spec. Publ. 87, London, pp. 77-86.

Eldridge, C.W., Barton, P.B., Ohmoto, H., 1983. Mineral textures and their bearing on formation of the Kuroko orebodies. Econ. Geol. Monograph 5, 241-281.

Escuder-Viruete, J., Díaz de Neira, A., Hernaiz Huerta, P.P., Monthel, J., García-Senz, J., Joubert, M., Lopera, E., Ullrich, T., Friedman, R., Mortensen, J., Pérez-Estaún, A., 2006. Magmatic relationships and ages of Caribbean island-arc tholeiites, boninites and related felsic rocks, Dominican Republic. Lithos 90, 161-186.

Escuder-Viruete, J., Contreras, F., Joubert, M., Urien, P., Stein, G., Weis, D., Pérez-Estaún, A., 2007a. Tectónica y geoquímica de la Formación Amina: registro del arco isla Caribeño primitivo en la Cordillera Central, República Dominicana. Bol. Geol. Min. 118, 221-242.

Escuder-Viruete, J., Contreras, F., Stein, G., Urien, P., Joubert, M., Pérez-Estaún, A., Friedman, R., Ullrich, T., 2007b. Magmatic relationships between adakites, magnesian andesites and Nb-

enriched basalt-andesites from Hispaniola: Record of a major change in the Caribbean island arc magma sources. Lithos 99, 151-177.

Escuder-Viruete, J., Pérez-Estaún, A., Weis, D., Friedman, R., 2009. Geochemical characteristics of the Río Verde Complex, Central Hispaniola: Implications for the paleotectonic reconstruction of the Lower Cretaceous Caribbean island-arc. Lithos 114, 168-185.

Escuder-Viruete, J., Castillo Carrión, M., and Pérez-Estaún, A., 2014. Magmatic relationships between depleted mantle harzburgites, boninitic cumulate gabros and subduction-related tholeiitic basalts in the Puerto Plata ophiolitic complex, Dominican Republic: Implications for the birth of the Caribbean island-arc. Lithos 196-197, 261-280.

Finlow-Bates, T. and Stumpfl, E.F., 1981. The behavior of so-called immobile elements in hydrothermally altered rocks associated with volcanogenic submarine-exhalative ore deposits. Miner. Deposita 16, 319-328.

Fouquet, Y., Stackelberg, U., Charlou, J.L., Erzinger, J., Herzig, P.M., Mühe, R., Wiedicke, M., 1993. Metallogenesis in Back-Arc Environments: The Lau Basin Example. Econ. Geol. 88, 2154-2181.

Franklin, J.M., Gibson, H.L., Jonasson, I.R., Galley, A.G., 2005. Volcanogenic Massive Sulfide Deposits, in: Hedenquist, J.W., Thompson, J.F.H., Goldfarb, R.J., Richards, J.P. (Eds.), Economic Geology 100th anniversary volume, 1905-2005. Littleton, pp. 523-560.

Freyssinet, Ph., Butt, C.R.M., Morris, R.C., 2005. Ore-forming processes related to lateritic weathering. Econ. Geol. 100th Anniversary Vol. 681-722.

Gallardo-Eupierre, E., 2001. Mineralización de sulfuros masivos en la Formación Los Pasos de Cuba Central. Empresa Geominera Centro, Cuba.

Galley, A.G. Hannington, M.D., Jonasson, I.R., 2007. Volcanogenic Massive Sulphide Deposits, in Goodfellow, W.D. (Ed.), Mineral Deposits of Canada: A Synthesis of Major Deposit-Types, District Metallogeny, the Evolution of Geological Provinces, and Exploration Methods. Geological Association of Canada, Mineral Deposits Division, Special Publication 5, 141-161.

García-Casco, A., Torres-Roldán, R.L., Iturralde-Vinent, M., Millán, G., Nuñez Cambra, K., Lázaro, C., Rodríguez Vega, A., 2006. High-pressure metamorphism of ophiolites in Cuba. Geol. Acta 4, 63-88.

García-Casco, A., Iturralde-Vinent, M.A., Pindell, J., 2008. Latest Cretaceous collision/accretion between the Caribbean plate and Caribeana: origin of metamorphic terranes in the Greater Antilles. Int. Geol. Rev. 50, 781-809.

García-Delgado, D.E., Pérez Pérez, C., Delgado Damas, R., Díaz Otero, C., Millán, G., Furrazola, G., Díaz de Villalvilla, L., García Cadiz, I., Sukar, K., Delgado Carballo, I., Bernal, L., Pardo, M., Rojas Agramonte, Y., Suárez Leyva, V., Duani Duarte, E., 1998. Mapa geológico de Cuba Central (provincias Cienfuegos, Villa Clara y Sancti Spiritus). Scale 1:100000. Instituto de Geología y Paleontología de Cuba, La Habana.

George, L., Cook, N.J., Ciobanu, C.L., Wade, B.P., 2015. Trace and minor elements in galena: A reconnaissance LA-ICP-MS study. Am. Mineral. 100, 548-569.

Gilgen, S.A., Diamond, L.W., Mercolli, I., Al-Tobi, K., Maidment, D.W., Close, R., Al-Towaya, A., 2014. Volcanostratigraphic Controls on the Occurrence of Massive Sulfide Deposits in the Semail Ophiolite, Oman. Econ. Geol. 109, 1585-1610.

Gilligan, L.B. and Marshall, B., 1987. Textural evidences for remobilization in metamorphic environments. Ore Geol. Rev. 2, 205-229.

Glasby, G.P., Iizasa, K., Hannington, M., Kubota, H., Notsu, K., 2008. Mineralogy and composition of Kuroko deposits from the northeastern Hohsu and their possible modern analogues from the Izu-Ogasawara (Bonin) Arc south of Japan: Implications for mode of formation. Ore Geol. Rev. 34, 547-560.

Govindaraju, K., 1994. Compilation of working values and sample description for 383 geostandards. Geostand. Geoanal. Res. 18, 1-158.

Haase, K.M., Worthington, T.J., Stoffers, P., Garbe-Schönberg., 2002. Mantle dynamics, element recycling, and magma genesis beneath the Kermadec Arc-Havre Trough. Geochem. Geophy. Geosy. 3, 1071-1093.

Hannington, M.D. and Scott, S.D., 1989. Sulfidation Equilibria as Guides to Gold Mineralization in Volcanogenic Sulfides: Evidence from Sulfide Mineralogy and the Composition of Sphalerite. Econ. Geol. 84, 1978-1995.

Hannington, M.D., Galley, A.G., Herzig, P.M., Petersen, S., 1998. Comparison of the TAG mound and stockwork complex with Cyprus-type massive sulfide deposits, in: Herzig, P.M.,

Humphris, S.E., Miller, D.J., Zierenberg, R.A. (Eds.), Proceedings of the Ocean Drilling Program, Scientific Results, 158, College Station, Texas, pp. 389-415.

Hannington, M.D., Bleeker, W., Kjarsgaard, I., 1999a. Sulfide Mineralogy, Geochemistry, and Ore Genesis of the Kidd Creek Deposit: Part II. The Bornite Zone. Econ. Geol. Monograph 10, 225-266.

Hannington, M.D., Poulsen, K.H., Thompson, J.F.H., Sillitoe, R.H., 1999b. Volcanogenic gold in massive sulfide environment. Rev. Econ. Geol. 8, 325-356.

Hart, T., Gibson, H.L., Lesher, C.M., 2004. Trace element geochemistry and petrogenesis of felsic volcanic rocks associated with volcanogenic Cu-Zn-Pb massive sulphide deposits. Econ. Geol. 99, 1003-1013.

Hawkesworth, C.J., Gallagher, K., Hergt, J.M., McDermott, F., 1993. Mantle and slab contributions in arc magmas. Annu. Rev. Earth Pl. Sc. 21, 175-204.

Herrington, R., Maslennikov, V., Zaykov, V., Seravkin, I., Kosarev, A., Buschmann, B., Orgeval, J.J., Holland, N., Tesalina, S., Nimis, P., Armstrong, R., 2005. 6: Classification of VMS deposits: Lessons from the Uralides. Ore Geol. Rev. 27, 203-237.

Herzig, P.M., 1988. A mineralogical, geochemical and thermal profile trough the Agrokipia "B" hydrothermal sulfide deposit, Troodos Ophiolite Complex, Cyprus, in: Friedrich, G.H. and Herzig, P.M. (Eds.), Base Metal sulfide deposits. Springer-Verlag, Berlin, pp. 182-215.

Herzig, P.M. and Hannington, M.D., 1995. Polymetallic massive sulfides at the modern seafloor: a review. Ore Geol. Rev. 10, 95-115.

Herzig P.M., Hannington, MD., Fouquet, Y., Von Stackelberg, U., Petersen, S., 1993. Gold-rich polymetallic sulfides from the Lay Back Arc and implications for the geochemistry of golg in sea-floor hydrothermal system of the Southwest Pacific. Econ. Geol. 88, 2182-2209.

Herzig, P.M., Petersen, S., Hannington, M.D., 1998. Geochemistry and sulfur isotopic composition of the TAG hydrothermal mound, Mid-Atlantic Ridge, 26°N. Proc. Ocean Drill Program Sci. Results 158, 47-68.

Hoefs, J., 2009. Stable isotope geochemistry, 6th edition. Springer, Heidelberg.

Hollis, S.P., Roberts, S., Earls, G., Herrington, R., Cooper, M.R., Piercey, S.J., Archibald, S.M., Moloney, M., 2014. Petrochemistry and hydrothermal alteration within the Tyrone Igneous

Complex, Northern Ireland: implications for VMS mineralization in the British and Irish Caledonides. Miner. Deposita 49, 575-593.

Horan, S.L., 1995. The geochemistry and tectonic significance of the Maimón-Amina schist's, Cordillera Central, Dominican Republic. Unpublished M.S. thesis, University of Florida, Gainesville, 172 pp.

Huston, D.L. and Large, R.R., 1989. A chemical model for the concentration of gold in volcanogenic massive sulphide deposits. Ore Geol. Rev. 4, 171-200.

Huston, D.L., Bottrill, R.S., Creelman, R.A., Zaw, K., Ramsden, T.R., Rand, S.W., Gemmell, J.B., Jablonski, W., Sie, S.H., Large, R.R., 1992. Geologic and geochemical controls on the mineralogy and grain size of gold-bearing phases, eastern Australian volcanic-hosted massive sulfide deposits. Econ. Geol. 87, 542-563.

Huston, D.L., Sie, S.H., Suter, G.F., Cooke, D.R., Both, R.A., 1995. Trace Elements in Sulfide Minerals from Eastern Australian Volcanic-Hosted Massive Sulfide Deposits: Part I. Proton Microprobe Analyses of Pyrite, Chalcopyrite, and Sphalerite, and Part II. Selenium Levels in Pyrite: Comparison with $\delta^{34}S$ Values and Implications for the Source of Sulfur in Volcanogenic Hydrothermal System. Econ. Geol. 90, 1167-1196.

Ishizuka, O., Tani, K., Reagan, M.K., Kanayama, K., Umino, S., Harigane, Y., Sakamoto, I., Miyajima, Y., Yuasa, M., and Dunkley, D.J., 2011. The timescales of subduction initiation and subsequent evolution of an oceanic island arc. Earth Planet. Sc. Lett. 306, 229-240.

Ishizuka, O., Tani, K., Reagan, M.K., 2014a. Izu-Bonin-Mariana Forearc Crust as a Modern Ophiolite Analogue. Elements 10, 115-120.

Ishizuka, O., Umino, S., Taylor, R.N., Kanayama, K., 2014b. Evidence for hydrothermal activity in the earliest stages of intraoceanic arc formation: implications for ophiolite-hosted hydrothermal activity. Econ. Geol. 109, 2159-2177.

Iturralde-Vinent, M.A., 1998. Sinopsis de la constitución Geológica de Cuba, in: Melgarejo J.C. and Proenza, J.A. (Eds.), Geología y Metalogénia de Cuba: Una Introducción. Acta Geologica Hispanica 33, 9-56.

Jochum, K.P. and Verma, S.P., 1996. Extreme enrichement of Sb, Tl and other trace elements in altered MORB. Chem. Geol. 130, 289-299.

Jochum, K.P. and Hofmann, A.W., 1997. Constraints on earth evolution from antimony in mantle-derived rocks. Chem. Geol. 139, 39-49.

Jolly, W.T., Lidiak, E.G., Dickin, A.P., Wu, T.W., 2001. Secular Geochemistry of Central Puerto Rican Island Arc Lavas: Constraints on Mesozoic Tectonism in the Eastern Greater Antiles. J. Petrol. 42, 2197-2214.

Keith, M., Haase, K.M., Schwarz-Schampera, U., Klemd, R., Petersen, S., Bach, W., 2014. Effect of temperature, sulfur and oxygen fugacity on the composition of sphalerite from submarine hydrothermal vents. Geology 42, 699-702.

Kerr, A.C., Iturralde-Vinent, M.A., Saunders, A.D., Babbs, T.L., Tarney, J., 1999. New plate tectonic model of the Caribbean: Implications from a geochemical reconnaissance of Cuban Mesozoic volcanic rocks. Geol. Soc. Am. Bull. 111, 1581-1599.

Kesler., S.E., Levy, E., Martín C., 1990. Metallogenic evolution of the Caribbean region, in: Dengo, G. and Case J.E. (Eds.), The Caribbean Region. The Geology of North America. Geological Society of America, Vol. H, 77-140.

Kesler, S., Russell, E.N., Reyes, C., Santos, L., Rodriguez, A., Fondeur, L., 1991. Geology of the Maimon Formation, Dominican Republic, in: Mann, P., Draper, G., Lewis, J.F. (Eds.), Geologic and tectonic development of the North America-Caribbean plate boundary in Hispaniola. Geol. S. Am. S. 262, 173-185.

Kesler, S.E., Campbell, I.H., Allen, C.M., 2005. Age of the Los Ranchos Formation, Dominican Republic: Timing and tectonic setting of primitive island arc volcanism in the Caribbean region. Geol. Soc. Am. Bulletin 117, 987-995.

Kessel, R., Schmidt, M.W., Ulmer, P., Pettke, T., 2005. Trace element signature of subduction-zone fluids, melts and supercritical liquids at 120-180 km depth. Nature 437, 724-727.

Kojima, S. and Sugaki, A., 1985. Phase relations in the Cu-fe-Zn-S system between 500ºC and 300ºC under hydrothermal conditions. Econ. Geol. 80, 158-171.

König, S., Luguet, A., Lorand, J.P., Wombacher, F., Lissner, M., 2012. Selenium and tellurium systematics of the Earth's mantle from high precision analyses of ultra-depleted orogenic peridotites. Geochim. Cosmochim. Ac. 86, 354-366.

Kretschmar, U. and Scott, S.D., 1976. Phase relations involving arsenopyrite in the system Fe-As-S and their application. Can. Mineral. 14, 364-386.

Langmuir, C.H., Bender, J.F., Bence, A.E., Hanson, G.N., Taylor, S.R., 1977. Petrogenesis of basalts from the FAMOUS area: mid-Atlantic ridge. Earth Planet. Sc. Lett. 36, 133-156.

Large, R.R., Gemmell, J.B., Paulick, H., Huston, D.L., 2001. The Alteration Box Plot: A Simple Approach to Understanding the Relationship between Alteration Mineralogy and Lithogeochemistry Associated with Volcanic-Hosted Massive Sulfide Deposits. Econ. Geol. 96, 957-971.

Larocque, A.C.L., Hodgson, C.J., Lafleur, P.J., 1993. Gold distribution in the Mobrun volcanic-associated massive sulfide deposit, Noranda, Quebec: a preliminary evaluation of the role of metamorphic remobilization. Econ. Geol. 88, 1443-1459.

Larocque, A.C.L., Hodgson, C.J., Cabri, L.J., Jackman, J.A., 1995. Ion-microprobe analysis of pyrite, chalcopyrite and pyrrhotite from the Mobrun VMS deposit in the Northwestern Quebec: evidence for metamorphic remobilization of gold. Can. Mineral. 33, 373-388.

Lesher, C.M., Gibson, H.L., Campbell, I.H., 1986. Composition-volume changes during hydrothermal alteration of andesite at Buttercup Hill, Noranda district, Quebec. Geochim. Cosmochim. Acta 50, 2693-2705.

Lewis, J.F. and Draper, G., 1990. Geology and tectonic evolution of the Northern Caribbean margin, in: Dengo, G., Case, J.E. (Eds.), The Caribbean region. Boulder, Colorado, Geol. Soc. Am., The Geology of North America H, 77-140.

Lewis, J.F., Astacio, V.A., Espaillat, J., Jiménez, J., 2000. The occurrence of volcanogenic massive sulfide deposits in the Maimón Formation, Dominican Republic: The Cerro de Maimón, Loma Pesada and Loma Barbuito deposits, in: Sherlock, R., Barsch, R., Logan, A. (Eds.), VMS deposits of Latin America. Geol. Soc. Can. Spec. Publ. 2, 213-239.

Lewis, J.F., Escuder Viruete, J., Hernaiz Huerta, P.P., Gutiérrez, G., Draper, G., 2002. Subdivisión geoquímica del arco de isla Circum-Caribeño, Cordillera Central Dominicana: implicaciones para la formación, acreción y crecimiento cortical en un ambiente intraoceánico. Acta Geologica Hispanica 37, 81-122.

Lewis, J.F., Draper, G., Proenza, J.A., Espaillat, J., Jiménez, J., 2006. Ophiolite-Related Ultramafic Rocks (Serpentinites) in the Caribbean Region: A Review of the Occurrence, Composition, Origin, Emplacement and Ni-Laterite Soil Formation. Geol. Acta 4, 237-263.

Lockington, J.A., Cook, N.J., Ciobanu, C.L., 2014. Trace and minor elements in sphalerite from metamorphosed sulfide deposits. Miner. Petrol. 108, 873-890.

Lydon, J.W., 1988. Volcanogenic massive sulfide deposits, Part 2: Genetic models. Geoscience Canada reprints Series 3, 155-182.

Mann, P., Draper, G., Lewis, J.F., 1991. An overview of the geologic and tectonic development of Española, in: Mann, P., Draper, G., Lewis, J.F. (Eds.), Geologic and Tectonic Development of the North-America-Caribbean Plate Boundary in Española. Geol. Soc. Am. Spec. Spec. Paper 262, 1-28.

Marshall, B. andGilligan, L.B., 1987. An introduction to remobilization: information from ore body geometry and experimental considerations. Ore Geol. Rev. 2, 87-131.

Marshall, B. and Gilligan, L.B., 1993. Remobilization, syn-tectonic processes and massive sulfide deposits. Ore Geol. Rev. 8, 39-64.

Marshall, B. and Spry, P.G., 2000. Discriminating between regional metamorphic remobilization and syntectonic emplacement in the genesis of massive sulfide ores, in: Spry, P.G., Marshall, B., Vokes, F.M. (Eds.), Metamorphosed and metamorphic ore deposits: Rev. Econ. Geol. 11, 39-79.

Marshall, B., Vokes, F.M., Larocque, A.C.L., 2000. Regional metamorphic remobilization: Upgrading and formation of ore deposits, in: Spry, P.G., Marshall, B., Vokes, F.M. (Eds.), Metamorphosed and metamorphic ore deposits. Rev. Econ. Geol. 11, 19-38.

Martín, M. and Draper, G., 1999. Mapa geológico de la hoja 6172-I (Hatillo) a escala 1:50 000 (SYSMIN, Proyecto C). Consorcio ITGE-PROINTEC-INYPSA. Dirección General de Minería, Santo Domingo.

McClay, K.R. and Ellis, P.G., 1983. Deformation and recrystallization of pyrite. Mineral. Mag. 47, 527-538.

McDonough, W.F. and Sun S.S., 1995. The composition of earth. Chem. Geol. 120, 223-253.

Meschede, M., 1986. A method of discriminating between different groups of mid-ocean ridge basalts and continental tholeiites with Nb-Zr-Y diagram. Chem. Geol. 56, 207-218.

Millán, G., 1996. Geología del complejo de Mabujina, in: Iturralde-Vinent, M.A. (Ed.), Ofiolitas y Arcos Volcánicos de Cuba. Miami, USA, IGCP Project 364 Special Contribution 1, 147-153.

Misra, K.C., 2000. Understanding Mineral Deposits. Kluwer Academic Publishers, Dordrecht.

Mishra, B. and Mookherjee, A., 1988. Geothermometry based on fractionation of Mn and Cd between coexisting sphalerite and galena from some carbonate-hosted sulfide deposits in India. Miner. Deposita 23, 179-185.

Nelson, C.E., Proenza, J.A., Lewis, J.F., López-Kramer, J., 2011. The metalogenic evolution of the Greater Antilles. Geol. Acta 9, 229-264.

Nelson, C.E., Stein, H.J., Dominguez, H., Carrasco, C., Barrie, T., Torró, L., Proenza J., 2015. Re-Os dating of molybdenite from the Pueblo Viejo (Au-Ag-Cu-Zn) and Douvray Cu-Au districts. Econ. Geol. 110, 1101-1110.

Noll, P.D., Newsom, H.E., Leeman, W.P., Ryan, J.G., 1996. The role of hydrothermal fluids in the production of subduction zone magmas: Evidence from siderophile and chalcophile trace elements and boron. Geochim. Cosmochim. Ac. 60, 587-611.

Ohmoto, H., 1986. Stable isotope geochemistry of ore deposits. Rev. Mineral. Geochem. 16, 491-559.

Ohmoto, H., and Goldhaber, M.B., 1997. Sulfur and carbon isotopes, in: Barnes, H.L. (Ed.), Geochemistry of hydrothermal ore deposits, 3rd edition. John Wiley and Sons, New York, pp. 517–611.

Pearce, J.A., 1996. A user's guide to basalt discrimination diagrams. Geological Association of Canada Special Publication 12, 79-113.

Pearce, J.A., 2008. Geochemical fingerprinting of oceanic basalts with applications to ophiolite classification and the search for Archaean oceanic crust. Lithos 100, 14-48.

Pearce, J.A., 2014. Immobile elements fingerprinting of ophiolites. Elements 10, 101-108.

Pearce, J.A. and Peate, D.W., 1995. Tectonic implications of the composition of volcanic arc magmas. Annu. Rev. Earth Pl. Sc. 23, 251-285.

Pearce, J.A., Harris, N.B.W., Tindle, A.G., 1984. Trace element discrimination diagrams for the tectonic interpretation of granitic rocks. J. Petrol. 25, 956-983.

Pearce, J.A., van der Laan, S.R., Arculus, R.J., Murton, B.J., Ishii, T., Peate, D.W., Parkinson, I.J., 1992. Boninite and harzburgite from Leg 125 (Bonin-Mariana forearc); a case study of magma genesis during the initial stages of subduction. Proceedings Ocean Drill Program Scientific Results 125, 623-659.

Pesquera, A. and Velasco, F., 1993. Ore metamorphism in sulfide mineralizations from the Cinco Villas massif (Western Pyrenees, Spain). Econ. Geol. 88, 266-282.

Petersen, S., 1992. Mineralogie und Geochemie goldführender Massivsulfide des Lau Back.Arc (Südwest-Pazifik). M.Sc. thesis, Aachen University of Technology, Aachen, 92pp.

Piercey, S.J., 2007. An overview of the use of petrochemistry in regional exploration for volcanogenic massive sulfide (VMS) deposits, in: Milkereit, B. (Ed.), Proceedings of exploration 07, Fifth Decennial International Conference on Mineral Exploration, 223-246.

Piercey, S.J., 2011. The setting, style, and role of magmatism in the formation of volcanogenic massive sulfide deposits. Miner. Deposita 46, 449-471.

Pindell, J.L., Maresch, W.V., Martens, U., Stanek, K.P., 2012. The Greater Antillean Arc: Early Cretaceous origin and proposed relationship to Central American subduction mélanges: Implications for models of Caribbean evolution. Int. Geol. Rev. 54, 131-143.

Pisutha-Arnond, V. and Ohmoto, H., 1983. Thermal history and chemical and isotopic compositions of the ore-forming fluids responsible for the Kuroko massive sulfide deposits in the Hokuroku District of Japan, in: Ohmoto, H., and Skinner, B.J. (Eds.), The Kuroko and related volcanogenic massive sulfide deposits. Econ. Geol. Monograph 5, 523-558.

Plank, T., 2005. Constraints from thorium/lanthanum on sediment recycling at subduction zones and the evolution of the continents. J. Petrol. 46, 921-944.

Poulsen, K.H. and Hannington, M.D., 1995. Volcanic-associated massive sulfide gold, in: Eckstrand, R.O., Sinclair, W.D., Thorpe, R.I. (Eds.), Geology of Canadian mineral deposit types. Geological Survey of Canada, Geology of Canada 8, 183-196.

Proenza, J.A. and Melgarejo, J.C., 1998. Una introducción a la metalogenia de Cuba bajo la perspectiva de la tectónica de placas. Acta Geologica Hispánica 33, 89-131.

Proenza, J.A., Díaz Martínez, R., Iriondo, A., Marchesi, C., Melgarejo, J.C., Gervilla, F., Garrido, C.J., Rodríguez-Vega, A., Lozano Santacruz, R., Blanco-Moreno, J.A., 2006. Primitive Cretaceous island-arc volcanic rocks in eastern Cuba: the Téneme Formation. Geol. Acta 4, 103-121.

Proenza, J.A., Zaccarini, F., Lewis, J.F., Longo, F., Garuti, G., 2007. Chromian spinel composition and the platinum-group minerals of the PGE-rich Loma Peguera chromitites, Loma Caribe peridotite, Dominican Republic. Can. Mineral. 45, 631-648.

Ramdohr, P., 1980. The ore minerals and their intergrowths, second ed. Pergamon Press, New York.

Reagan, M.K., Ishizuka, O., Tsukuaba, H., Stern, R.J., Kelley, K.A., Ohara, Y., Blichert-Toft, J., Bloomer, S.H., Cash, J., Fryer, P., Hanan, B.B., Hickey Vargas, R., Ishii, T., Kimura, J.I., Peate, D.W., Rowe, M.C., Woods, M., 2010. Forearc basalts and subduction initiation in the Izu-Bonin-Mariana system. Geochem. Geophy. Geosy. 11, doi: 10.1029/2009GC002871.

Rojas-Agramonte, Y., Neubauer, F., Bojar, A.V., Hejl, E., Handler, R., García-Delgado, D.E., 2006. Geology, age and tectonic evolution of the Sierra Maestra Mountains, southeastern Cuba. Geol. Acta 4, 123-150.

Rojas-Agramonte, Y., Neubauer, F., Garcia-Delgado, D.E., Handler, R., Friedl, G., Delgado-Damas, R., 2008. Tectonic evolution of the Sierra Maestra Mountains, SE Cuba, during Tertiary times: From arc-continent collision to transform motion. J. S. Am. Earth Sci. 26, 125-151.

Rojas-Agramonte, Y., Kröner, A., García-Casco, A., Somin, M., Iturralde-Vinent, M.A., Mattinson, J.M., Millán Trujillo, G., Sukar, K., Pérez Rodríguez, M., Carrasquilla, S., Wingate, M.T.D., Liu, D.Y., 2011. Timing and Evolution of Cretaceous Island Arc Magmatism in Central Cuba: Implications for the History of Arc System in the Northwestern Caribbean. J. Geol. 119, 619-640.

Russell, N., Moreira, J., Sánchez, R., 2002. Volcanogenic massive sulfide deposits of Cuba. , in: Sherlock, R., Barsch, R., Logan, A. (Eds.), VMS deposits of Latin America. Geol. Soc. Can. Spec. Publ. 2, 241-258.

Sack, R.O., Kuehner, S.M., Hardy, L.S., 2002. Retrograde Ag-enrichment in fahlores from the Coeur d'Alene mining district, Idaho, USA. Mineral. Mag. 66, 215-229.

Sack, R.O., Lynch, J.V.G., Foit, F., 2003. Fahlore as petrogenetic indicator: Keno Hill Ag-Pb-Zn District, Yukon, Canada. Mineral. Mag. 67, 1023-1038.

Sales, R.H. and Meyer, C., 1951. Effect of post-ore dike intrusion on Butte ore minerals. Econ. Geol. 46, 813-820.

Sangster, D.F., 1971. Sulphur isotopes, stratabound sulphide deposits, and ancient seas. Soc. Mining Geol. Japan. Spec. Issue Proc. IMA-IAGOD Meeting'70 3, 295-299.

Sangster, D.F., 1976. Sulphur and lead isotopes in strata-bound deposits, in: Wolf. K.H. (Ed.), Handbook of strata-bound and stratiform ore deposits vol. 2. Elsevier, Amsterdam, pp. 219-266.

Schulz, K.J., 2012. Regional environment in volcanogenic massive sulfide occurrence model, in: Shanks III, W.C. and Thurston, R. (Eds.), Volcanogenic massive sulfide occurrence model, U.S. Geological Survey Scientific Investigation Report 2010-5070-C, Reston, pp. 5-8.

Scott, S.D., 1973. Experimental calibration of the sphalerite geobarometer. Econ. Geol. 68, 466-474.

Scott, S.D., 1976. Application of sphalerite geobarometer to regionally metamorphosed terrains. Am. Mineral. 61, 661-670.

Scott, S.D., 1983. Chemical behaviour of sphalerite and arsenopyrite in hydrothermal and metamorphic environments. Mineral. Mag. 47, 427-435.

Scott, S.D. and Barnes, H.L., 1971. Sphalerite geothermometry and geobarometry. Econ. Geol. 66, 653-669.

Seal II, R.R. and Piatak, N., 2012. Geoenvironmental features in volcanogenic massive sulfide occurrence model, in: Shanks III, W.C. and Thurston, R. (Eds.), Volcanogenic massive sulfide occurrence model, U.S. Geological Survey Scientific Investigation Report 2010-5070-C, Reston, pp. 319-339.

Shanks III, W.C.P. and Koski, R.A., 2012. Introduction to Volcanogenic massive sulfide occurrence model, in: Shanks III, W.C. and Thurston, R. (Eds.), Volcanogenic massive sulfide

occurrence model, U.S. Geological Survey Scientific Investigation Report 2010-5070-C, Reston, pp. 5-8.

Shanks III, W.C., Bischoff, J.L., Rosenbauer, R.J., 1981. Seawater sulfate reduction and sulfur isotope fractionation in basaltic systems: interaction of seawater with fayalite and magnetite at 200–350°C. Geochim. Cosmochim. Ac. 45, 1977-1995.

Shanks III, W.C., Böhlke, J.K., Seal II, R.R., 1995. Stable isotopes in midocean ridge hydrothermal systems: interaction between fluids, minerals and organisms, in: Humphris, S.E., Zierenberg, R.A., Mullineaux, L.S., Thomson, R.E. (Eds.), Seafloor hydrothermal systems: physical, chemical, biological, and geological interactions. Geophys. Mon. 91, American Geophysical Union, Washington, DC, pp. 194-221.

Sharman, E.R., Taylor, B.E., Minarik, W.G., Dubé, B., Wing, B.A., 2015. Sulfur isotope and trace element data from ore sulfides in the Noranda district (Abitibi, Canada): implications for volcanogenic massive sulfide deposit genesis. Miner. Deposita DOI 10.1007/s00126-014-0559-7.

Shervais, J.W., 1982. Ti-V plots and the petrogenesis of modern and ophiolitic lavas. Earth Planet. Sc. Lett. 59, 101-118.

Singer, D.A., 1986. Descriptive model of Cyprus massive sulfide, in: Cox, D.P. and Singer, D.A. (Eds.), Mineral deposit models. U.S. Geological Survey Bulletin 1693, pp. 131-132.

Solomon, M., Eastoe, C.J., Walshe, J.L., Green, G.R., 1988. Mineral deposits and sulfur isotope abundances in the Mount Read volcanics between Que River and Mount Darwin, Tasmania. Econ. Geol. 83, 1307-1328.

Solomon, M., Gemmell, J.B., Zaw, K., 2004. Nature and origin of the fluids responsible for forming the Hellyer Zn–Pb–Cu, volcanic-hosted massive sulphide deposit, Tasmania, using fluid inclusions, and stable and radiogenic isotopes. Ore. Geol. Rev. 25, 89-124.

Stanton, R.L., 1990. Magmatic evolution and the ore type-lava type affiliations of volcanic-exhalative ores, in: Hughes, F.E. (Ed.), Geology of the mineral deposits of Australia and Papua New Guinea. Aus. I. M. M. Bull. 14, 101-108.

Stern, R.A., 2004. Subduction initiation: spontaneous and induced. Earth Planet. Sc. Lett. 226, 275-292.

Stern, R.A. and Bloomer, S.H., 1992. Subduction zone infancy; examples from Eocene Izu-Bonin-Mariana and Jurassic California arcs. Geol. Soc. Am. Bull. 104, 1621-1636.

Sun, S.S. and McDonough, W.F., 1989. Chemical and isotopic systematics of oceanic basalts: implication for mantle composition and processes, in: Saunder, A.D. and Norry, M.J. (Eds.), Magmatism in the ocean basin. Geol. Soc. Sp. 42, 313-345.

Tesfaye Firdu, F. and Taskinen, P., 2010. Sulfide mineralogy-Literature review. Aalto University Publications in Material Science and Engineering, Helsinki.

Timm, C., De Ronde, C.E.J., Leybourne, M.I., Layton-Matthews, D., Graham, I.J., 2012. Sources of Chalcophile and Siderophile Elements in Kermadec Arc Lavas. Econ. Geol. 107, 1527-1538.

Tolkunov, A.E., Malinovski, E.P., Cabrera, R., Carassou, G., 1974. Características comparativas de los yacimientos de cobre de Cuba, in: Geología de los yacimientos minerales útiles de Cuba, A.C.C., Havana, pp. 7-61.

Tornos, F., 2006. Environment of formation and styles of volcanogenic massive sulfides: The Iberian Pyrite Belt. Ore Geol. Rev. 28, 259-307.

Torres-Zafra, J.L., 2013. Perspectivas para metales base y preciosos en el arco volcánico cretácico de Cuba central. Anuario de la Sociedad Cubana de Geología 1, 65-76.

Torró, L., León, P., Proenza, J.A., Farré de Pablo, J., Melgarejo, J.C., Reyes, E., Chávez, C., Lewis, J.F., 2014. Mineralogy of the Doña Amanda prospect, Bayaguana, Dom. Rep.: a transitional epithermal-porphyry deposit in Los Ranchos Formation? Macla, 19 (in press).

Torró, L., Proenza, J.A., García-Casco, A., Farré de Pablo, J., del Carpio, R., León, P., Chávez, C., Domínguez, H., Brower, S., Espaillat, J., Nelson, C.E., Lewis, J.F., 2015. La geoquímica de la Formación Maimón (Cordillera Central, República Dominicana) revisada. Boletín Geológico y Minero (in press).

Toulmin, P. and Barton, P.B., 1964. A thermodynamic study of pyrite and pyrrothite. Geochim. Comochim. Ac. 49, 2221-2237.

Trout, P. and Chavez, C., 2013. Perilya limited: successful mining and exploration in the Dominican Republic. Proceedings of the X CONGRESO CUBANO DE GEOLOGÍA, Sociedad Cubana de Geologia, Havana, GE04-07.

Velasco, F., 2014. El Oro Asociado a los Sulfuros Masivos de la Faja Pirítica Ibérica. Macla 19 (in press).

Velasco, F., Sánchez-España, J., Boyce, A.J., Fallick, A.E., Sáez, R., Almodóvar, G.R., 1998. A new sulfur isotopic study of some Iberian Pyrite Belt deposits: evidence of a textural control on sulphur isotope composition. Miner. Deposita 34, 4-18.

Vokes, F.M., 1969. A review of metamorphism of sulphide deposits. Earth Sci. Rev. 6, 99-143.

Watkins, J., 1990. Geologic Setting of the Cerro de Maimón Deposit, Dominican Republic. Geologic report for Falconbridge Dominicana, Santo Domingo, 43 pp.

Winchester, J.A. and Floyd, P.A., 1977. Geochemical discrimination of different magma series and their differentiation products using immobile elements. Chem. Geol. 20, 325-343.

Yesares, L., Sáez, R., Nieto, J.M., Ruiz de Almodóvar, G., Cooper, S., 2014. Supergene enrichment of precious metals by natural amalgamation in the Las Cruces weathering profile (Iberian Pyrite Belt, SW Spain). Ore Geol. Rev. 58, 14-26.

Zheng, B., Zhu, Y., An, F., Huang, Q., Qiu, T., 2015. As-Sb-Bi-Au mineralization in the Baogutu gold deposit, Xinjiang, NW Xina. Ore Geol. Rev. 69, 17-32.

FIGURE CAPTIONS

Figure 1: (A) Geographic location of the PIA series (green) and ophiolitic peridotites (black) of the Greater Antilles. (B) Location map of the VMS deposits and occurrences in the Maimón Formation; geological map of the Maimón Formation and surrounding units modified from Martín and Draper (1999). (C) Location map of the VMS deposits and occurrences in the Los Pasos Formation; geological map modified from Gallardo-Eupierre (2001).

Figure 2: Detailed cross sections of (A) the Cerro de Maimón, (B) San Fernando and (C) Antonio ore bodies and their host formations.

Figure 3: (A) Alteration (major-element mobility) box plot (Large et al., 2001) for analyzed volcanic rocks from the Maimón and Los Pasos Formations. Least altered box: BA, basaltic andesite; BAS, basalt; DAC, dacite; RHY, rhyolite. Arrows show six common trends during hydrothermal alteration. Alteration mineralogy: carb, carbonate; chl, chlorite; kfeld, K-feldspar; py, pyrite; ser, sericite. (B) Zr/Ti vs. Nb/Y classification diagram (Pearce, 1996 after Winchester and Floyd, 1977) for mafic and felsic volcanic rocks from the Maimón and Los Pasos Formations.

Figure 4: Geochemical diagrams for basaltic rocks from the Maimón Formation including compositional fields from other complexes/sources for comparison. (A) Tectonic discrimination Nb-Zr-Y diagram after Meschede (1986). (B) Ti-V diagram (Shervais, 1982) including field nomenclatures as recommended by Pearce (2014). (C-F) Chondrite-normalized extended REE diagrams for the different basalt types described in the main text; normalization values are after McDonough and Sun (1995); NMORB values are from Sun and McDonough (1989) with the exception of V (average value of MORB from the FAMOUS area, Langmuir et al., 1977). Geochemical data of samples from the Los Pasos Formation include analyses of Díaz de Villalvilla et al. (2003). IBM: Izu-Bonin-Marianas.

Figure 5: Geochemical diagrams for rhyodacitic rocks from the Maimón and Los Pasos Formations including compositional fields from other complexes/sources for comparison. (A) Chondrite-normalized extended REE diagram; normalization values are after McDonough and Sun (1995). (B) Nb-Y tectonic discrimination diagram for granites of Pearce et al. (1984); prospective fields are after Piercey (2007). (C) La/Yb_{CN} vs. Yb_{CN} discrimination diagram of Hart et al. (2004); chondrite normalization values are after McDonough and Sun (1995). (D) Zr/Y vs. Y discrimination diagram of Lesher et al. (1986). Geochemical data of samples from the Los Pasos Formation include analyses of Díaz de Villalvilla et al. (2003) and Kerr et al. (1999).

Figure 6: Ore mineralogy of Cerro de Maimón massive sulfide lens. (A) Paragenetic sequence deduced for ores in the massive sulfide body; width of bars approximates the abundance of minerals; the bright gray rectangle indicates lack of primary textures due to total obliteration by metamorphism. (B) Feather-shaped quartz in pressure shadow adjacent to pyrite porphyroclast; transmitted light, crossed polars image [CM-299-318.30]. (C) Partially welded anhedral to subhedral pyrite crystals enveloped in a matrix of gangue, chalcopyrite, sphalerite and minor tetrahedrite; polarized reflected light image [CM-306-228.50]. (D) Individual fine- to medium-grained anhedral pyrite crystals enveloped in a matrix of abundant chalcopyrite and subordinate sphalerite and tetrahedrite; polarized reflected light image [CM-322-260.22]. (E) Equilibrium textures in composed sulfide inclusion within pyrite; polarized reflected light image [CM-353-214.50]. (F) Cataclastic textures and microfracturing with blow-apart structures in pyrite; polarized reflected light image [CM-307-150.00]. (G) Rotational fabric in a big pyrite crystal wrapped by muscovite; polarized reflected light image [CM-299-318.30]. (H) Welded pyrite crystal aggregates with frequent foam or annealing textures; polarized reflected light image [CM-286-195.15]. (I) Hessite infillings (in voids) and sphalerite and galena mineral inclusions within pyrite; SEM-BSE image [CM-322-260.22]. (J) Hessite grains concentrated along the margins of a tennantite crystal; SEM-BSE image [CM-330-270.55]. (K) Bornite replacement by flame-like aggregates of covellite-chalcocite; polarized reflected light image [CM-370-8.10]. Abbr.: qtz: quartz; ser: sericite; py: pyrite; cpy: chalcopyrite; sph: sphalerite; tn: tennantite; gn: galena; bn: bornite; hess: hessite; cv: covellite; cc: chalcocite.

Figure 7: Mineralogy of the San Fernando sulfide deposits. (A) Paragenetic sequence in the stockwork, stratabound and stratiform mineralization types; width of bars approximates the abundance of minerals and discontinuous lines indicate rare occurrence of mineral formation. (B-K) Photomicrographs with polarized reflected light (B-C) and SEM-BSE (D-K). (B) Recrystallized massive pyrite from the stratiform mineralization showing strongly indented grains in a chalcopyrite-gangue matrix; note the subtle preservation of spongy texture in the core of some pyrite crystals with zoned overgrowth [SF97-25-107]. (C) Pyrite and minor sphalerite vein cuts a massive mineralization of pyrite [SF97-22-134]. (D) Grain boundaries at 120º among chalcopyrite, sphalerite and tennantite that contrast with irregular outlines of galena; minute hessite grains occur along sphalerite-chalcopyrite contacts [SF97-127-10]. (E) Annealing texture in a tennantite, hessite and electrum inclusion within sphalerite [SF97-127-10]. (F) Symplectic replacement of tennantite; note the triple junctions at 120º between the tennantite, pyrite and chalcopyrite crystals [SF97-133-8]. (G) Detail of symplectic replacement of tennantite by sphalerite, chalcopyrite, löllingite and matildite [SF97-133-8]. (H) Replacement of pyrite by chalcopyrite and tornebohmite [SF97-125-4].

(I) Interstitial mineralization of sphalerite, arsenopyrite (partially recrystallized to löllingite), tetrahedrite and electrum within chalcopyrite [SF97-133-8]. (J) (Ag,Hg) amalgam as replacement of acanthite along a late vein cutting a chalcopyrite-pyrite assemblage [SF97-133-8]. (K) Replacement of sphalerite by an assemblage of zinalsite and armenite [SF97-127-10] Abbr.: qtz: quartz; chl: chlorite; py: pyrite; cpy: chalcopyrite; sph: sphalerite; tn: tennantite; td: tetrahedrite; gn: galena; hess: hessite; el: electrum; bt: biotite; mat: matildite; lö: löllingite; torn: tornebohmite; aspy: arsenopyrite; acan: acanthite; zls: zinalsite; armn: armenite.

Figure 8: Mineralogy of the Antonio sulfide deposit. (A) Paragenetic sequence in the stockwork, stratabound and stratiform mineralization types; width of bars approximates the abundance of minerals and discontinuous lines indicate rare occurrences of mineral formation. (B-E) Polarized reflected light and (F-G) SEM-BSE images. (B) Remnant of framboidal-spheroidal overgrowth of pyrite with microcrystallite textures [AM-11]. (C) Extensive spongy texture in pyrite [AM-294]. (D) Coarser-grained pyrite preserving relict of zoned overgrowths with largely inclusion free rims and subtle spongy cores; chalcopyrite is often concentrated along growth faces in pyrite [AM-264]. (E) Sphalerite and subordinate chalcopyrite in the matrix of zoned pyrite largely with spongy cores and porosity-free overgrowths [AM-285]. (F) Barite vein crosscuts pyrite containing inclusions of sphalerite [AM-286]. (G) Altaite and kochkarite partially or totally infill micro-voids in pyrite [AM-4]. Abbr.: py: pyrite; cpy: chalcopyrite; sph: sphalerite; bar: barite; alt: altaite; Koch: kochkarite

Figure 9: Mineral chemistry of ores from the Cerro de Maimón, San Fernando and Antonio deposits. (A) Fe (wt. %) vs. Zn (wt. %) in sphalerite; note the tight negative correlation between Fe and Zn. (B) Fe (wt. %) vs. Cu (wt. %) in sphalerite diagram as tool for discriminating non-primary Cu enrichment. (C) S (wt. %) vs. Fe/Zn in sphalerite; discriminant fields (sediment-covered and sediment-starved) are after Keith et al. (2014). (D) Sb(Sb+As) vs. Ag/(Ag+Zn+Cu+Fe) in tetrahedrite group minerals(fahlores). Abbr.: stock: stockwork; stb: stratabound; str: stratiform; u: upper; i: intermediate; l: lower.

Figure 10: Histogram of $\delta^{34}S$ values of sulfides from the Cerro de Maimón (Dominican Republic), San Fernando and Antonio (Cuba) VMS deposits. Abbr.: Cpy: chalcopyrite; Sph: sphalerite; Py: pyrite.

Figure 11: (A) Th/Yb vs. Nb/Yb plots (modified from Pearce and Peate, 1995) for basaltic rocks from the Maimón and Los Pasos Formations including the mantle array from depleted to enriched sources. DM: depleted mantle; NMORB: normal MORB; E-MORB: evolved MORB; OIB: oceanic island basalts. (B) La-Yb plot for basaltic rocks from the Maimón and Los Pasos Formations; La-Yb abundances in modern island arc basalts are from compilation by Jolly et al. (2001).

Figure 12: Schematic diagram showing the tectonic and magmatic environment for the VMS-forming hydrothermal activity within the framework of the birth of the Caribbean island-arc (after Escuder-Viruete et al., 2014). (A) Initiation of W-dipping subsidence of the Proto-Caribbean plate and high-degree decompression-driven partial melting of a depleted mantle generating FAB magmas. Extension is general in the over-riding plate and facilitated the hydrothermal activity for the formation of VMS deposits in the Maimón Formation; however, capping by FAB of VMS bodies was not observed. (B) The depleted mantle is fluxed with fluids from the downgoing oceanic crust and melts at shallow levels generating boninitic and LOTI magmas. Continued extensional regime in the over-riding plate caused by slab rollback and trench migration promoted the circulation of hydrothermal fluids that led the formation of VMS deposits hosted in the Maimón and Los Pasos Formation. (A, B) Hydrothermal activity would have taken place in a terrigenous sediment-poor deep-sea environment. (C) Once the magmatic front stabilizes, upwelling of fertile mantle in presence of slab-derived fluids in the supra-subduction zone triggers the generation of normal IAT magmas. Note that the VMS from the Maimón Formation are represented at deeper levels in the boninitic-LOTI sequence than those hosted in the Los Pasos Formation as a representation of formation in a slightly more primitive setting.

Table 1: Chemical composition and structural formulas of selected sulfides from the Cerro de Maimón, San Fernando and Antonio deposits (electron-microprobe data).

wt. %			S	Fe	Cu	Zn	As	Se	Ag	Cd	Sb	Te	Au	Hg	Pb	Bi	Sum
		d.l.	0.01	0.02	0.03	0.03	0.05	0.05	0.02	0.08	0.05	0.06	0.06	0.15	0.07	0.11	
Sph	C M	Str.	34.27	6.02	0.15	60.22	d.l.	n.a.	n.a.	0.35	n.a.	n.a.	d.l.	n.a.	0.21	n.a.	101.22
Sph	C M	Str.	32.35	1.54	1.16	64.21	d.l.	d.l.	d.l.	0.49	0.14	d.l.	d.l.	n.a.	0.10	d.l.	100.09
Sph	C M	Str.	31.39	0.05	0.03	66.26	n.a.	n.a.	n.a.	0.49	n.a.	n.a.	n.a.	n.a.	0.24	n.a.	98.48
Sph	SF	Sbd.	32.14	1.38	d.l.	65.27	d.l.	d.l.	d.l.	0.32	d.l.	d.l.	d.l.	0.38	d.l.	d.l.	99.53
Sph	SF	L. Str.	32.80	2.44	d.l.	63.84	d.l.	d.l.	d.l.	0.46	d.l.	0.08	d.l.	0.44	d.l.	d.l.	100.17
Sph	SF	I. Str.	33.19	3.89	n.a.	62.31	d.l.	n.a.	0.04	0.49	n.a.	n.a.	n.a.	d.l.	n.a.	n.a.	99.92
Sph	SF	U. Str.	32.42	4.10	d.l.	61.82	d.l.	0.08	d.l.	0.44	d.l.	d.l.	d.l.	0.35	d.l.	d.l.	99.25
Sph	A	Stck.	32.83	1.23	0.38	64.37	d.l.	d.l.	d.l.	0.11	0.07	d.l.	d.l.	0.37	0.07	d.l.	99.47
Sph	A	L. Str.	32.36	1.65	0.08	64.01	d.l.	d.l.	0.02	d.l.	d.l.	d.l.	d.l.	0.42	d.l.	d.l.	98.64
Sph	A	U. Str.	32.06	0.66	d.l.	66.16	d.l.	d.l.	0.02	0.12	d.l.	d.l.	d.l.	0.48	d.l.	d.l.	99.64
Tn	C M	Str.	27.19	0.19	44.28	7.97	16.09	d.l.	0.08	0.19	d.l.	3.85	d.l.	n.a.	0.20	d.l.	100.04
Tn	C M	Str.	27.56	0.34	43.26	8.07	17.76	d.l.	0.12	0.23	d.l.	1.48	0.29	n.a.	d.l.	d.l.	99.17
Tn	SF	Sbd.	27.28	3.39	41.51	4.34	16.34	n.a.	0.60	n.a.	5.94	n.a.	n.a.	0.19	0.08	0.11	99.78
Tn	SF	I. Str.	26.92	6.60	36.90	1.52	18.90	n.a.	8.22	n.a.	1.96	n.a.	n.a.	0.17	d.l.	0.44	101.63
Tn	SF	U. Str.	27.28	5.37	42.05	2.49	17.97	n.a.	0.86	n.a.	3.83	n.a.	n.a.	d.l.	0.10	0.57	100.58
Tn	A	Stck.	25.96	3.33	37.33	4.97	10.78	0.14	4.37	d.l.	11.88	d.l.	d.l.	0.47	d.l.	d.l.	99.38
Tn	A	L. Str.	27.12	3.52	40.80	6.66	19.13	0.15	d.l.	d.l.	0.36	d.l.	d.l.	0.28	0.07	d.l.	98.11
Tn	A	U. Str.	27.78	4.77	41.06	5.45	19.76	n.a.	d.l.	n.a.	1.03	n.a.	n.a.	d.l.	d.l.	0.39	100.26
Td	SF	I. Str.	22.83	4.83	24.99	2.05	2.87	n.a.	19.55	n.a.	22.79	n.a.	n.a.	d.l.	d.l.	1.42	101.34
Td	SF	U. Str.	25.17	4.06	37.08	4.30	4.42	n.a.	4.34	n.a.	20.40	n.a.	n.a.	d.l.	d.l.	0.51	100.28
Gn	C M	Str.	13.08	d.l.	0.09	0.11	d.l.	0.64	0.16	0.23	d.l.	0.09	0.22	n.a.	85.29	d.l.	100.04
Gn	SF	U. Str.	10.78	0.03	0.05	d.l.	d.l.	0.22	0.43	d.l.	0.11	0.43	d.l.	d.l.	84.57	0.71	97.35
Aspy	SF	I. Str.	14.02	31.42	n.a.	n.a.	54.32	n.a.	n.a.	n.a.	n.a.	n.a.	n.a.	n.a.	n.a.	n.a.	99.82
Elec.	SF	I. Str.	n.a.	0.68	1.05	n.a.	n.a.	n.a.	43.30	n.a.	n.a.	n.a.	56.40	0.57	n.a.	n.a.	102.00
atom %			**S**	**Fe**	**Cu**	**Zn**	**As**	**Se**	**Ag**	**Cd**	**Sb**	**Te**	**Au**	**Hg**	**Pb**	**Bi**	
Sph	C M	Str.	50.80	5.12	0.11	43.77	-	-	-	0.15	-	-	-	-	0.05	-	
Sph	C	Str.	49.3	1.35	0.89	48.0	-	-	-	0.2	0.06	-	-	-	0.02	-	

	M		6			4				1						
	C		48.9			50.6				0.2						
Sph	M	Str.	6	0.04	0.02	8	-	-	-	2	-	-	-	-	0.06	-
			49.3			49.1				0.1				0.0		
Sph	SF	Sbd.	7	1.22	-	6	-	-	-	4	-	-	-	9	-	-
			49.8			47.6				0.2		0.0		0.1		
Sph	SF	L. Str.	9	2.13	-	2	-	-	-	0	-	3	-	1	-	-
			50.1			46.2				0.2						
Sph	SF	I. Str.	9	3.38	-	0	-	-	0.02	1	-	-	-	-	-	-
		U.	49.6			46.4		0.0		0.1				0.0		
Sph	SF	Str.	4	3.60	-	2	-	5	-	9	-	-	-	9	-	-
			50.1			48.2				0.0				0.0		
Sph	A	Stck.	8	1.08	0.30	4	-	-	-	5	0.03	-	-	9	0.02	-
			49.9			48.4								0.1		
Sph	A	L. Str.	1	1.46	0.07	1	-	-	0.01	-	-	-	-	0	-	-
		U.	49.3			49.8				0.0				0.1		
Sph	A	Str.	0	0.58	-	9	-	-	0.01	5	-	-	-	2	-	-
	C		44.2		36.3		11.1			0.0		1.5				
Tn	M	Str.	0	0.18	2	6.35	9	-	0.04	9	-	7	-	-	0.05	-
	C		44.6		35.3		12.3			0.1		0.6				
Tn	M	Str.	7	0.32	8	6.41	2	-	0.06	1	-	0	0.08	-	-	-
			44.6		34.2		11.4							0.0		0.0
Tn	SF	Sbd.	5	3.19	8	3.48	5	-	0.29	-	2.56	-	-	5	0.02	3
			43.9		30.4		13.2							0.0		0.1
Tn	SF	I. Str.	7	6.19	2	1.22	1	-	3.99	-	0.84	-	-	4	-	1
		U.	44.0		34.2		12.4									0.1
Tn	SF	Str.	9	4.98	9	1.97	3	-	0.41	-	1.63	-	-	-	0.03	4
			44.5		32.2			0.1						0.1		
Tn	A	Stck.	0	3.28	9	4.18	7.91	0	2.23	-	5.36	-	-	3	-	-
			44.1		33.5		13.3	0.1						0.0		
Tn	A	L. Str.	7	3.29	3	5.32	3	0	-	-	0.16	-	-	7	0.02	-
		U.	44.3		33.0		13.4									0.1
Tn	A	Str.	1	4.37	4	4.26	9	-	-	-	0.43	-	-	-	-	0
			43.5		24.0				11.0		11.4					0.4
Td	SF	I. Str.	0	5.28	3	1.92	2.34	-	7	-	4	-	-	-	-	2
		U.	44.1		32.8											0.1
Td	SF	Str.	9	4.09	5	3.70	3.32	-	2.27	-	9.43	-	-	-	-	4
	C		48.6					0.9		0.2		0.0			49.1	
Gn	M	Str.	6	-	0.17	0.20	-	7	0.18	4	-	8	0.13	-	0	-
		U.	44.2					0.3				0.4			53.6	0.4
Gn	SF	Str.	1	0.08	0.11	-	-	6	0.53	-	0.11	5	-	-	7	5
Asp			25.3	32.6			42.0									
y	SF	I. Str.	3	0	-	-	1	-	-	-	-	-	-	-	-	-
Elec									55.8				39.8	0.4		
.	SF	I. Str.	-	1.69	2.30	-	-	-	1	-	-	-	1	0	-	-

d.l.: detection limit; n.a.: not analyzed; Sph: sphalerite; Tn: tennantite; Td: tetrahedrite; Gn: galena; Aspy: arsenopyrite; Elec: electrum; CM: Cerro de Maimón; SF: San Fernando; A: Antonio; Str: stratiform; Sbd: stratabound; Stck: stockwork; U: upper; I: Intermediate; L: Lower

Table 2: Summary of element concentrations in sphalerite, tennantite and tetrahedrite from the Cerro de Maimón, San Fernando and Antonio deposits (electron-microprobe data).

wt. %				S	Fe	Cu	Zn	As	Se	Ag	Cd	Sb	Te	Au	Hg	Pb	Bi
Sphalerite	Cerro Maimón	Stratiform	MIN	30.81	d.l.	d.l.	60.22	d.l.	d.l.	d.l.	0.23	d.l.	d.l.	d.l.	d.l.	d.l.	d.l.
			MA	34.27	6.02		67.06		0.07		0.93		0.09			0.27	0.36
		n=48	X			1.16		0.09		0.21		0.28		d.l.	d.l.		
			Av	32.27	1.16	0.21	64.89	0.01	0.01	0.03	0.41	0.08	0.03	-	-	0.10	0.09
	San Fernando	Stratabound	MIN	31.40	0.75	d.l.	62.87	d.l.	d.l.	d.l.	0.13	d.l.	d.l.	d.l.	d.l.	d.l.	d.l.
			MA	32.22	3.01		65.27		0.07		0.55		0.09		0.85	0.16	
		n=17	X			0.14		d.l.		0.07		0.08		d.l.			d.l.
			Av	31.83	1.69	0.02	64.29	-	0.01	0.01	0.33	0.02	0.02	-	0.28	0.03	-
		Lower stratiform	MIN	31.34	1.28	d.l.	62.93	d.l.	d.l.	d.l.	0.24	d.l.	d.l.	d.l.	d.l.	d.l.	d.l.
			MA	32.80	3.17		65.19		0.10		0.59		0.09		0.60	0.17	0.13
		n=13	X			0.12		d.l.		d.l.		0.09		d.l.			
			Av	31.98	2.06	0.02	64.18	-	0.02	-	0.38	0.03	0.03	-	0.35	0.07	0.01
		Intermediate stratiform	MIN	31.70	2.13	d.l.	61.25	d.l.	d.l.	d.l.	0.33	d.l.	d.l.	d.l.	d.l.	d.l.	d.l.
			MA	33.19	3.89		64.32		0.10		0.52				0.40	0.12	
		n=7	X			0.92		d.l.		0.04		d.l.	d.l.	d.l.			d.l.
			Av	32.43	2.99	0.24	62.88	-	0.04	0.01	0.42	-	-	-	0.24	0.05	-
		Upper stratiform	MIN	31.07	4.10	d.l.	58.30	d.l.	d.l.	d.l.	0.36	d.l.	d.l.	d.l.	0.17	d.l.	d.l.
			MA	32.42	5.86		61.82		0.10		0.90		0.16		0.54	0.20	0.09
		n=12	X			0.81		0.06		0.06		0.10		d.l.			
			Av	31.60	4.94	0.20	59.76	0.01	0.04	0.01	0.70	0.02	0.03	-	0.36	0.06	0.02
	Antonio	Stockwork	MIN	31.84	0.35	0.05	63.42	d.l.	d.l.	d.l.	d.l.	d.l.	d.l.	d.l.	d.l.	d.l.	d.l.
			MA	32.83	1.70		66.70		0.06		0.22				0.46		
		n=7	X			0.38		d.l.		d.l.		0.07	d.l.	d.l.		d.l.	d.l.
			Av	32.25	1.12	0.17	64.87	-	0.04	-	0.14	0.02	-	-	0.20	-	-
		Lower stratiform	MIN	32.01	1.44	0.08	63.64	d.l.	d.l.	d.l.	d.l.	d.l.	d.l.	d.l.	0.40	d.l.	d.l.
			MA	32.36	1.65		64.01		0.06		0.05				0.42		
		n=2	X			0.12		d.l.		d.l.		d.l.	d.l.	d.l.		d.l.	d.l.
			Av	32.19	1.55	0.10	63.83	-	0.03	-	0.03	-	-	-	0.41	-	-
		Upper stratiform	MIN	32.01	0.46	d.l.	60.62	d.l.	d.l.	d.l.	d.l.	d.l.	d.l.	d.l.	0.11	d.l.	d.l.
			MA	33.35	3.83		66.21		0.06		0.23		0.05		0.48	0.05	0.13
		n=6	X			d.l.		d.l.		0.06		0.05	d.l.	d.l.			
			Av	32.54	1.47	-	64.27	-	0.02	0.03	0.12	0.01	-	-	0.25	0.00	0.05
Tennantite	Cerro Maimón	Stratiform	MIN	26.06	0.19	40.58	6.55	16.09	d.l.	d.l.	d.l.	d.l.	0.57	d.l.	d.l.	d.l.	d.l.
			MA	28.27	1.86	44.63	8.91	18.50	d.l.	3.48	0.33	2.92	3.96	0.46	d.l.	2.92	d.l.
		n=25	X														
			Av	27.25	0.94	42.65	7.68	17.49	-	0.27	0.19	0.62	1.73	0.09	-	0.60	-

				26.9	3.2	41.0		16.3								
		Stratabound	MIN	9	4	6	4.34	4	d.l.	0.59	d.l.	5.94	d.l.	d.l.	d.l.	d.l.	d.l.
			MA	27.2	3.4	41.9		17.0							0.1	0.0	0.2
		n=4	X	8	1	1	4.60	8	d.l.	0.74	d.l.	6.13	d.l.	d.l.	9	8	0
				27.1	3.3	41.4		16.7							0.0	0.0	0.1
			Av	8	5	5	4.46	6	-	0.64	-	6.07	-	-	6	5	1
				26.5	6.1	34.9		17.8									0.4
			MIN	1	3	0	1.24	1	d.l.	8.08	d.l.	1.86	d.l.	d.l.	d.l.	d.l.	1
		Intermediate	MA	27.5	7.9	38.1		18.9							0.1	0.0	0.9
		stratiform	X	0	6	9	1.57	0	d.l.	9.85	d.l.	2.54	d.l.	d.l.	7	9	8
				26.9	6.7	36.9		18.5							0.0	0.0	0.5
	San Fernando	n=5	Av	6	5	5	1.43	2	-	8.68	-	2.08	-	-	4	2	5
		Upper		27.2	4.5	42.0		17.8									0.0
		stratiform	MIN	4	0	4	2.21	4	d.l.	0.67	d.l.	3.55	d.l.	d.l.	d.l.	d.l.	9
			MA	27.9	5.6	43.5		18.2							0.1	0.3	0.7
		n=13	X	2	6	5	3.29	5	d.l.	1.08	d.l.	3.89	d.l.	d.l.	9	0	3
				27.6	5.2	42.4		18.0							0.0	0.1	0.4
			Av	1	5	8	2.81	1	-	0.85	-	3.76	-	-	7	1	3
				25.3	1.4	35.3			0.1								
		Stockwork	MIN	6	0	4	4.31	9.16	0	d.l.	d.l.	0.49	d.l.	d.l.	d.l.	d.l.	d.l.
			MA	30.1	6.3	43.2		20.4	0.2			14.3			0.4	0.1	0.2
		n=19	X	7	8	6	8.83	6	3	5.60	d.l.	1	d.l.	d.l.	7	7	5
				27.4	3.1	41.0		17.2	0.1						0.1	0.0	0.0
			Av	4	9	0	6.01	8	4	0.96	-	3.34	-	-	6	4	9
		Lower		27.1	2.3	40.7		18.3	0.0								
		stratiform	MIN	1	8	1	4.96	0	9	d.l.	d.l.	0.22	d.l.	d.l.	d.l.	d.l.	d.l.
			MA	28.2	5.2	42.3		19.7	0.1						0.6	0.2	0.3
		n=4	X	0	9	6	7.17	9	8	0.13	d.l.	3.11	d.l.	d.l.	1	7	9
				27.3	3.6	40.7		18.6	0.1						0.4	0.0	0.0
			Av	3	6	9	6.52	4	5	0.01	-	0.37	-	-	3	4	2
		Upper		27.4	2.3	40.9		18.3									0.1
		stratiform	MIN	1	8	7	4.96	0	d.l.	d.l.	d.l.	0.98	d.l.	d.l.	d.l.	d.l.	2
			MA	28.2	5.2	42.3		19.7							0.2	0.2	0.3
		n=9	X	0	9	6	7.17	9	d.l.	0.13	d.l.	3.11	d.l.	d.l.	5	7	9
				27.7	3.7	41.6		19.1							0.0	0.0	0.2
			Av	2	7	4	6.09	1	-	0.04	-	1.93	-	-	8	8	8
				22.0	4.4	23.1				18.2		22.0					0.6
			MIN	2	4	8	1.88	0.92	d.l.	0	d.l.	5	d.l.	d.l.	d.l.	d.l.	8
		Intermediate	MA	22.8	5.1	25.8				20.2		26.3			0.0	0.1	2.0
		stratiform	X	6	7	6	6.27	3.74	d.l.	3	d.l.	6	d.l.	d.l.	9	6	0
				22.5	4.8	24.5				19.5		23.8			0.0	0.0	1.3
Tetrahedrite	San Fernando	n=9	Av	5	7	7	2.62	2.19	-	4	-	6	-	-	2	6	4
		Upper		24.6	3.6	35.4						20.4					0.2
		stratiform	MIN	9	6	2	4.30	3.07	d.l.	4.34	d.l.	0	d.l.	d.l.	d.l.	d.l.	6
			MA	25.1	4.0	37.0						24.9				0.0	0.5
		n=3	X	7	6	8	4.69	4.42	d.l.	5.31	d.l.	4	d.l.	d.l.	d.l.	7	1
				24.9	3.9	36.3						22.4				0.0	0.3
			Av	4	1	2	4.48	3.86	-	4.83	-	1	-	-	-	4	7

d.l.: detection limit.

Table 3: Sulfur isotope compositions in sulfides from the Cerro de Maimón, San Fernando and Antonio VMS deposits.

Deposit	**Mineral**	**$\delta^{34}S$ (‰)**
Cerro de Maimón	Pyrite	-1.3, -0.3, -0.2, 0.0, 0.1, 0.4, 0.4, 0.4, 0.4, 0.4, 0.5, 0.8, 0.9, 1.0, 1.1, 1.6, 1.7, 1.8, 2.0, 2.8, 3.0
	Chalcopyrite	-0.7, -0.6, 0.4, 0.4, 0.6, 1.5
	Sphalerite	1.5
San Fernando	Pyrite	-0.5, 0.9, 2.5, 2.6, 2.6, 2.6, 2.6, 2.6, 2.7, 2.9, 3.0, 3.1, 3.5, 3.7, 4.0, 4.2, 4.4, 4.6, 4.8, 5.2, 5.7, 7.0
	Chalcopyrite	0.3, 0.4, 0.5, 1.6, 1.7, 1.8, 1.8, 2.0, 2.1, 2.2, 2.6, 2.7, 3.1
	Sphalerite	1.7, 1.9
Antonio	Pyrite	0.0, 0.7, 0.8, 0.9, 1.3, 1.5, 1.5, 1.6, 1.8, 2.2, 2.3, 2.4, 2.5, 2.7, 3.6, 3.8, 3.9, 4.9, 5.8
	Chalcopyrite	5.7

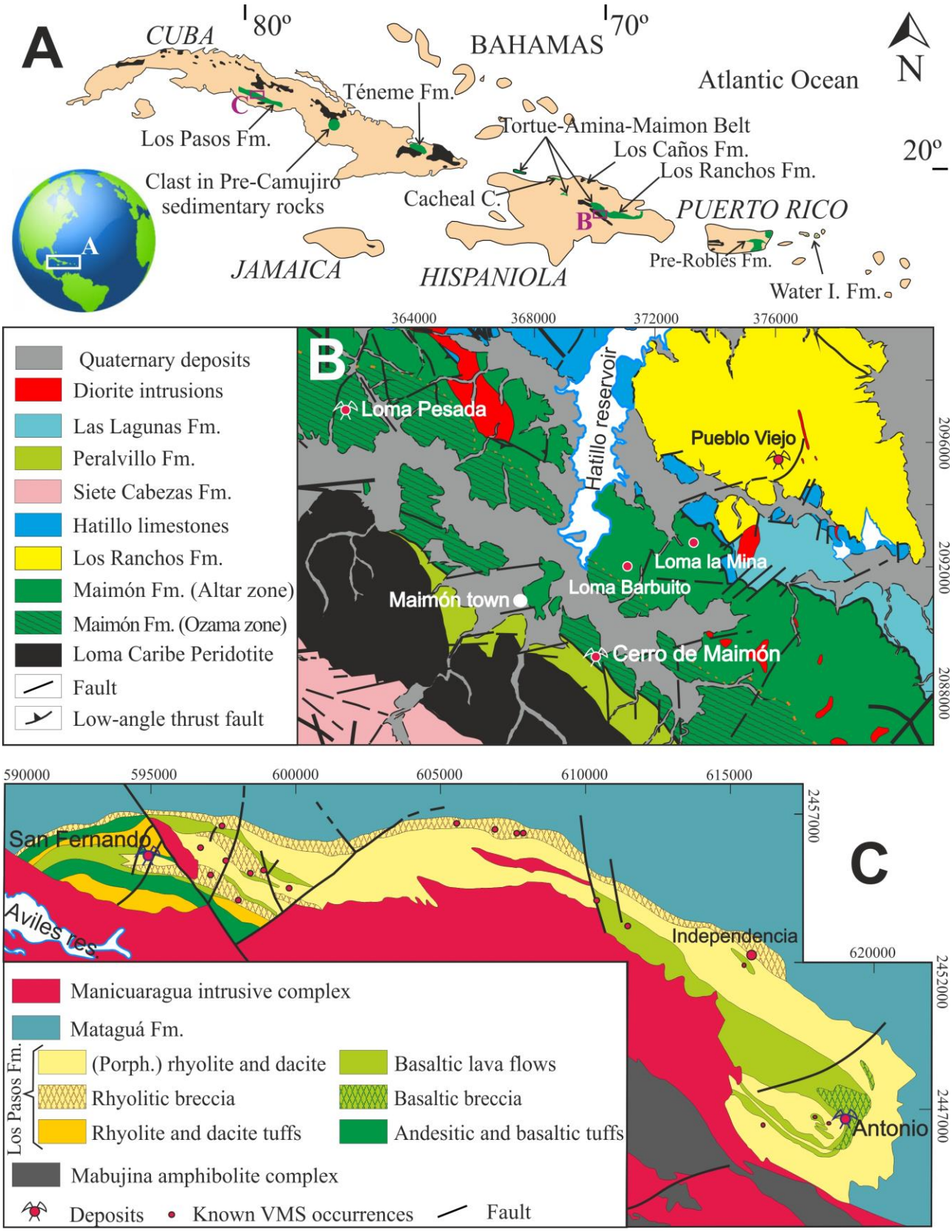

Figure 1

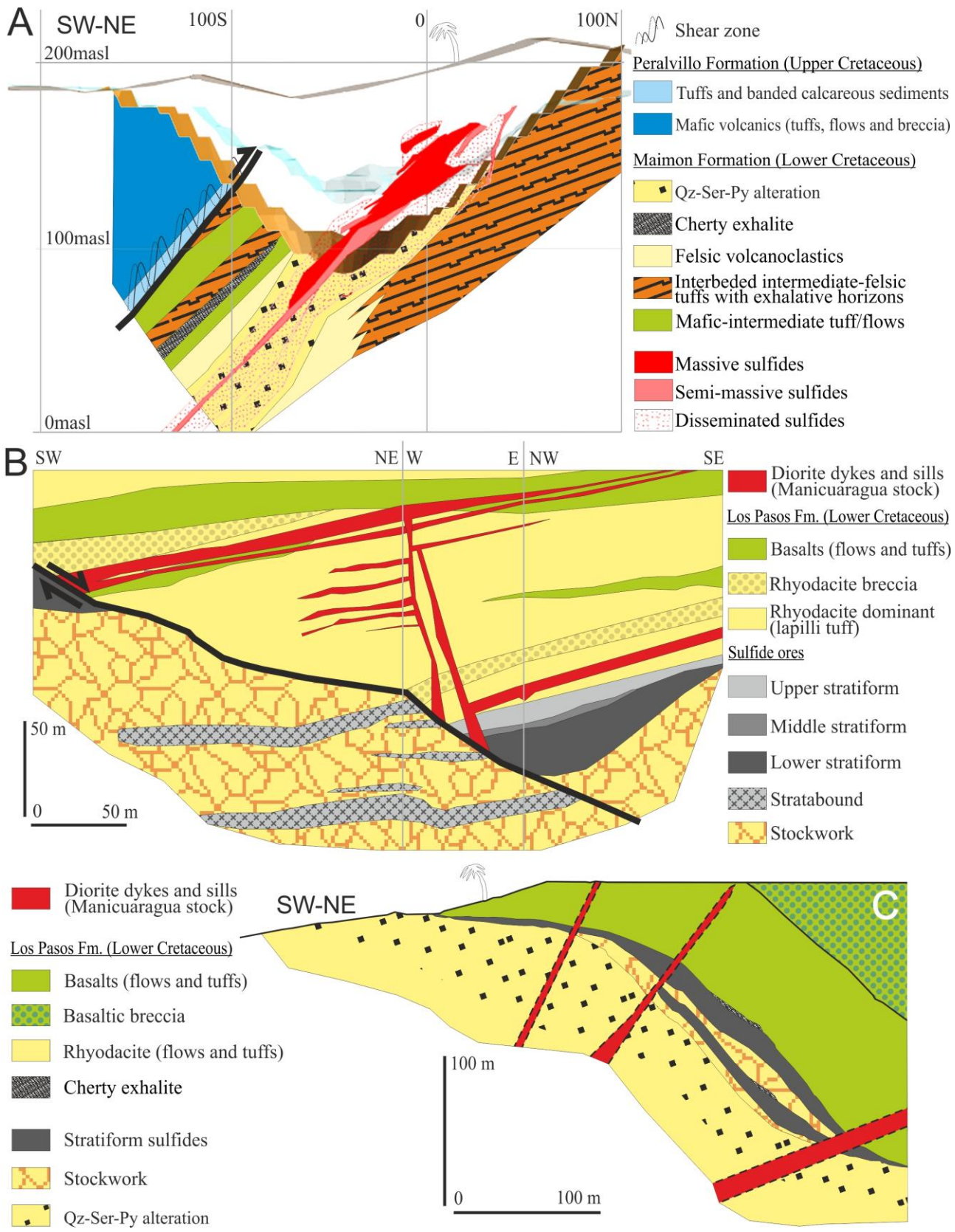

Figure 2

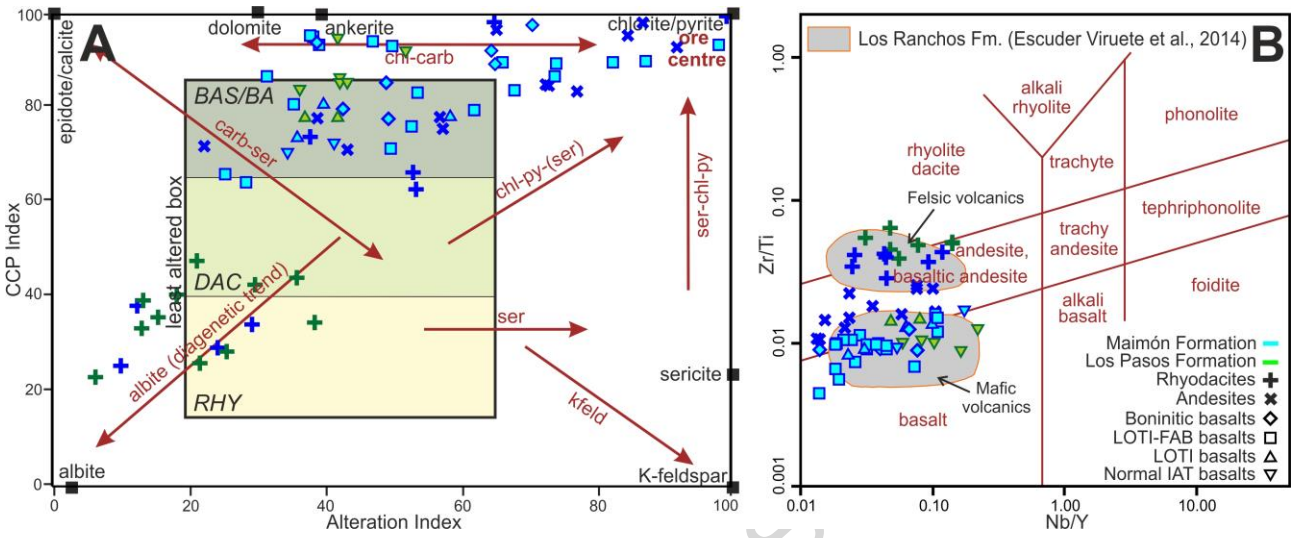

Figure 3

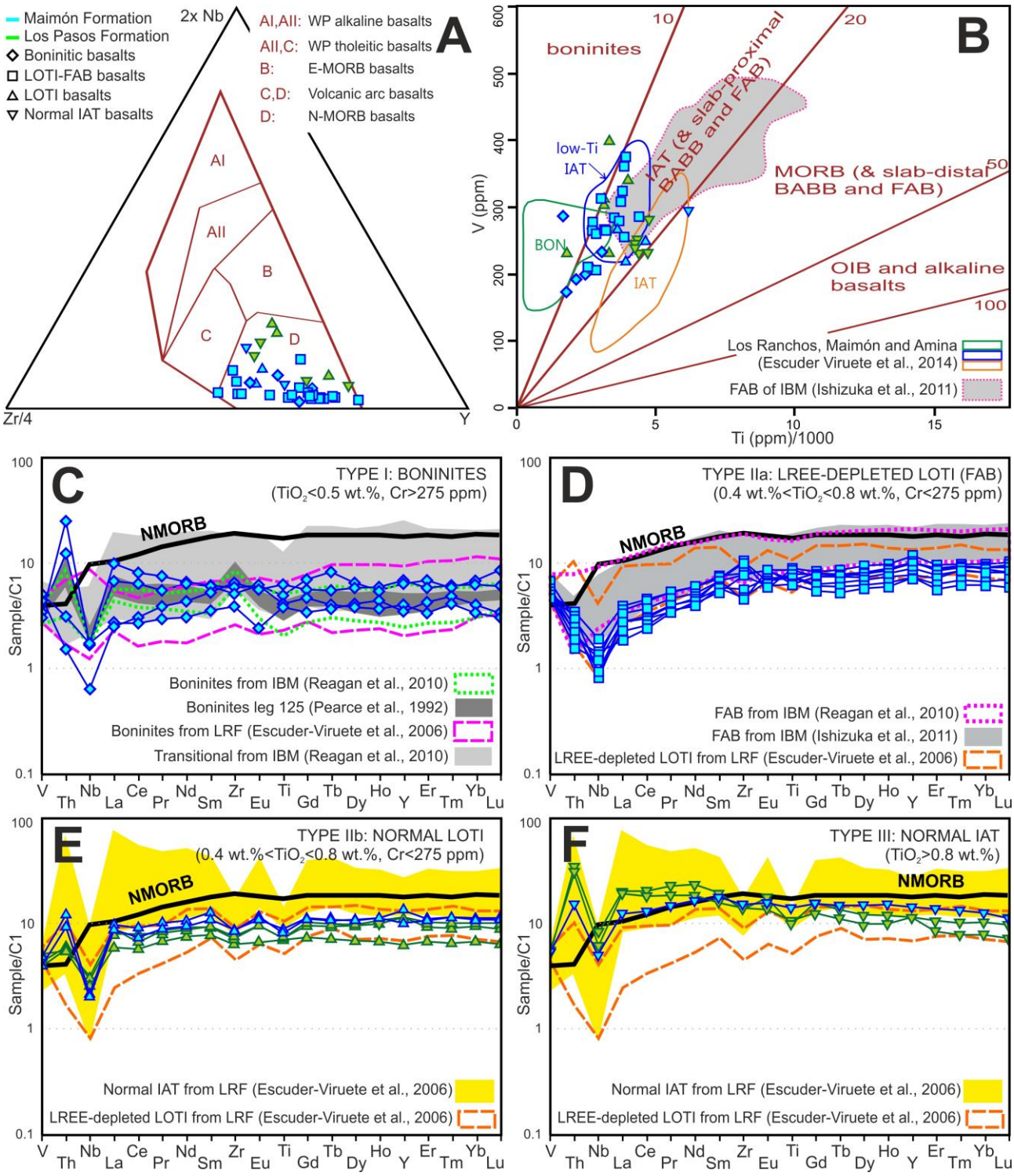

Figure 4

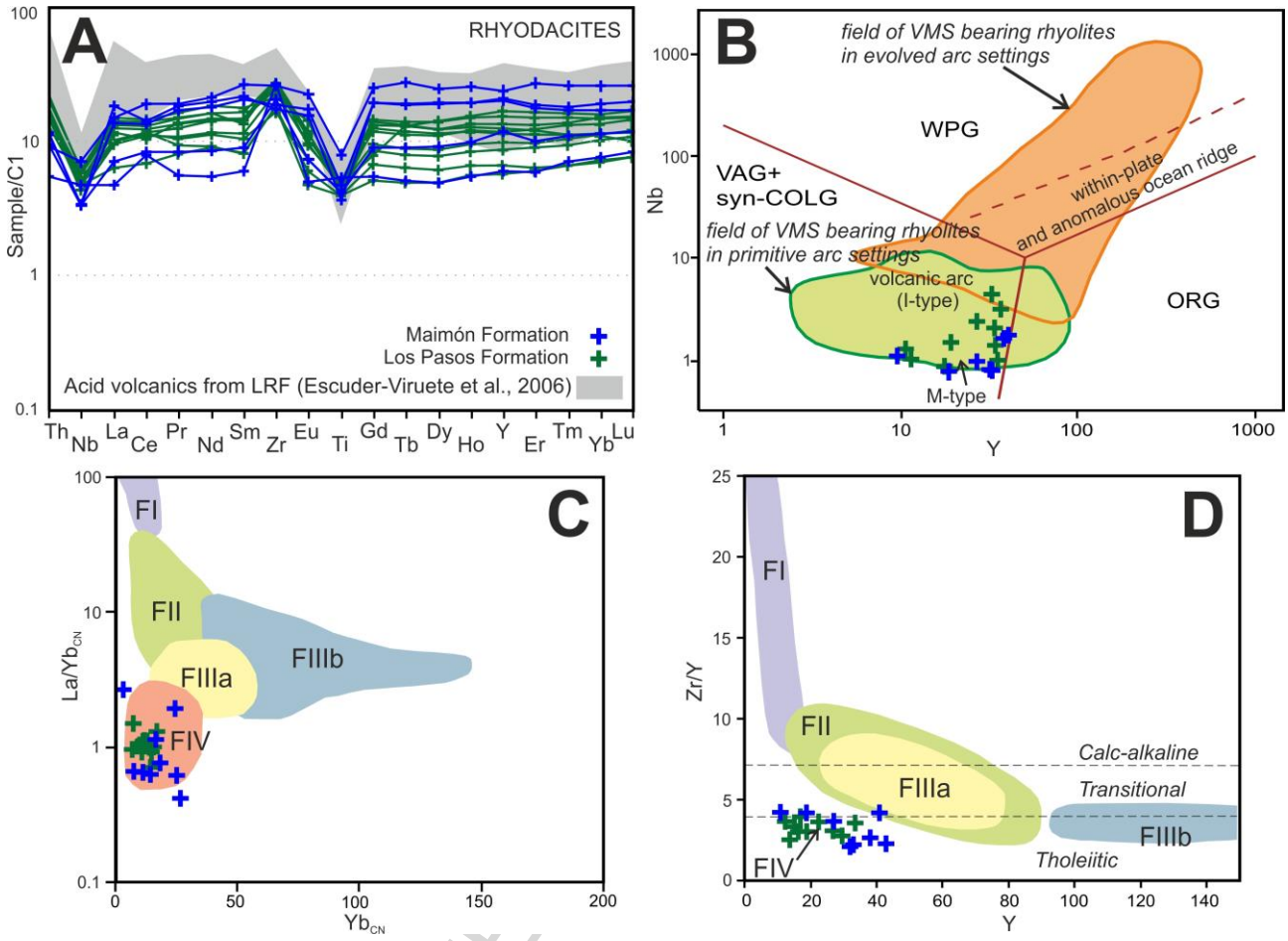

Figure 5

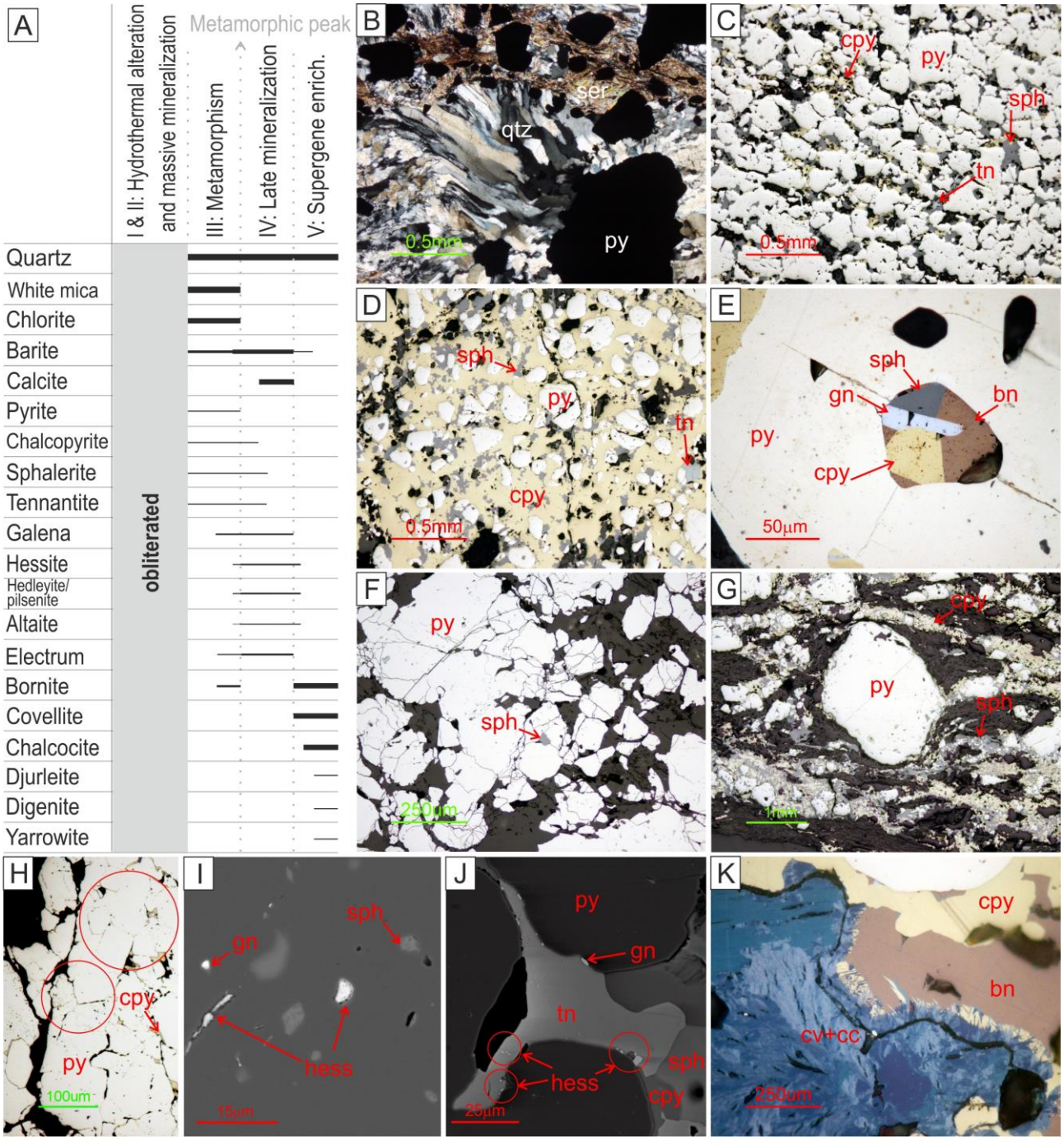

Figure 6

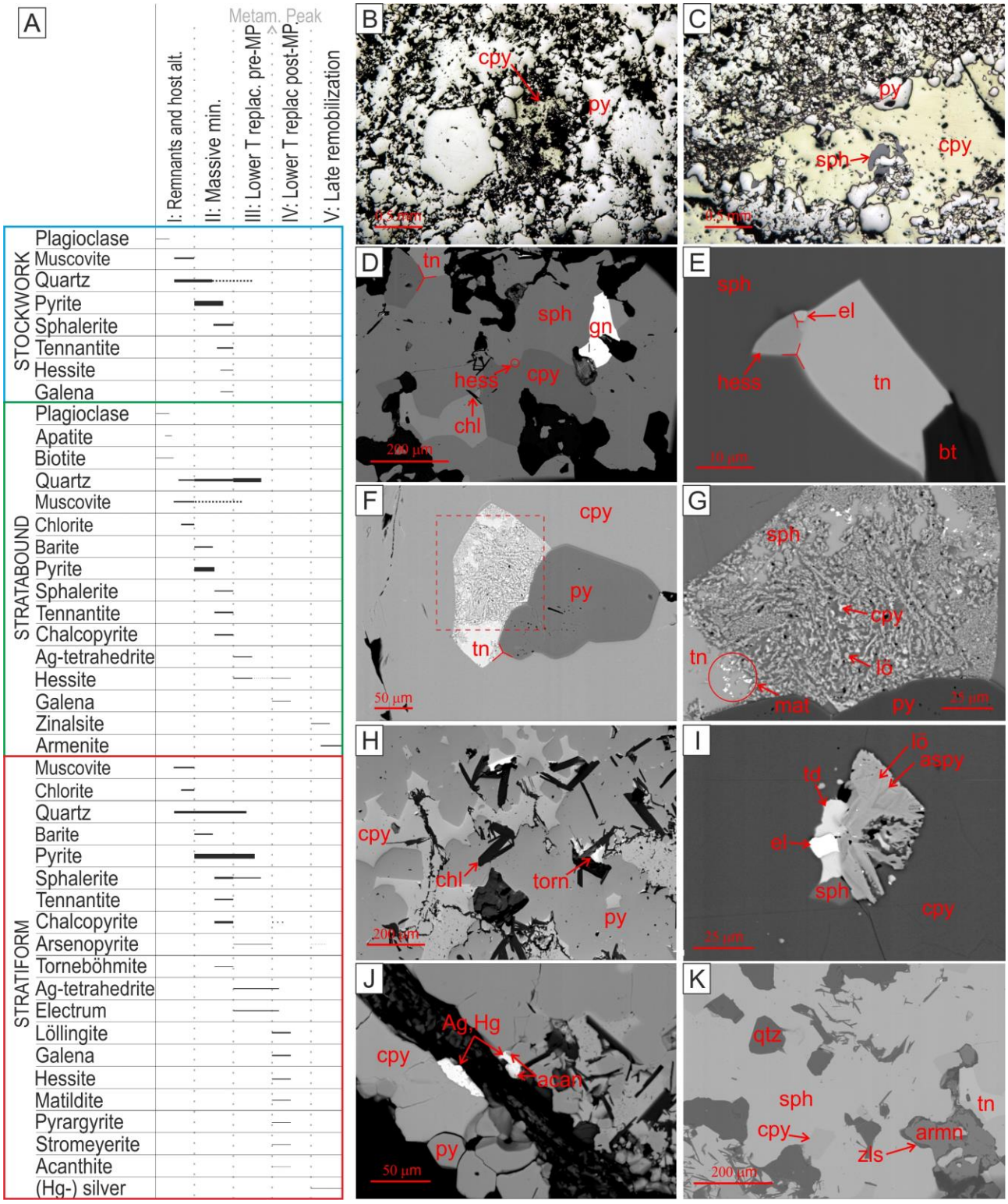

Figure 7

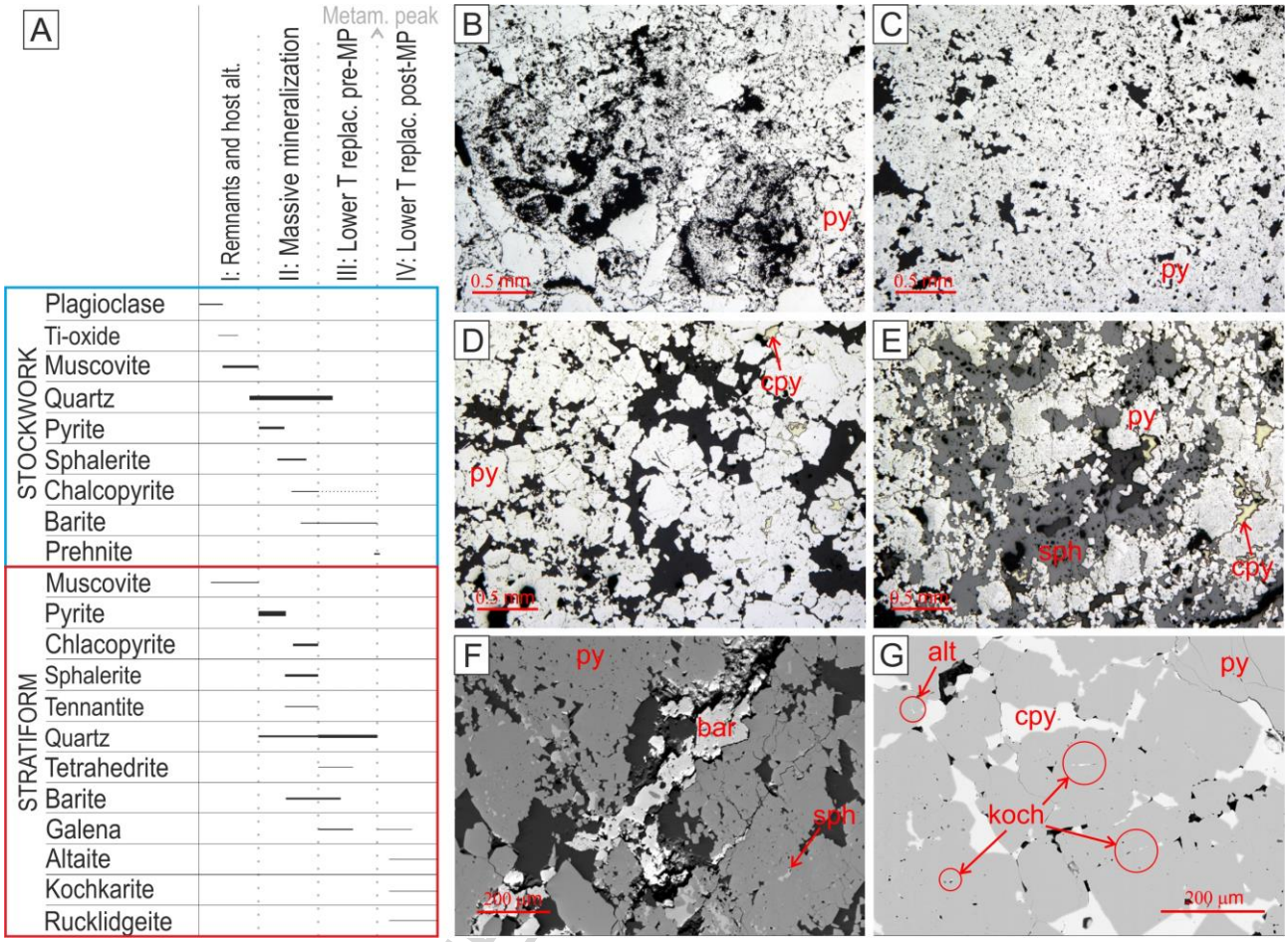

Figure 8

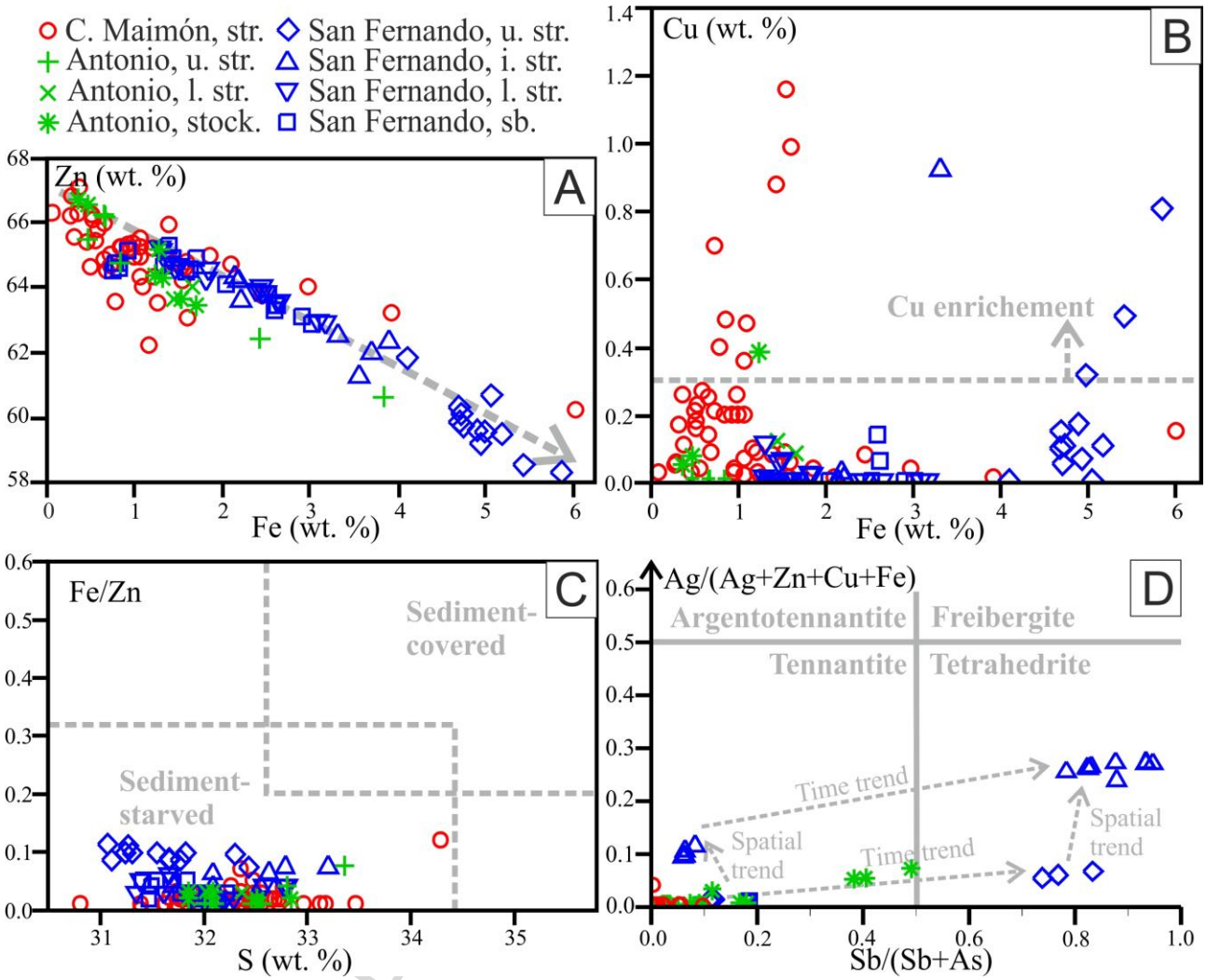

Figure 9

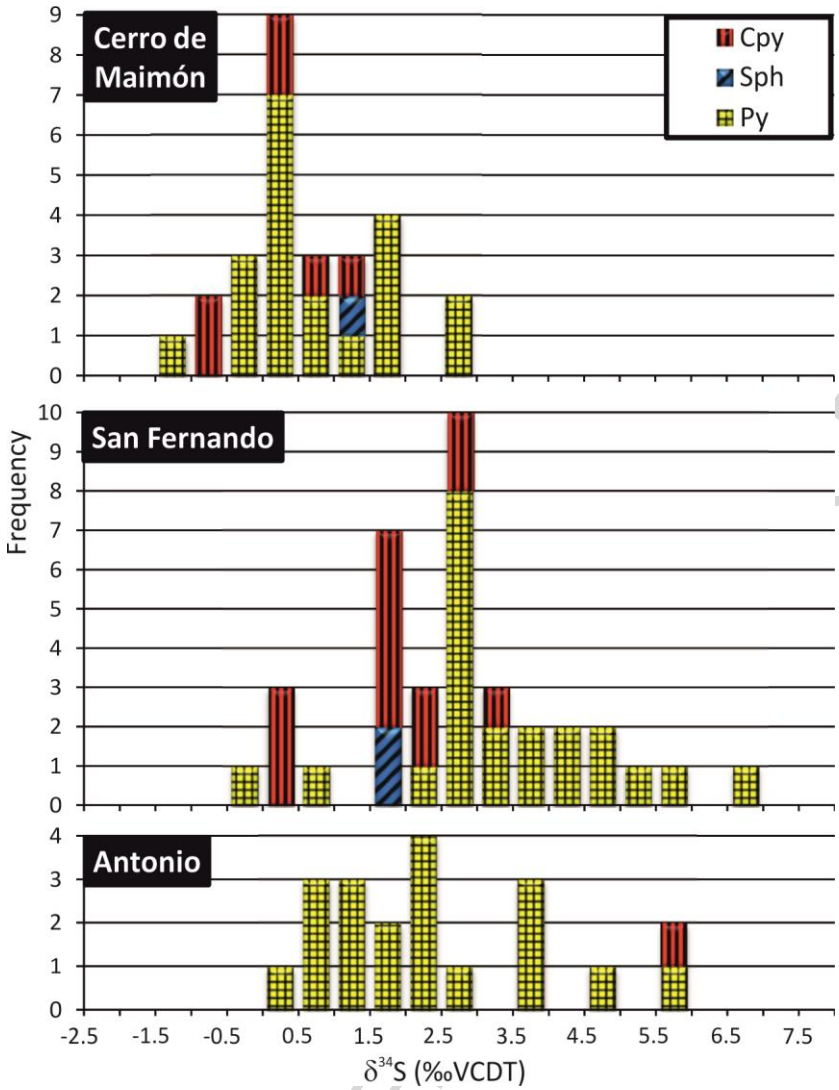

Figure 10

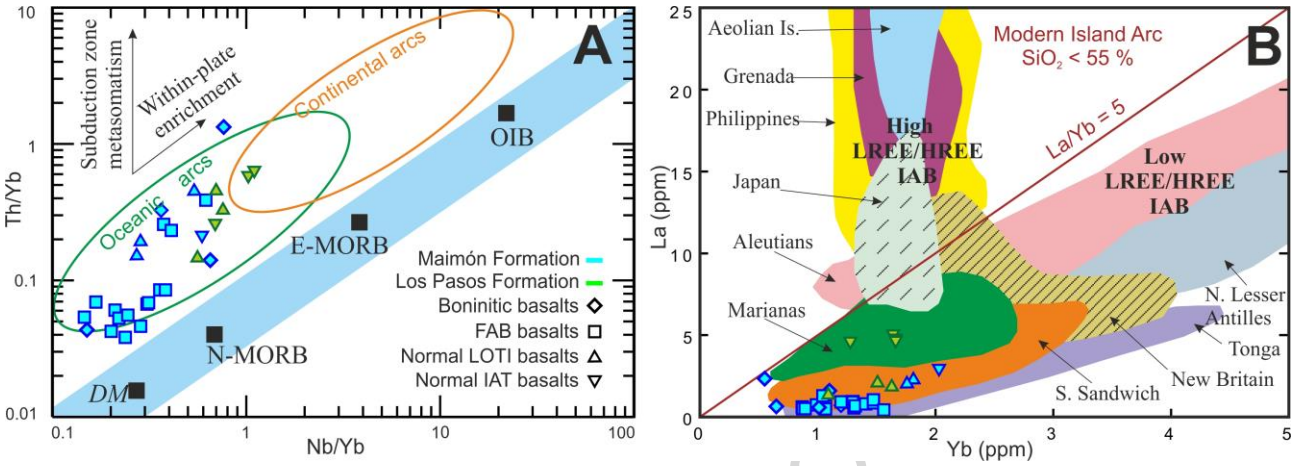

Figure 11

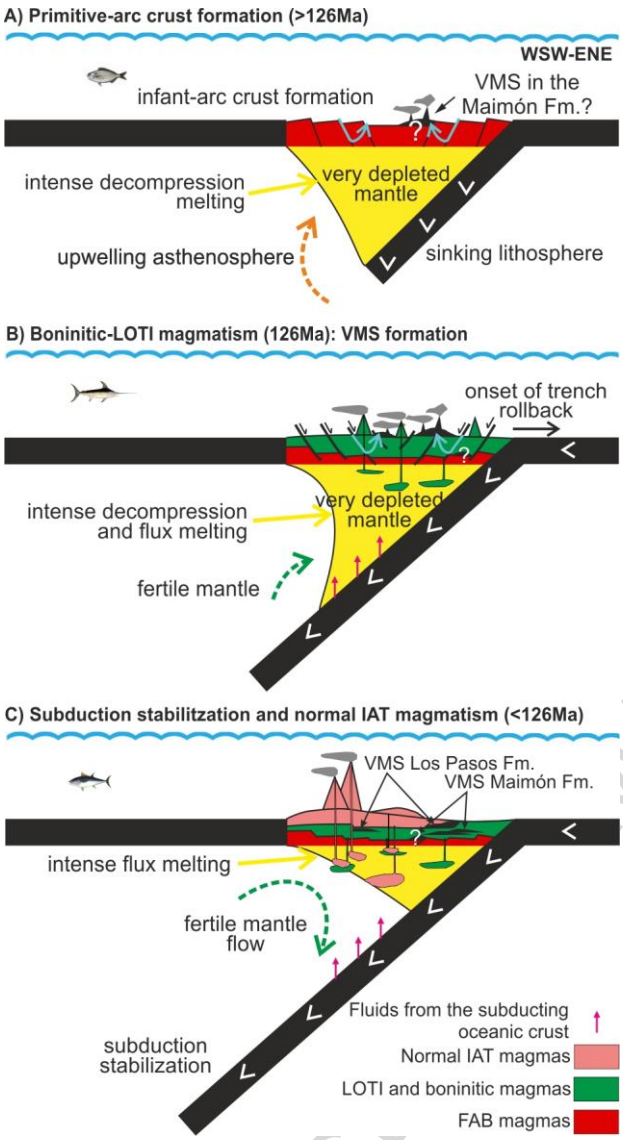

Figure 12

HIGHLIGHTS (for review)

This is a quite long manuscript, including 12 figures, that gathers mineralogical and geochemical data on ore and hosting volcanic samples from the Dominican Cerro de Maimón and the Cubans San Fernando and Antonio VMS deposits. Analyzed samples are among those collected over the last 20 years by our research team from the most prominent VMS deposits of the Greater Antilles. The long list of authors is indeed a reflection of the long-lived collaboration with the Cuban- and Dominican-based mining companies.

Lithochemistry of the hosting volcanics from the Maimón and Los Pasos Formations points to an exceptional record of the very first magmatic expressions connected to the subduction initiation of an intraoceanic case. This makes the joint study of the VMS mineralizations hosted in both Formations an appealing opportunity to describe and understand VMS mineralizing systems linked to the most primitive arc volcanism in fore-arc settings.

The work here presented is based in new unpublished data complemented and supported by previous results, which confers to it an indisputable review character. It is authors' opinion that the review and regional perspective of this article makes it very suitable for publication in your journal.

In accordance with the "Guide for authors" on the webpage of your journal, we have submitted the original manuscript with figures and table online. Due care has been taken to ensure the integrity of the work. No conflict of interest exists in the submission of this manuscript. This research article is part of the PhD thesis of the corresponding author.

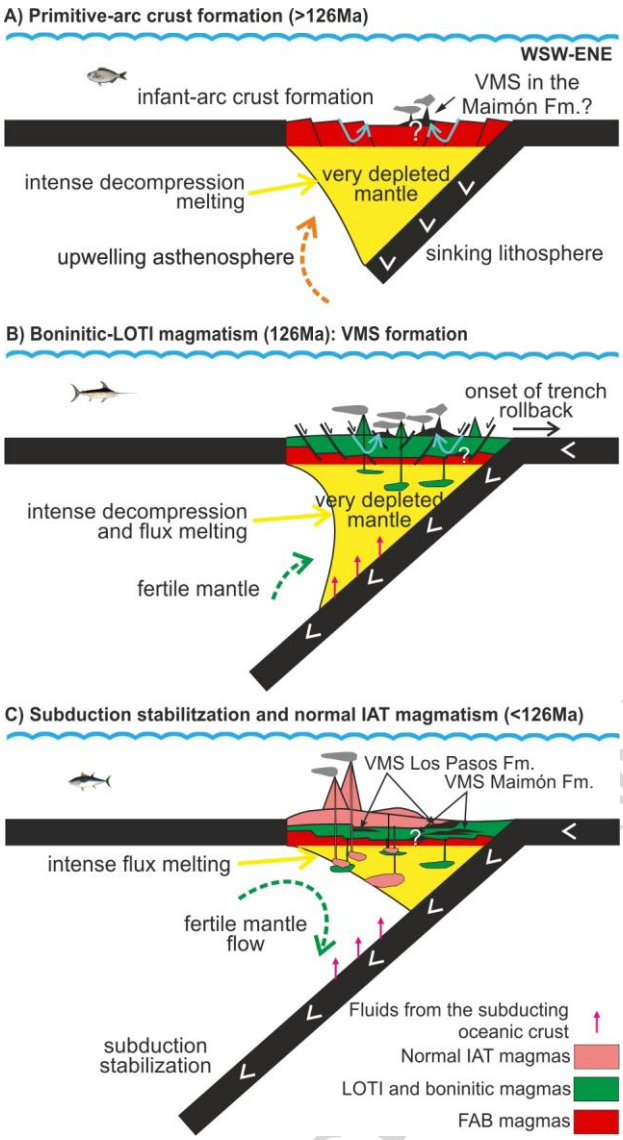

Graphical Abstract